Studies on Thin Films of Liquid Crystalline Molecules

THESIS

Submitted in partial fulfilment
of the requirements for the degree of
DOCTOR OF PHILOSOPHY

by

C. KARTHIK

Under the Supervision of

Prof. R. K. Gupta

BIRLA INSTITUTE OF TECHNOLOGY AND SCIENCE, PILANI

2015

BIRLA INSTITUTE OF TECHNOLOGY AND SCIENCE, PILANI

CERTIFICATE

This is to certify that the thesis entitled "Studies on thin films of liquid crystalline molecules" and submitted by C. Karthik ID No 2010PHXF401p for award of Ph.D. of the Institute embodies original work done by him under my supervision.

Supervisor:
Prof. R. K. GUPTA
Associate Professor
Department of Physics

Date:

Dedicated to my loving maa and papa

ACKNOWLEDGEMENTS

At the outset, I would like to express my deepest heart-felt gratitude to Prof. Raj Kumar Gupta for his expert guidance, suggestions and continuous encouragement to me at all phases of my work and providing unrestricted environment during the entire course of my research. His constant support, understanding and involvement in the minutest of the details has given this thesis the present form. I am indebted to him for the help rendered to me. It has been an honor for me to be his first Ph.D. student. I thank GOD for giving me such a patient, caring and friendly mentor. I am also grateful to Prof. Manjuladevi V. for her invaluable guidance, her constant support and motivation throughout my PhD work. I deeply acknowledge the invaluable support of my DAC members Prof. Debashis Bandhyopadhyay and Prof. Manjuladevi V. for reviewing my work and giving valuable suggestions, feedback and constructive comments during the course of my research work. I am grateful to Prof. B. N. Jain, Vice-Chancellor (BITS) and Director (Pilani campus), for allowing me to carry out my doctoral research work in the institute. I am thankful to Prof. S. K. Verma, Dean, Academic research division, BITS, Pilani, Prof. Hemant Jadhav, Associate Dean, Academic research division, BITS, Pilani for their co-operation and encouragement at every stage of my PhD programme. I would like to thank Prof. Sunil Bhand, Dean, Sponsored Research and consulting division and Prof. Sanjeev Kumar, Associate Dean, Sponsored Research and consulting division for providing me their valuable supports. I would like to express my gratitude to Prof. D. D. Pant, Head of Physics Department and Prof. Rakesh Choubisa, DRC Convener for providing me all the necessary departmental facilities at various stages of my research work. I would like to thank all the faculty members of Physics Department for their support and encouragement during my PhD tenure. I would like to thank Dr. Anshuman, Unit Chief, Estate Management, BITS, Pilani for helping me with a pleasant stay at BITS, Pilani. I would like to acknowledge all deans and associate deans, BITS, Pilani for their support. I would like to thank BITS, Pilani for providing central facilities to carry out my research work.

I wish to place on record my special thanks to Raman Research Institute, Bengaluru for providing the experimental facilities for my research work. I am grateful to our collaborators Prof. Sandeep Kumar and Dr. Mahesh C. Varia of Raman Research Insitute, Bengaluru for providing us with molecules for carrying out the research work. I would like to thank Mr. A. Dhason and Mrs. K.N Vasudha, Scientific Assistants of Raman Research Institute, Bengaluru for helping me with the Field emission SEM and XRD experiments. These were the most important inputs for my present research study.

I owe this doctorate degree especially to my maa, Mrs. C. Kalpana and my papa, Mr. K. Chandrashekar whose dreams have come true with my achievement of this stage in

my education. This has been possible because of all the prayers and sacrifices of my parents, their love, affection and blessings. Thank you mom and dad for everything. Your motivation and warm encouragement helped me in overcoming tough times. I would like to thank all my family members including my Uncle and inspiration, Prof. K. Jayaraman, Michigan State University, U.S.A and my Aunt Mrs. Jayashri Iyer for her blessings and support. I wish to express my sincere gratitude to Mr. Edwin (Director, IIM Coimbatore) for his guidance and counselling in choosing my present career.

I would also like to offer my special thanks to my roommate, best friend and brother, Kapil Dhaka, research scholar, Department of Physics, BITS, Pilani for his love, extraordinary tolerant support, motivation, and all the good times during my PhD work. I would like to thank Dr. Neha Gupta for helping, supporting and motivating me constantly during my PhD work. I would like to thank Mr. M. C. Pandey and Mrs. Poonam Pandey for their blessings and support throughout my journey. I would like to thank Mr. Rohit Pant, Mrs. Pankaja Pant, Mr. Rajan Pandey and Mrs Indu Nitendra Singh for their support and blessings. I would also like to thank Mrs. Kitab Kaur, Mr. Rajesh Dhaka and Mrs. Sapana Poonia Dhaka for their blessings and invaluable support. I want to thank Dr. Anil Rai, HOD Music, BITS, Pilani for his blessings and members of Gurukul, Department of Music, BITS, Pilani for their support. I would like to thank Dr. Sanjeev Gupta, CSIR-CEERI, Pilani for helping me with my research work. I want to extend my thanks to my Lab-mates, Keerti Choudhary, Monika Poonia, Jeetendra Kumar, Devnarayanan V.P. and Akshatha for helping me to carry out my research work. I am thankful to the office staff of Academic research division, Mr. Mahipal, and Mr. Raghuvir for all the help and good wishes. I express my thanks to the office staff of Physics Department, BITS, Pilani, including Mr. Srikant Sharma, Mr. Rajiv Gaur and Mr. C. P. Soni for providing all the necessary support whenever needed. I would like to acknowledge all research scholars of Physics Department, BITS, Pilani. I take this opportunity to thank one and all for their help directly or indirectly in my present achievement. I deeply acknowledge BITS, Pilani and UGC-BSR for the financial assistance throughout my PhD tenure.

In the end once again my humble thanks to Prof. Raj Kumar Gupta and Prof. Manjuladevi V. This is the perfect opportunity to tell you and Mam, how special you are and how much you mean to me. Thank you for everything. You will live with me forever even if we are miles apart. I will always need your blessings.

C. Karthik

Date:

ABSTRACT

A thin film is a layer of material whose thickness ranges from a fraction of nanometer to several micrometers. The surface to volume ratio of a material increases enormously when spread on to a substrate to form thin film which results in enhancement of performance and efficiency of the thin film based devices. The physicochemical properties of the thin film are governed by several parameters including molecular aggregation and density. In this thesis, we are primarily focusing on surface behavior of several liquid crystal (LC) molecules possessing different intermolecular interaction and shape anisotropy. The Langmuir monolayer (LM) of the molecules were formed at the air-water (A-W) interfaces and the surface phases were characterized by surface manometry, Brewster angle microscopy (BAM) and epifluorescence microscopy. The LM of the molecules were transferred to solid substrates by Langmuir Blodgett (LB), horizontal transfer and Schaefer methods and the surface morphology was studied using scanning probe microscopy (SPM) and field emission scanning electron microscopy (FESEM). The LM of a tricycloquinazoline (TCQ) based amphiphilic discotic liquid crystal (DLC) with 6 ethelenoxy side chains (AmTCQ) was found to be very stable at A-W interface. Due to weak pi - pi interaction, the LM of AmTCQ exhibits a high density liquid phase (L_{12}) wherein the molecules prefer both face-on and edge-on conformations. The LB films of AmTCQ deposited onto silicon substrates at different target surface pressure (π_t) shows the stable triangular shaped nanostructure. The number of such triangular domains increase polynomially with the increase in π_t. In order to study the effect of change in intermolecular interaction on the surface behavior, the side chain of the AmTCQ is replaced by rod shaped cyanobiphyenyl (TCQCB molecule). The LM of such molecule exhibits gas, low density and high density liquid phases. The LB films of such molecules reveal a morphological transformation from random shape to elongated domain to granular texture with the increase in π_t of deposition. The AmTCQ molecule was fluorescent in nature and therefore we present systematic photophysical properties of the molecule. We demonstrated that the AmTCQ molecules can be employed as molecular probe for imaging another discotic system and LM at the A-W interface. The LB films of hybrid system comprising of hexaalkoxy triphenylene DLC (HAT5) molecule and TiO_2 nanoparticles were fabricated at different experimental conditions. Here we found that the energy gap of such hybrid system can be altered systematically by altering the wt.% of TiO_2 nanoparticles and π_t of the LB deposition. We found that the LM can be used as a template for the fabrication of nanoparticles at the A-W interface. We synthesized

the cadmium sulfide (CdS) nanoparticles by forming LM of octadecanethiol (ODT) over an aqueous subphase containing cadmium chloride ($CdCl_2$) salt. Such nanoparticles were embedded into the LM of rod shaped LC, 4-octyl-cyanobiphenyl (8CB). We demonstrated that with the LB film of 8CB+CdS nanoparticles as alignment layer, the bulk LC in the cell can align planar. The presence of CdS nanoparticles in the LB film of 8CB enhances the planar orientation in the bulk LC. The LM and LB film of H-shaped LC molecules show interesting results. Since the molecule possesses azo group, the surface morphology of the LB film of such molecules showed dependence on the nature of exposed radiation during the LB film fabrication. Such system can potentially be used in molecular electronic switches and memory devices.

Contents

Certificate **i**

Acknowledgements **iii**

Abstract **v**

List of Tables **x**

List of Figures **xi**

Abbreviations **xviii**

Symbols **xxi**

1 Introduction **1**
1.1 Langmuir monolayer (LM) at air-water (A-W) interface 2
1.2 Thin films at air-solid(A-S) interface 8
1.2.1 LB technique 8
1.2.2 Horizontal transfer and Langmuir Schaefer's techniques . . . 10
1.2.3 Characterization techniques 11
1.3 Materials 13
1.3.1 Liquid crystals (LC) 13
1.3.1.1 Thermotropic LCs 14
1.3.1.2 Lyotropic LCs 15
1.3.1.3 Nanomaterials and nanostructures 16
1.3.1.4 Biological systems 16

2 Ultrathin films of Tricycloquinazoline (TCQ) based discotic liquid crystal molecules at different interfaces **25**
2.1 Introduction 25
2.2 Experimental Methods 27
2.3 Results and discussion 29
2.4 Conclusion 43

3 Effect of modification of side chains of TCQ based discotic molecules on its surface behavior at different interfaces 48
3.1 Introduction . . . 48
3.2 Experimental Methods . . . 49
3.3 Results and Discussion . . . 50
3.4 Conclusions . . . 55

4 Fluorescence behavior of AmTCQ discotic LC molecules and its application for imaging in bulk and Langmuir monolayer 58
4.1 Introduction . . . 58
4.2 Materials and methods . . . 60
4.2.1 Experimental methods . . . 61
4.2.2 Computational methods . . . 61
4.2.3 Theoretical methods . . . 62
4.3 Results and Discussion . . . 64
4.4 Conclusions . . . 72

5 Studies on thin films of discotic liquid crystal, hexa-alkoxy triphenylene (HAT5) doped with TiO_2 nanoparticles 78
5.1 Introduction . . . 78
5.2 Experimental Methods . . . 80
5.3 Results and Discussion . . . 80
5.4 Conclusions . . . 86

6 Langmuir monolayer assisted fabrication of cadmium sulfide (CdS) nanoparticles and its role in surface manometry and alignment of rod shaped liquid crystal 89
6.1 Introduction . . . 89
6.2 Experimental Methods . . . 91
6.2.1 Materials . . . 91
6.2.2 Methods . . . 91
6.2.2.1 Surface manometry measurements . . . 91
6.2.2.2 Langmuir Blodgett deposition . . . 92
6.2.2.3 UV-VIS Spectroscopic Measurements . . . 92
6.2.2.4 Field Emission Scanning Electron Microscopy . . . 92
6.2.2.5 Atomic Force Microscopy . . . 92
6.2.2.6 X-Ray Diffraction . . . 93
6.2.2.7 Zeta potential Measurements . . . 93
6.3 Results and Discussion . . . 93
6.3.1 Fabrication of CdS nanoparticles at air-water interface . . . 93
6.3.2 Incorporation of CdS nanoparticles in a liquid crystal matrix at air-water and air-solid interfaces and its role in alignment of bulk liquid crystal . . . 100
6.4 Conclusions . . . 104

7 Langmuir monolayer (LM) and Langmuir-Blodgett (LB) films of H-Type liquid crystal molecule 108

7.1 Introduction 108
7.2 Experimental Methods 110
7.3 Results and Discussion 111
7.4 Conclusions 121

8 Conclusions and future scope of our studies 124
8.1 Conclusions 124
8.2 Future Scope 132

A LIST OF PUBLICATIONS 135

B LIST OF PRESENTATIONS 137

C BIOGRAPHY OF THE CANDIDATE 139

D BIOGRAPHY OF THE SUPERVISOR 140

List of Tables

1.1 Some of the possible hydrophobic (HPB) and hydrophilic (HPL) groups of amphiphilic molecules 3
1.2 Thermotropic LCs forming stable LM 15
1.3 Lyotropic LCs forming stable LM 16
1.4 Nanomaterials forming stable LM 16
1.5 Biological systems forming stable LM 17

2.1 The absorbance values and relative comparison (A/B) as obtained from RAIRS spectra for the AmTCQ monolayer deposited at different π_t on the gold deposited Si substrate. The value of absorbance (Abs.) at a characteristic peak is estimated after baseline correction with a linear fit. 37

4.1 Spectral data: emission wavenumbers (v_f), absorption wavenumbers (v_a), Stoke's shift (v_f - v_a) and arithmetic mean of Stoke's shift ((v_f + v_a)/2) 65
4.2 Dielectric constants (k), refractive index (n) of the solvents, Lippert ($F(k,n)$), Bakhshiev ($F_1(k,n)$), Kawski Chamma Viallet ($F_2(k,n)$) solvent polarity function 66
4.3 Estimated values of ground state p_g and excited state p_e dipole moment 68
4.4 Absorbance (A), Absorbance at excitation wavelength (390 nm) (A*), Polarity (P), Quantum Yield (ϕ_1/ϕ_2) 69
4.5 Molar absorbance (ϵ), Band shift at half maxima (Δv_a), oscilator strength (f), transition dipole moment (μ_t) 69

6.1 Variation of energy gap (E_g) as the function of $CdCl_2$ concentration in the subphase and the target surface pressure (π_t) of LB deposition of ODT 96
6.2 Variation of energy gap (E_g) as a function of target surface pressure (π_t) of LB deposition of ODT from the substrate at 10^{-5} M $CdCl_2$ concentration. The LB films were dispersed in $CHCl_3$ solvent by ultrasonication and then the UV-VIS spectra were collected. 98

7.1 Surface manometry results for HLC molecule 112
7.2 Minimum average step height of HLC layers observed in AFM. . . . 118

List of Figures

1.1 A schematic diagram of an amphiphilic molecule indicating polar head group and a non-polar tail group. 2

1.2 (a) shows a typical π – A_m isotherm indicating the different phases in a LM. (b) shows the molecular arrangement in different phases. The symbols L_1, L_2 and S represent liquid expanded, liquid condensed and solid phases, respectively. 4

1.3 A schematic diagram showing the experimental setup for the measurement of π - A_m isotherms. The basic parts of the setup are as follows; (1) Teflon trough, (2) Teflon barriers, (3) subphase (ion-free water), (4) Wilhemy plate (filter paper), (5) π sensor, (6) computer, (7) connecting wires. 6

1.4 Schematic diagrams showing the working principle of a BAM. θ_B is the Brewster angle for water with respect to air. The different parts are as follows; polarizer (P), charge coupled device (CCD) camera and monolayer at the A-W interface (S). (a) and (b) are the BAM setups without and with monolayer at the A-W interface, respectively. 7

1.5 A schematic diagram showing the experimental setup for forming Langmuir-Blodgett films. The parts are as follows; (1) teflon trough with a well in the center, (2) barriers, (3) subphase, (4) substrate (5) dipper. 9

1.6 (a) The mechanism of formation of multilayer by the Langmuir-Blodgett technique. (A) first upstroke, (B) first downstroke and (C) second upstroke. (b) The structure of different types of multilayer obtained by LB technique, namely X-, Y- and Z-type. 10

1.7 Schematic diagram of AFM. 11

1.8 Schematic diagram of DLC in (a) columnar and (b) nematic phase . 14

2.1 DLC molecule possessing TCQ core and six ethelenoxy side chains. 27

2.2 Surface pressure (π) - area per molecule (A_m) isotherm of the AmTCQ molecule. The arrows a, b and c are drawn to indicate the onset of low density liquid (L_1), high density liquid (L_{12}) phases and collapse during compression. 30

2.3 Variation of normalized area ($A_t/A_{t=0}$) with time (t) at different π. Here A_t is the A_m at a time t and $A_t = 0$ is the initial A_t. 30

2.4 (a) Variation of π with time during the determination of the equilibrium spreading pressure (ESP) of AmTCQ molecules. (b) Isocycle by compression and expansion of the monolayer. 31

2.5 BAM images of the monolayer of AmTCQ molecules. The images were captured at an A_m shown below the respective images. (a) Coexistence of dark and gray domains. (b) Very uniform gray texture. (c) Coexistence of bright domains in the gray background. The scale bar represents a length of 500 μm. 32
2.6 AFM images in SRI mode for the monolayer of AmTCQ molecules deposited at different π_t as indicated in the caption of the respective images. The top and bottom images are topographic and I_t map measured simultaneously in the SRI mode. The line profiles are drawn at the same location of both the maps and the corresponding graphs are shown below each images. The various features in the image (d) are labeled with A, B, and C. The corresponding points are indicated in the graphs by vertical lines. The scale bar in the image (a) and (b–d) represent lengths of 1 μm and 0.25 μm, respectively. 34
2.7 The RAIRS spectra of the films deposited at different π_t (π_t). The curves are relatively shifted vertically by absorbance value of 0.25 for visual clarity. 36
2.8 (a) The possible molecular conformation of AmTCQ molecules at the A-W interface in L_1 phase. (b) The possible molecular conformation of AmTCQ molecules at the A-W interface in L_{12} phase. 38
2.9 $\pi - A_m$ isotherm of the AmTCQ molecule. The AFM images of the LB film on Si substrate deposited at the target surface pressure (π_t) as indicated by the arrows in the isotherm. 39
2.10 AFM images of LB film of AmTCQ molecules deposited at π_t of (A) 0 mN/m, (B) 1 mN/m, (C) 10 mN/m and (D) 15 mN/m. The height profile corresponding to the black line drawn over each image is shown below respective images. 41
2.11 Percentage area coverage (c) of triangular domains in the LB films deposited at different target surface pressure (π_t). The dark circles are the experimental data points. The solid line is a fit polynomial curve: $c = 0.4 - 0.32\pi_t + 0.12\pi_t^2$. 42

3.1 The chemical structure of the TCQCB molecule. 50
3.2 Surface pressure (π) - area per molecule (A_m) isotherm (solid line) and in-plane elastic modulus (E) - A_m of the TCQCB molecule (dashed line). 51
3.3 Isocycles obtained during repeated compression and expansion of the TCQCB monolayer at A-W interface. 52
3.4 (Top) AFM image of a bare glass coverslip. (Below) Height profile is drawn along the white line on the AFM image. The scale bar represent a length of 0.25 μm. Dashed line represent the average height of the image. 53

3.5 AFM images of LB films of TCQCB molecule. The target surface pressure (π_t) for LB films deposition corresponding to the images A, B, C and D are 10, 20, 30 and 35 mN/m, respectively. The height profile along the dark line drawn on the images are shown below the respective images. The scale bar represent a length of 200 nm. 54
3.6 (a) The possible molecular conformation of TCQCB molecules at the A-W interface in L_1 phase. (b) The possible molecular conformation of TCQCB molecules at the A-W interface in L_2 phase. 55

4.1 Ball and stick model of AmTCQ molecule 59
4.2 Solution of AmTCQ molecule prepared in $CHCl_3$ (0.26 mg/ml). The color of the solution appears to be yellowish-green. 61
4.3 The UV-VIS (left side) and fluorescence (right side) curves of AmTCQ in various solvents. 65
4.4 The plot (a) is stokes shift versus Lippert polarity function (F(k, n)), (b) is stokes shift versus Bakshiev polarity function ($F_1(k,n)$) and (c) is arithmetic mean of emission/absorption wavenumbers versus Kawski Chamma Vallet polarity function ($F_2(k,n)$) of AmTCQ in various solvents: (1) chloroform, (2) acetone, (3) acetonitrile, (4) Dimethyl formamide, (5) toluene, (6) Dichloromethane, (7) Carbon tetrachloride, (8) THF. (———Linear fit) 67
4.5 The plot shows variation of transition dipole moment (Top) and Oscillator strength (Below) as the function of emission wavenumber for AmTCQ in various solvents: (1) chloroform, (2) acetone, (3) Dimethyl formamide, (4) acetonitrile, (5) toluene, (6) Carbon tetrachloride,(7) Dichloromethane, (8) THF. 70
4.6 The fluorescence microscopy images of (a) AmTCQ molecue (Bright green region) (Inset shows fluorescence microscopy image of HAT5 (Dark region)) and HAT5 doped with (b) 1 (c) 5 (d) 10 mole percent of AmTCQ. 71
4.7 (a) Isotherm of LM of AmTCQ molecule at A-W interface. The arrows on the isotherm indicate the position at which the epifluorescence images were captured. (b) The epifluorescence images of LM of AmTCQ captured at A and B as indicated in the isotherm. Image A shows gas-liquid like coexistence phase and Image B shows liquid like phase. The scale bar is 500 μm in length. 72
4.8 Schematic view of fluorescence imaging on HAT5 with the aid of fluorescent AmTCQ molecule in a) columnar phase b) nematic phase. 73

5.1 Chemical structure of hexalkoxytriphenylene (HAT5). 79
5.2 Surface pressure (π)- Area (A) isotherms of Langmuir monolayer of the pure HAT5 (inset) and HAT5+TiO_2 nanocomposite with TiO_2 nanoparticles at different wt.% at the air-water interface. 81
5.3 The variation of lift-off area (A_i) as a function of wt.% of TiO_2 nanoparticles in the HAT5 monolayer. The continuous line is to indicate the non-linear behavior of the variation. 82

5.4 UV-VIS (a) (Left side) UV-Vis absorption spectra measurements for LB films of HAT5, HAT5+TiO_2 nanocomposites with 5 and 20 wt % of TiO_2 deposited on the glass coverslips at a target surface pressure (π_t) of 2 mN/m. (Right side) Plot indicating decrease in energy gap (eV) value on increasing the dopant concentration. (b) (Left side) Absorption spectra measurements for LB films of HAT5, HAT5+TiO_2 nanocomposites with 5 and 20 wt % of TiO_2 nanoparticles deposited on the coverslips at π_t of 20 mN/m. (Right side) Plot indicating decrease in energy gap (eV) value on increasing the dopant concentration. 83
5.5 Variation of energy band gap of the LB films deposited at π_t of 2 mN/m and 20 mN/m for 5 and 20 wt.% of TiO_2 in HAT5. 83
5.6 The AFM images of LB films of (a) HAT5 (b) HAT5+TiO_2 nanocomposite with 5 wt.% of TiO_2 nanoparticles and (c) HAT5+TiO_2 nanocomposite with 20 wt.% of TiO_2 nanoparticles. The films were deposited at the $\pi_t = 2$ mN/m. The scale bar for image A is 0.5 μm in length and the scale bar for image B and C is 0.2 μm in length. 84
5.7 The AFM images of LB films of (a) HAT5, (b) HAT5+TiO_2 nanoparticles, 5 wt.% and (c) HAT5+TiO_2 nanoparticles, 20 wt.%. The films were deposited in the L_2 phase at the $\pi_t = 20$ mN/m. The scale bar for image A is 0.5 μm in length and the scale bar for image B and C is 0.2 μm in length. 85
5.8 Variation of size of clusters of TiO_2 nanoparticles of the LB films deposited at π_t of 2 mN/m and 20 mN/m for 5 and 20 wt.% of TiO_2 in HAT5. 85

6.1 Schematic diagram of formation of cadmium sulfide (CdS) nanoparticles. 90
6.2 The surface pressure (π) - area per molecule (A_m) isotherm of octadecanethiol molecule with different concentration of $CdCl_2$ in the subphase. Inset shows the isotherm of octadecanethiol (ODT) molecule on ultrapure ion free water. 94
6.3 Plot of elastic modulus (E) vs. area per molecule (A_m) of octadecanethiol monolayer with different concentration of $CdCl_2$ in the subphase. 94
6.4 Average transfer ratio of LB films of ODT-Cd^{2+} complex at different concentration (10^{-x}M) of $CdCl_2$ in the aqueous subphase 95
6.5 UV-VIS spectra of the LB film of ODT-Cd^{2+} complex deposited from the subphase having different concentration of $CdCl_2$ onto quartz plates at different π_t. 96
6.6 Plot of energy gap (E_g) of the LB films of ODT-Cd^{2+} complex deposited from different concentration (10^{-x}M) of $CdCl_2$ in aqueous subphase 97
6.7 UV-VIS spectra of the chloroform deposited LB film of ODT transferred from the subphase having 10^{-5} M concentration of $CdCl_2$. 97
6.8 XRD profile of CdS nanoparticles formed at π_t of 30 mN/m. The concentration of Cd^{2+} ion in the subphase was 10^{-4} M. 98

6.9 FESEM image of the LB film of ODT-Cd^{2+} complex deposited at π_t of 30 mN/m from the aqueous subphase of 10^{-4} M concentration of $CdCl_2$. The scale bar in (a) is 100 nm in length. The scale bar in (b), (c) and (d) is 2 μm in length. 99
6.10 AFM images of the LB film of ODT-Cd^{2+} complex deposited at π_t of 30 mN/m from the aqueous subphase of 10^{-4} M concentration of $CdCl_2$. The scan area of the figure (A) 5×5 μm^2 and (B) 0.5×0.5 μm^2. 100
6.11 Zeta potential results of the ethanol dispersed LB film of ODT-Cd^{2+} complex deposited at π_t of 30 mN/m from the aqueous subphase of 10^{-4} M concentration of $CdCl_2$. 100
6.12 (a) The surface pressure (π) - area per molecule (A_m) isotherms of mixed monolayer system of 8CB with different mole percent of ODT at the ultrapure ion-free water subphase. (b) The surface pressure (π) - area per molecule (A_m) isotherms of mixed monolayer system of 8CB with different mole percent of ODT on the aqueous subphase containing 10^{-4} M concentration of $CdCl_2$. 101
6.13 (a) The AFM image of LB film of 8CB with 10 mole percent of ODT deposited at π_t of 2 mN/m from the ultrapure ion-free water subphase. (b) The AFM image of LB film of 8CB with 10 mole percent of ODT deposited at the π_t of 2 mN/m from the aqueous subphase containing 10^{-4} M concentration of $CdCl_2$. The scale bar is 0.5 μm in length. 102
6.14 Schematic diagram showing LC-cell fabricated using LB film as an alignment layer. 103
6.15 The polarizing microscopy textures of the LC-cell fabricated using LB films. The LB film of 8CB with 10 mole percent of ODT was deposited at π_t of 2 mN/m from the ultrapure ion-free water subphase. The intensity does not change in sequence from (a) to (b) on rotation of the LC-cell mounted on the microscope stage between crossed polarizers. 103
6.16 The polarizing microscopy textures of the LC-cell fabricated using LB films. The LB film of 8CB with 10 mole percent of ODT was deposited at π_t of 2 mN/m from the aqueous subphase containing 10^{-4} M concentration of $CdCl_2$. The change in intensity from maximum to zero can be obtained in sequence from (a) to (d) on rotation of the LC-cell mounted on the microscope stage between crossed polarizers. 104

7.1 Chemical structure of H shaped LC (HLC) molecule. 109
7.2 Surface pressure (π) - area per molecule (A_m) isotherm of HLC molecule at air-water (A-W) interface under different illumination - bright and UV light and under dark condition. Different regions of the isotherms are labelled from A to K. 111
7.3 Chemical structure of H shaped LC (HLC) molecule indicating the 1) backbone, 2) photoactive area and the 3) hydrophilic part. 113
7.4 In-plane elastic modulus (E) - A_m of the HLC molecule under different illumination - bright and UV light and under dark condition. 114

7.5 Isocycles obtained during repeated compression and expansion of the HLC monolayer at A-W interface under bright light. With respect to the first isocycle, the second and third cycles have been shifted by 0.3 and 0.6 nm^2 respectively on x-axis for visual clarity. . 114
7.6 BAM images of LM of HLC molecule under bright light at A-W interface. The size of the image is 6.4 x 4.8 mm^2. 115
7.7 FESEM image of HLC molecule under different illumination - (a) Bright light (b) UV light (c) Dark condition at π_t of 1 mN/m. The scale bar is 100 μm in length. 116
7.8 FESEM image of HLC molecule under different illumination - (a) Bright light (b) UV light (c) Dark condition at π_t of 20 mN/m. The scale bar is 20 μm in length for images A and C. The scale bar is 30 μm in length for the image B. 117
7.9 AFM images of single LB film of HLC molecule under different illumination - (a) UV light (b) Bright light (c) Dark condition at π_t of 1 mN/m. The scale bar is 0.5 μm in length for images A and C. The scale bar is 0.25 μm in length for image B. 119
7.10 AFM images of single LB film of HLC molecule under different illumination - (a) UV light (b) Bright light (c) Dark condition at π_t of 20 mN/m. The scale bar is 0.5 μm in length. 120

8.1 Discotic liquid crystal (DLC) molecule possessing tricycloquinazoline (TCQ) core and six ethelenoxy side chains (AmTCQ). 126
8.2 The possible molecular conformation of AmTCQ molecules at the A-W interface in a) L_1 and b) L_{12} phases. 126
8.3 Triangular domain of AmTCQ molecule. 127
8.4 Percentage area coverage (c) of triangular domains in the LB films of AmTCQ deposited at different target surface pressure (π_t). The dark circles are the experimental data points. The solid line is a fit polynomial curve: $c = 0.4 - 0.32\pi_t + 0.12\pi_t^2$. 128
8.5 The possible molecular conformation of TCQCB molecules at the A-W interface in a) L_1 and b) L_2 phases. In L_1 phase, the molecules may prefer edge on conformation with a tilt. In L_2 phase, the molecules exhibit edge-on conformation in a highly dense surface layer where the side chains of the molecules are shown interdigitated with the side chains of the neighbouring molecules 128
8.6 Graphical abstract of Chapter 4 129
8.7 Variation of a) energy gap b) size of clusters of TiO_2 nanoparticles of the LB films deposited at π_t of 2 mN/m and 20 mN/m and 5 and 20 wt.% of TiO_2 in HAT5. 130
8.8 The AFM images of LB film of HAT5+ 20 wt.% of TiO_2 nanoparticles. The films were deposited in the L_2 phase at π_t of 20 mN/m. The scale bar is 0.2 μm in length. 130
8.9 FESEM image of the LB film of ODT-Cd^{2+} complex deposited at π_t of 30 mN/m from the aqueous subphase of 10^{-4} M concentration of $CdCl_2$. The scale bar is 2 μm in length. 131

8.10 The polarizing microscopy textures of the LC-cell fabricated using LB films. The LB film of 8CB with 10 mole percent of ODT was deposited at the π_t of 2 mN/m from the aqueous subphase containing 10^{-4} M concentration of $CdCl_2$. The change in intensity from maximum to zero can be obtained in sequence from (a) to (d) on rotation of the LC-cell mounted on the microscope stage between crossed polarizers. 132
8.11 Chemical structure of H shaped LC (HLC) molecule. 133
8.12 FESEM image of HLC molecule indicating flower like patterns under dark condition at π_t of 20 mN/m. The scale bar is 20 μm in length. 133

Abbreviations

MEMS	Microelectromechanical systems
CVD	Chemical vapour deposition
PVD	Physical vapour deposition
LB	Langmuir Blodgett
SA	Self assembly
HPB	Hydrophobic
HPL	Hydrophilic
LM	Langmuir monolayer
A-W	Air-water
A-S	Air-solid
LC	Liquid crystal
LCs	Liquid crystals
TiO_2	Titanium dioxide
DLCs	Discotic liquid crystals
DLC	Discotic liquid crystal
AFM	Atomic force microscopy
BAM	Brewster angle microscopy
FTIR	Fourier transform infrared spectroscopy
SEM	Scanning electron microscopy
SPM	Scanning probe microscopy
FE	Field emission
FESEM	Field emission scanning electron microscopy
UV-VIS	Ultraviolet-visible spectroscopy
SRI	Spreading resistance imaging
LaB_6	Lanthanum hexaboride

SA	Stearic acid
1D	1 dimensional
2D	2 dimensional
3D	3 dimensional
TCQ	Tricycloquinazoline
AmTCQ	Tricycloquinazoline with six ketone groups
TCQCB	Tricycloquinazoline with six cyano biphenyl groups
8CB	4-octyl-cyanobiphenyl
CNT	Carbon nanotube
CCD	Charge coupled device
HAT5	Hexa-alkoxytriphenylene
HPLC	High performance liquid chromatography
DNA	deoxyribonucleic acid
ESP	Equilibrium spreading pressure
HOPG	Highly ordered pyrolytic graphite
ITO	Indium tin oxide
DFT	Density functional theory
NSOM	Near-field scanning optical microscopy
$CHCl_3$	Chloroform
DMF	Dimethylformamide
DCM	Dichloromethane
CCl_4	Carbontetrachloride
THF	Tetrahydrofuran
IR	Infrared
H_2SO_4	Sulfuric acid
H_2O_2	Hydrogen peroxide
HMDS	Hexamethyldisilazane
$CdCl_2$	Cadmium chloride
CdS	Cadmium sulfide
QDs	Quantum dots
ODT	Octadecanethiol
XRD	X-Ray diffraction

-CN	Cyano group
HLC	H-Type liquid crystal dimer
UV	Ultraviolet
CFL	Compact fluorescent lamp

Symbols

A_m	Area per molecule
A_i	Lift-off area per molecule
A_o	Limiting area per molecule
π	Surface pressure
E	Elastic modolus
A_L	Area of monolayer from water
A_S	Area of the substrate covered with monolayer
T_R	Transfer ratio
$\tan(\theta_B)$	Brewster angle
n	refaractive index
n_1	Refractive index of the medium
n_2	Refractive index of the reflecting material
γ_0	Surface tension of water without monolayer
γ	Surface tension of water with monolayer
L_1	Liquid expanded phase or low density liquid phase
L_2	Liquid condensed phase or high density liquid phase
L_{1H}	Low density liquid phase of HLC molecules
L_{2H}	High density liquid phase of HLC molecules
L_{12}	Liquid like phase where face-on and edge-on configuration coexist
π_t	Target surface pressure
π_c	Collapse surface pressure
I_t	Tunneling current
Si	Silicon
O	Oxygen

C	Carbon
N	Nitrogen
H	Hydrogen
ν_a	Absorption wavenumber
ν_f	Emission wavenumber
F (k,n)	Lippert's polarity function
F_1 (k,n)	Bakshiev's polarity function
F_2 (k,n)	Kawski Chamma Viallet's polarity function
k	Dielectric constant
p_g	Ground state dipole moment
p_e	Excited state dipole moment
a	Onsager radius cavity
ϕ	Angular seperation
f	Oscillator strength
ϕ_1	Quantum yield of AmTCQ in various solvents
ϕ_2	Quantum yield of AmTCQ in DCM
μ	Transition dipole moment
ν_{max}	Maximum absorption wavenumber
ϵ_{max}	Molar absorbance at maximum absorption wavenumber
$\nu_{1/2}$	Maximum absorption wavenumber
Cd^{2+}	Cadmium ion
a.u.	Arbitrary unit

Chapter 1

Introduction

A thin film is a layer of material whose thickness ranges from a fraction of nanometer to several micrometers. The surface to volume ratio of a material when spread on to a substrate to form a thin film increases enormously. Therefore, the sensitivity and efficiency of thin film devices increase manifold. The physicochemical properties of the thin film may depend on the nature of molecular aggregation onto the substrate. The structures of the thin films on a surface can lead to the growth of bulk material, and hence the material properties can be controlled by manipulating the structures of the thin films [1]. The form of such structures depends on the molecule-substrate and intermolecular interactions. Thin films find application in microelectronics, optical devices, microelectromechanical systems (MEMS), photovoltaics and as an anti corrosion agent.

A single layer of molecules onto the substrate can be considered as ultrathin film. The possibility of molecules to orient in ultrathin films has been used for amazingly diverse purposes from semiconductor devices to manufacture of membranes for oxygen-enhancement, and for a simulation of the human tongue's taste ability [2–9]. Ultrathin films can be fabricated using different techniques e.g. chemical vapour deposition (CVD), plating, physical vapour deposition (PVD), dip coating, spin coating, self assembly and Langmuir Blodgett (LB). CVD generally uses a gas-phase precursor, often a halide or hydride of the element to be deposited. Plating relies on liquid precursors, often a solution of water with a salt of the metal to be deposited. PVD uses mechanical, electromechanical or thermodynamic means to produce a thin film of solid. Dip-coating methods are frequently employed to produce thin films of organic/inorganic materials from sol-gel precursors. Spin coating is a method to produce uniform thin organic films

over large areas. Self assembly is a spontaneous and reversible organization of molecular units into ordered structures by specific local interactions among the units. In LB technique, the monolayer of organic molecules in a particular phase at the air-water (A-W) interface is transferred layer by layer onto a solid substrate by vertically moving the substrate in and out of the aqueous subphase in a highly controlled manner. In this thesis, we report the formation of stable LM of various mesogenic materials and transfer them onto solid substrate by LB technique. The LM and LB films were characterized by different techniques.

1.1 Langmuir monolayer (LM) at air-water (A-W) interface

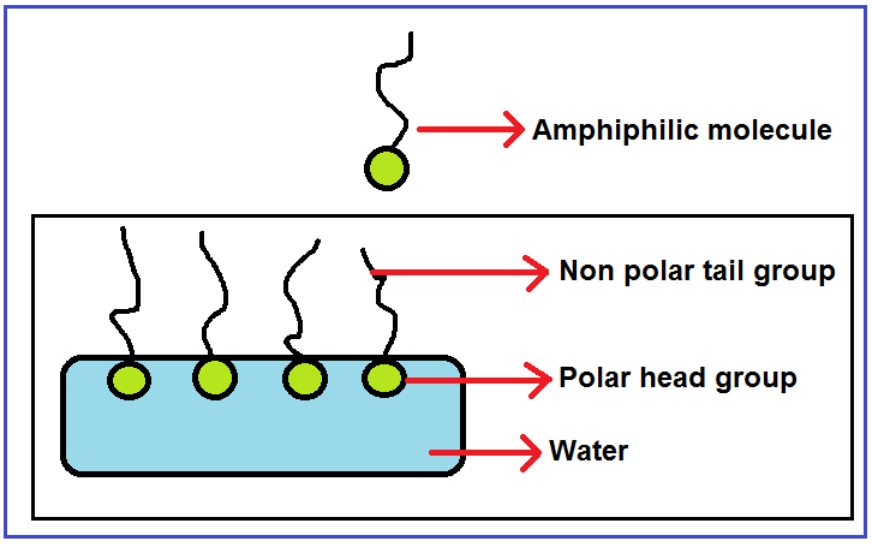

FIGURE 1.1: A schematic diagram of an amphiphilic molecule indicating polar head group and a non-polar tail group.

Amphiphilic molecules (Figure 1.1), which are usually organic in nature, possess polar 'head' and non-polar 'tail' groups. When spread at the A-W interface, the hydrophilic head group of the amphiphilic molecules gets anchored to the water surface whereas the hydrophobic part stays away from the water surface [10]. The stability of the monolayer at the A-W interface is determined by the strength of polarity of the head group and the hydrophobicity of tail group of the molecules. A balance between hydrophilicity and hydrophobicity of the amphiphilic molecule will yield a stable monolayer at the A-W interface. Such stable film at A-W interface can be termed as LM [11]. Table 1.1 shows the possible hydrophobic (HPB) and hydrophilic (HPL) groups of amphiphilic molecules.

TABLE 1.1: Some of the possible hydrophobic (HPB) and hydrophilic (HPL) groups of amphiphilic molecules

Hydrophobic (HPB) groups	**Hydrophilic (HPL) groups**
Hydrocarbon chains (e.g. methyl)	Hydroxyl ($-OH$)
Fluorocarbon chains	Sulphates ($-SO_4$)
Phenyl	Sulfhydry ($-SH$)
Polycyclic	Carbonyl ($C=O$)
	Amino ($-NH_2$)
	Carboxyl ($-COOH$)
	Phosphate ($-PO_4$)

LM is an ideal system to study the thermodynamics of two dimensional (2D) film where 2D plane is provided by smooth water surface. Surface manometry is a standard technique to study the thermodynamics and the surface phases in a LM. The presence of a monolayer at the A-W interface reduces the surface tension of water. Such reduction in the surface tension is defined as surface pressure (π). It is given by

$$\pi = \gamma_o - \gamma \tag{1.1}$$

where γ_o is the surface tension of pure water and γ is the surface tension of water with monolayer [11]. In surface manometry, surface density of the molecules adsorbed at the interface is varied and π is recorded simultaneously at a constant temperature. This yields a π - surface density isotherm. The area per molecule (A_m) is defined as the inverse of surface density.

A typical π – A_m isotherm is shown in Figure 1.2a. The isotherm shows discontinuities in the form of kinks and plateau at few values of A_m. The kink or plateau in the isotherm indicate phase transitions. Due to practical limitations, the weak phase transitions sometimes does not appear exclusively as a prominent kink or plateau in the isotherm. Such weak phase transition can be studied by calculating in-plane elastic modulus (E) from the isotherm. E is an appropriate quantity for distinguishing very weak phase transitions and elastic nature of the monolayer in a given phase. The isothermal in-plane E [12] is defined as

$$E = -A_m \times (\frac{d\pi}{dA_m}) \tag{1.2}$$

At very large A_m, the molecules do not interact with each other resulting in zero π. On compression of the monolayer, the isotherm indicates very small and finite values of π. The A_m at which such initial rise in π occurs is known as lift-off

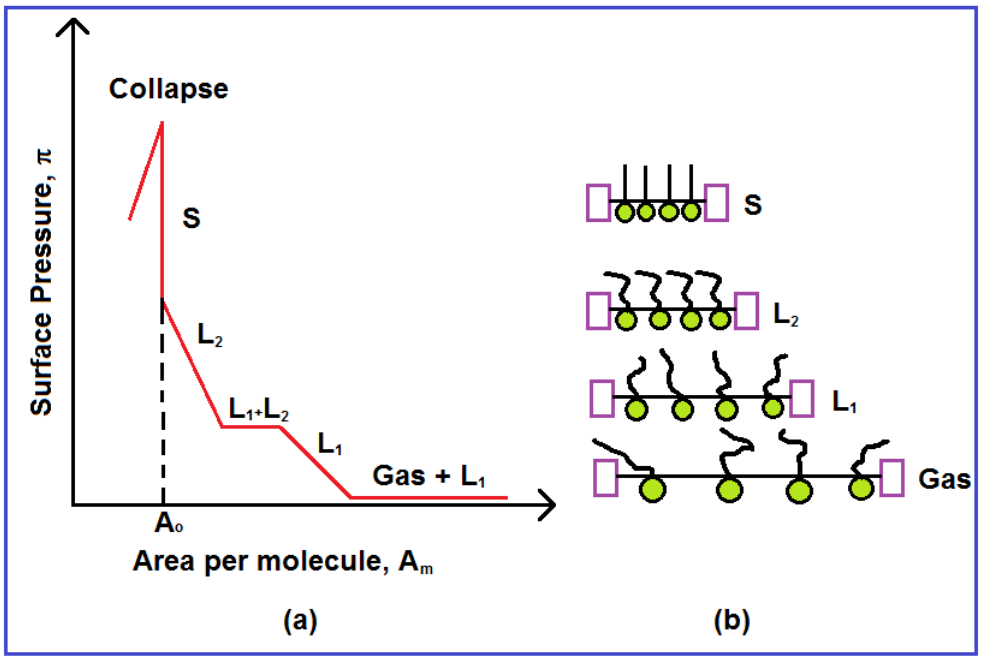

FIGURE 1.2: (a) shows a typical $\pi - A_m$ isotherm indicating the different phases in a LM. (b) shows the molecular arrangement in different phases. The symbols L_1, L_2 and S represent liquid expanded, liquid condensed and solid phases, respectively.

area per molecule (A_i). The average area occupied by the molecules in a phase is determined by extrapolating the corresponding region of the isotherm to the zero π on the A_m axis. The extrapolation of the steep region (S phase in Figure 1.2a) of the isotherm to zero π is called limiting area per molecule (A_0). This is the minimum area to which the molecules can be compressed on the water surface without collapsing the monolayer. The orientational state (tilt or untilt) of the molecules in a phase can be estimated qualitatively by comparing the extrapolated A_m with that of molecular cross-sectional area in the bulk single crystal.

At large A_m, the molecules do not interact with each other and exhibit neither orientational nor positional order. This is a gas phase (Figure 1.2b). The gas phase is identified experimentally by the zero π region of the isotherm at large A_m. On reduction of A_m, molecules interact and condense to yield a 2-dimensional (2D) liquid like phase or liquid expanded phase (L_1) (Figure 1.2b). The L_1 is a low density liquid phase where there is no positional order in the head groups and orientational order in the tail groups. The phase is identified experimentally by the onset of a slow or gradual rise in π in the isotherm. Typically, the in-plane E values between 12.5 and 50 mN/m corresponds to the L_1 phase [13]. On further reduction of A_m, a high density liquid phase (liquid condensed phase, L_2) is observed (Figure 1.2b). In the π - A_m isotherm, the condensed phase is identifed as a rapid increase in the value of π. The phase is less compressible and it shows

higher values of in-plane E as compared to that of L_1 phase. In L_2 phase, there may be a quasi long range orientational order in the tail group. On further reduction of A_m, 2D solid phase is obtained (Figure 1.2b). In this phase, the molecules usually orient normal to the interface exhibiting a long range positional and orientational order. The in-plane E of the phase is very high (e.g. 1000 mN/m for stearic acid (SA) monolayer). The monolayer collapses on further decrease in A_m. The collapsed state is generally indicated either by a sharp decrease in π value or a plateau in the isotherm [14]. In the collapsed state, the monolayer destabilizes and the molecules go to the third dimension. A plateau in the collapse state may indicate the formation of multilayer, whereas a sharp decrease may indicate a random crystallization into the 3 dimensional (3D) crystals. The nature of collapse varies from molecules to molecules. It also depends on the experimental conditions. The monolayer may fold or bend in the collapsed state [15]. The LM of fatty acid is known to exhibit 17 different phases. These phases are dependent on surface density, temperature and ion content of the aqueous subphase [16–19].

The equilibrium spreading pressure (ESP) is the value of π of a monolayer co-existing with its bulk phase at the interface. The monolayer of the molecule becomes metastable if the value of π becomes larger than the ESP of the molecules. The π above ESP leads to the formation of critical nuclei and the collapsed state becomes more probable [20]. The isocycles of LM can be obtained by repeated compression and expansion of the monolayer. Small hysteresis and retraceable isocycles indicate stable and reversible phases of the LM. The shift in the isocycle curves towards the lower or higher A_m indicate unstable LM. The instability may arise due to dissolution of the molecules or the formation of irreversible aggregates on the water surface.

The schematic of instrument for the measurement of π – A_m isotherm is shown in Figure 1.3. A LB trough (LB 2007DC, Apex Instruments) consists of a trough (1) and barriers (4). The material used for all parts of the trough that come into direct contact with the subphase should be chemically inert and able to withstand the organic solvents used for the monolayer spreading and cleaning. In order to improve experimental accuracy, the amphiphilic molecules should not get adsorbed on the barriers and the walls of the trough. Therefore, the trough should be made of material (e.g. Teflon) which is both oleophobhic and hydrophobic in nature. The LB trough is kept inside a glass box to avoid any thermal or air drift.

Proper cleaning of the trough before monolayer spreading is very essential. The usual approach is to first fill the trough with dilute sulphuric acid and leave it

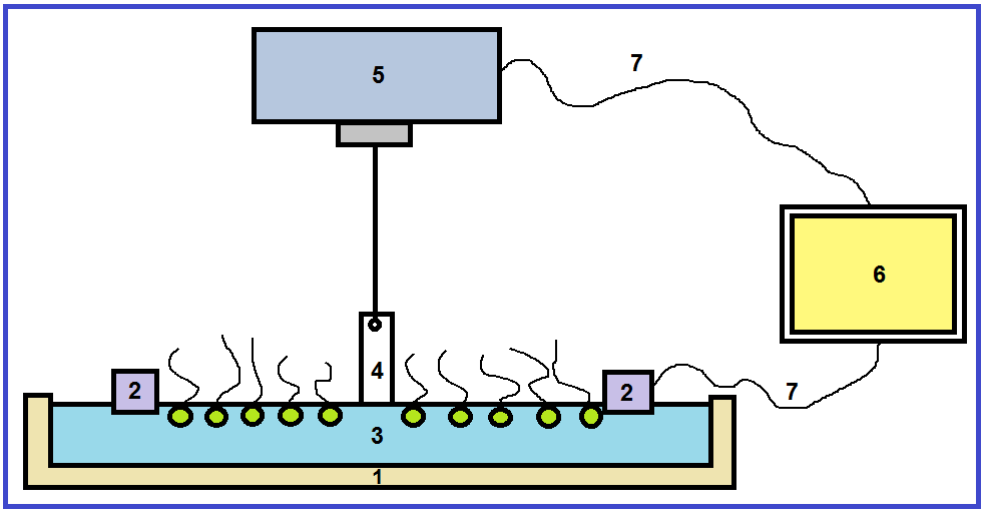

FIGURE 1.3: A schematic diagram showing the experimental setup for the measurement of π - A_m isotherms. The basic parts of the setup are as follows; (1) Teflon trough, (2) Teflon barriers, (3) subphase (ion-free water), (4) Wilhemy plate (filter paper), (5) π sensor, (6) computer, (7) connecting wires.

overnight. Then the dilute sulphuric acid is suctioned out through a pump and the trough is rinsed thoroughly with ultrapure ion free water followed by cleaning using organic solvents like alcohol and chloroform.

The subphase (2) used for the experiments is ultrapure ion free water. The ultrapure ion-free water (resistivity $\geq$18 MΩ-cm) is obtained by feeding reverse osmosis (RO) water into the Millipore Milli-Q (DQ5) filtering system. Monolayer forming materials are spread on to the subphase by first dissolving them into appropriate solvent to obtain a solution of known concentration. The solvent should be chemically inert and volatile so as to evaporate within a reasonable time period to leave no trace on the water surface. We have used mostly chloroform as the dispersing solvent for our research work. The solution of the samples is spread on the water subphase between the barriers using a precisely calibrated microsyringe (Hamilton). The solvent is allowed to evaporate by waiting for 15 minutes before starting the compression.

The surface density of the molecules in the monolayer is varied by changing the area available for the molecules by moving the two barriers laterally. The barriers are driven by motors which are controlled by a computer (6). They are coupled to each other so that it ensures a symmetric compression of the monolayer. The π is measured using a Wilhemy plate method [11, 21]. We use filter paper of appropriate size as the Wilhemy plate (4). The filter paper is suspended from the balance and made just to touch the surface of the water. The filter paper is allowed to soak water fully and the reading of the sensor (5) is made zero. A_m is changed

by symmetric compression of the barriers and π is measured simultaneously at a constant temperature using a computer. The LM at the A-W interface can be imaged by BAM and epifluorescence microscopy.

Brewster angle microscopy (BAM)

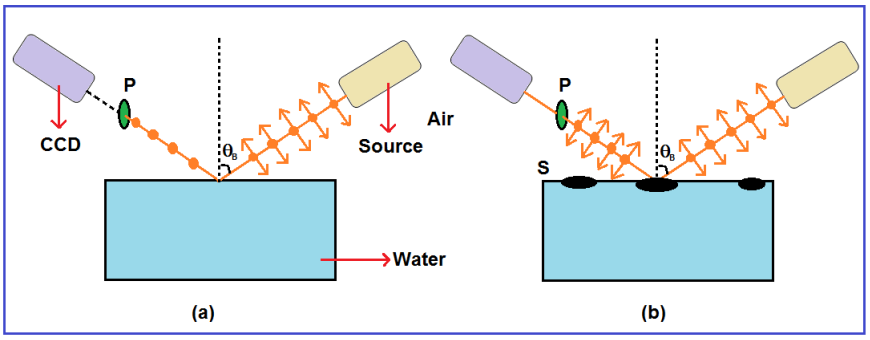

FIGURE 1.4: Schematic diagrams showing the working principle of a BAM. θ_B is the Brewster angle for water with respect to air. The different parts are as follows; polarizer (P), charge coupled device (CCD) camera and monolayer at the A-W interface (S). (a) and (b) are the BAM setups without and with monolayer at the A-W interface, respectively.

The angle of incidence at which an unpolarized light acquires a linearly polarized state after reflection from the plane of an interface is known as Brewster angle [22, 23] of the reflecting material. The state of polarization of the reflected light at the Brewster angle (θ_B) is perpendicular (s-polarized) to the plane of incidence. At Brewster angle of incidence

$$\tan(\theta_B) = \frac{n_2}{n_1} \tag{1.3}$$

where n_2 is the refractive index of the reflecting material and n_1 is the refractive index of the medium through which the light is incident. We have utilized a commercial setup, MiniBAM Plus from Nanofilm Technologie for imaging. In the microscope, a polarized light source from a 30 mW laser of wavelength 660 nm falls on the water surface at the Brewster angle of A-W interface (53°). The reflected light is allowed to pass through a polarizer which allows only the p-component of the reflected light to enter a CCD camera, as shown in Figure 1.4. Since the angle was set for the Brewster angle of A-W interface, the reflected intensity in the CCD camera was minimum for pure water. Any domain of the monolayer changes the refractive index at the interface and hence the Brewster angle for A-W interface gets altered. This in turn reflects some light which was collected by the CCD to form the images of the monolayer domains. The intensity of the reflected light depends on the thickness of the film and the surface density of the molecules. The

optical anisotropy in the BAM images arises due to a difference in tilt-azimuth variation of the molecules in the monolayer and the anisotropy in the unit cell [24]. The Brewster angle microscopy (BAM) imaging of a LM reveals dark region for the gas phase due to very low surface density of the molecules. The BAM image shows an uniform texture for liquid expanded phase and uniform bright texture for liquid condensed phase.

There is another kind of monolayer at the A-W interface known as Gibbs monolayer [11, 25]. In Gibbs monolayer, the molecules from the bulk solution adsorb spontaneously at the interface and establish a dynamical equilibrium between the molecules at the interface to the molecules in the solution. Here, the molecules are more hydrophilic and hence soluble in aqueous solution.

1.2 Thin films at air-solid(A-S) interface

1.2.1 LB technique

The monolayer in a particular phase at the A-W interface can be transferred layer by layer onto a solid substrate by vertically moving the substrate in and out of the aqueous subphase in a highly controlled manner. This technique is known as LB technique. LB technique exhibit numerous advantages over any other thin film deposition techniques. It provides precise control over the film thickness and intermolecular separation. A hybrid thin film of organic and inorganic materials can be fabricated by LB deposition technique. Such hybrid thin films can be potentially employed for numerous technological applications [26, 27].

In order to transfer LM at a given phase, the monolayer is held at a target surface pressure (π_t) and the solid substrate is immersed in and withdrawn from the subphase by vertical motion of the dipper at a defined rate (Figure 1.5) [28, 29]. Each stroke of the dipper may deposit a single layer of molecules onto the substrate. Various substrates like coverslip, quartz plate, silicon wafer, highly ordered pyrolytic graphite (HOPG), indium tin oxide (ITO) plates and mica are used for LB deposition. Prior to deposition, substrates like coverslips and silicon wafer are treated hydrophilically by boiling them in piranha solution (3:1, conc H_2SO_4:H_2O_2) for 1 minute, and then rinsed successively with ion-free water, absolute alcohol and acetone solvents. The substrates were then dried by blowing hot air at 70 °C. The substrates are treated hydrophobically by immersing the hydrophilically treated substrates in a solution (1:9, Hexamethyldisilazane

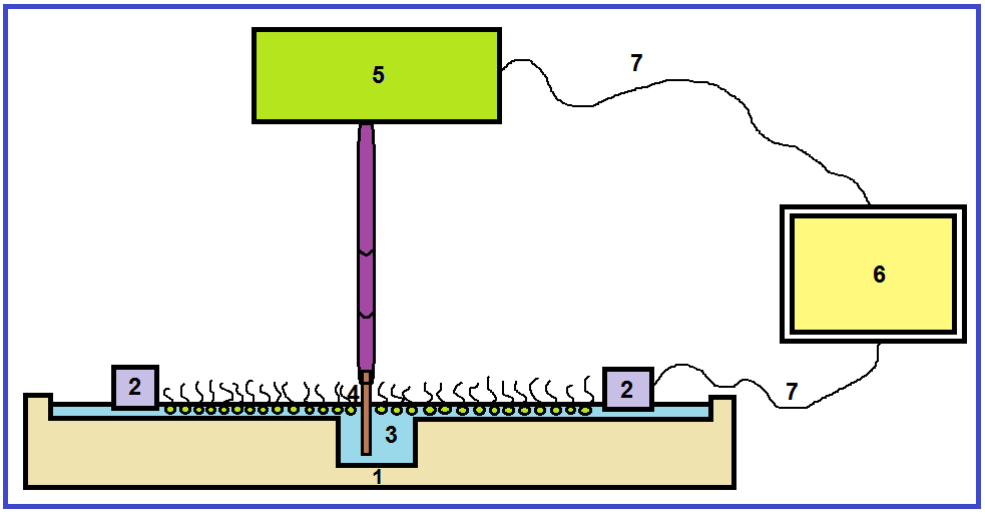

FIGURE 1.5: A schematic diagram showing the experimental setup for forming Langmuir-Blodgett films. The parts are as follows; (1) teflon trough with a well in the center, (2) barriers, (3) subphase, (4) substrate (5) dipper.

(HMDS) : Chloroform) for 12 hours. Depending on the nature of the substrate, molecules in LB films aggregate differently on the solid surface. When hydrophilic substrate is used, on the first upstroke of the dipper, the hydrophilic polar head group adheres to the substrate thereby yielding the hydrophobic surface (Scheme A in Figure 1.6). When hydrophobic substrate is used, on the first downstroke of the dipper, the hydrocarbon chain adhere to the substrate thereby yielding the hydrophilic surface (Scheme B in Figure 1.6). In case of multilayer deposition, if the monolayer deposits during both the upstroke and downstroke of the dipper, such deposition is known as Y-type of LB deposition. On the other hand, if the deposition takes place only with either downstrokes or upstrokes, they are termed as X or Z-type of LB deposition, respectively (Figure 1.6). The nature of LB deposition depends on various experimental conditions including ion-contents in the subphase, temperature, pH, humidity and molecule-substrate interaction.

The transfer efficiency of LB film can be quantified by measuring the transfer ratio (T_R) [30]

$$T_R = \frac{A_L}{A_S} \tag{1.4}$$

where A_L is the decrease in monolayer area from the water surface during the deposition and A_S is the area of the substrate to be covered by the monolayer. The T_R equal to one indicate defectless LB film whereas T_R equal to zero indicates

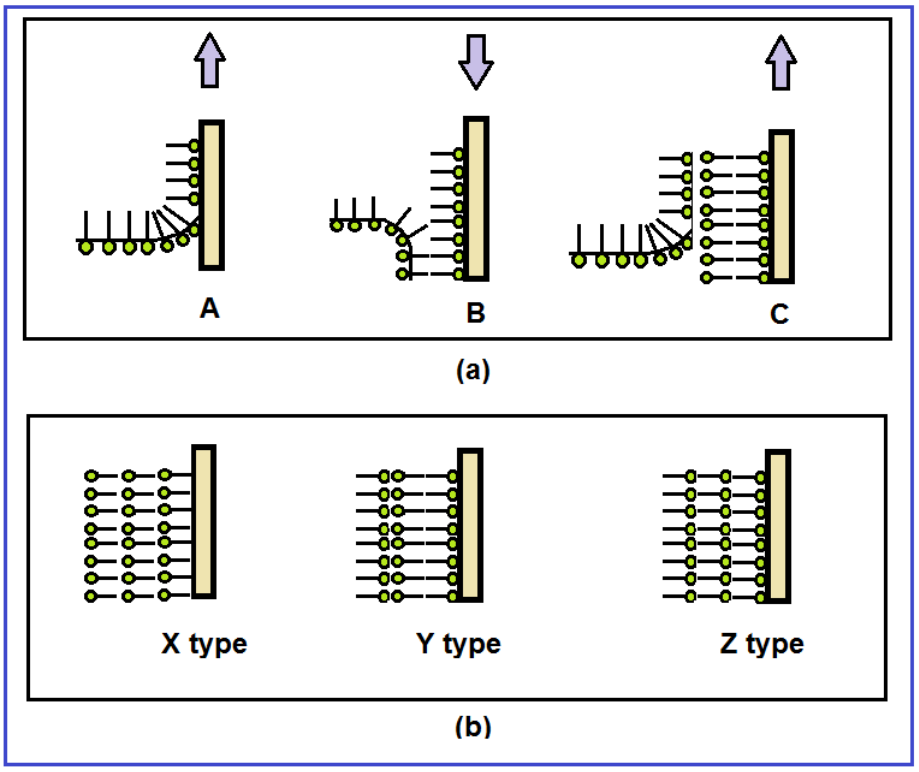

FIGURE 1.6: (a) The mechanism of formation of multilayer by the Langmuir-Blodgett technique. (A) first upstroke, (B) first downstroke and (C) second upstroke. (b) The structure of different types of multilayer obtained by LB technique, namely X-, Y- and Z-type.

no deposition. The negative value of T_R indicates desorption of the LB film from the substrate.

1.2.2 Horizontal transfer and Langmuir Schaefer's techniques

The monolayer at the A-W interface can be transferred onto substrates by two other different techniques. These are called horizontal transfer method and Schaefer's method. In the horizontal transfer method, a hydrophilic substrate is kept immersed horizontally in the subphase and then the monolayer is formed at the A-W interface. The monolayer is compressed to achieve a required target value of π. Then the aqueous subphase is siphoned out very slowly from the other side of the barriers. The monolayer gets adsorbed onto the substrate as the water drains out. In the Schaefer's method, a hydrophobic substrate is allowed to touch the monolayer on the water surface. The hydrophobic part of the molecules gets adsorbed to the substrate. To facilitate the drainage of water, the substrates in either cases can be tilted by a small angle prior to the adsorption. Spin coating method is also one of the widely used deposition technique to create thin films of

viscous materials like polymers, onto a substrate. However, there is no control of thickness of the film and the phases of the material.

1.2.3 Characterization techniques

LB film can be characterized by various techniques like atomic force microscopy (AFM), scanning electron microscopy (SEM), UV visible (UV-VIS) spectroscopy, Fourier transform infrared (FTIR) spectroscopy and X Ray diffraction (XRD) method [31–33].

Atomic force microscopy

The discovery of scanning probe microscopy (SPM) by Binning and coworkers has revolutionized the field of surface science [34]. Its versatile range of applications have made it an indispensable tool in the fields of surface science and other branches of soft condensed matter. It is useful in the study of the surface topography, electronic properties of the film, film growth, adhesion, friction, lubrication, dielectric and magnetic properties. It has also been used in molecular or atomic manipulation. Among the various SPM, AFM [35] is widely used to study LB films.

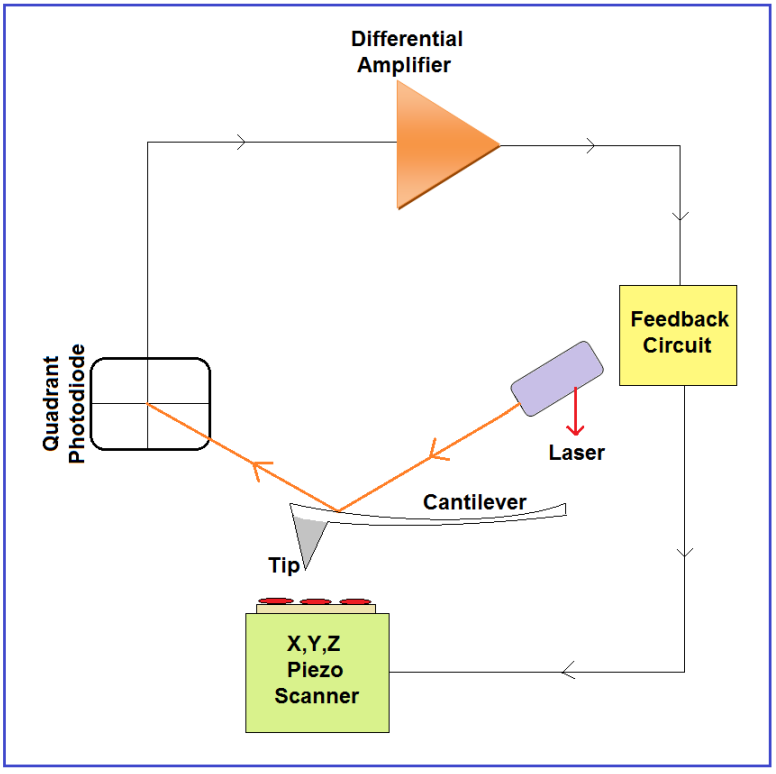

FIGURE 1.7: Schematic diagram of AFM.

AFM techniques yields the topographic images by sensing the atomic forces between a sharp tip and the sample. A schematic diagram of AFM is shown in Figure 1.7. Here, a sharp tip is grown on a cantilever. The head of the tip is coated with a reflecting material like gold and it is illuminated with a laser light. The reflected light is collected on a quadrant photodiode. Any deflection in the tip due to its interaction with the sample is monitored by measuring a distribution of light intensity in the photodiode. There are numerous modes of operation of AFM. We have utilized tapping, contact and spreading resistance imaging modes of AFM. In contact mode, the tip is brought into direct contact with sample and the surface is scanned. It is also known as constant force mode. Here, the force between the tip and the sample is kept constant and by monitoring the bending of the cantilever as a function of (x, y), a topographic image can be obtained. In tapping mode, the tip is allowed to oscillate nearly to its resonant frequency on the sample at a given amplitude and frequency. Due to interaction between the tip and the sample, the amplitude and phase of oscillation of the cantilever change. The change in amplitude can be used to obtain a topographic map of the sample. The phase change gives an insight about the chemical nature of the sample. The LB films are scanned in spreading resistance imaging (SRI) mode using diamond coated conducting tips (DCP11 series) having spring constants in the range of 5.5-10 N/m. In the SRI mode [36], the tip scans the sample while in contact with the surface maintaining a constant force between tip and sample. In our study, a constant force between the tip and sample was maintained at 12 nN. The bias voltage applied between tip and sample was 0.2 V. The SRI mode provides valuable information on the height map and tunneling current map of the film simultaneously.

In order to probe about the molecular structure and any chemical complexation of the species in the LB films, various spectroscopy techniques like UV-VIS, reflection absorption infrared spectroscopy (RAIRS) using FTIR spectrometer and fluorescence microscopy [37, 38] have been utilized. The molecular aggregation and complexation in LB film of liquid crystals (LCs) can be studied by these spectroscopic techniques.

Field emission scanning electron microscopy

Electron microscopes use a beam of highly energetic electrons to probe objects on a very fine length scale [39, 40]. In standard electron microscopes, electrons are mostly generated by "heating" a tungsten filament (electron gun). They are also produced by heating a crystal of lanthanum hexaboride (LaB_6). The use

of LaB_6 results in a higher electron density in the beam and a better resolution than that with the conventional device. In a field emission scanning electron microscope (FESEM), on the other hand, no heating but a so-called “cold" source is employed. Field emission is the emission of electrons from the surface of a conductor caused by a strong electric field. An extremely thin and sharp tungsten needle (tip diameter 10–100 nm) is employed as a cathode. The field emission (FE) source reasonably combines with scanning electron microscopes (SEMs) whose development has been supported by advances in secondary electron detection technology. The acceleration voltage between cathode and anode is commonly $\sim$ 0.5 kV to 30 kV, and the apparatus requires an extreme vacuum (10^{-6} Pa) in the column of the microscope. Because the electron beam produced by the FE source is about 1000 times smaller than that in a standard microscope with a thermal electron gun, the image quality will be markedly improved; for example, resolution of the order of 2 nm at 1 keV and 1 nm at 15 keV can be obtained. FESEM is a very useful tool for high resolution surface imaging in the fields of nanomaterials science. We have used FESEM from ZEISS, Sigma for obtaining surface morphology of LB film.

1.3 Materials

There are numerous materials which can form stable LM and can be transferred to solid substrates by LB technique. Conventionally, amphiphilic molecules like long chain fatty acids [41–46], cholesterol and its derivatives [47–50] form LM at the A-W interface and have been widely studied. Thermotropic LCs of different shape anisotropy form stable LM at the A-W interface [51–59]. Other non-traditional materials like carbon nanotubes (CNT) [60–63], quantum dots (QDs) [64–66], nanoparticles [67–70], graphene [71–73], lipids [74–76] and proteins [77–79] form LM and can be transferred to various solid substrates by LB technique for basic science research and applications.

1.3.1 Liquid crystals (LC)

LCs are states of condensed matter whose symmetries lie between those of 3D ordered crystals and completely disordered isotropic liquid. LCs exhibit anisotropies in physical properties such as refractive indices, dielectric constants and diamagnetic susceptibilities like crystals and flow like liquids. The thin films of

LC exhibit interesting properties. The formation of nanostructure in the thin film is governed by molecular interaction and external parameters like temperature, surface density, etc. The surface can be patterned and the nanostructures can be controlled by an appropriate choice of LC molecules. LC molecules with different shape anisotropy are reported in literature [51–59]. Such molecules exhibit numerous mesophases. LCs can be classified into thermotropic and lyotropic LCs. The phases of thermotropic LCs depend on temperature whereas that of lyotropic LCs depend on temperature, concentration, pH and ion contents.

1.3.1.1 Thermotropic LCs

LCs which exhibit mesophases as a function of temperature are known as thermotropic LCs.

The three fundamental and commonly observed mesophases of thermotropic LC are:

1. Nematic
2. Cholesteric
3. Smectic

In the nematic phase, the molecules have a long range orientational order but no translation order. On an average the long axis of the molecules are oriented along a particular direction called the director. The cholesteric phase is exhibited by optically active or chiral molecules. In this phase, the director is no longer constant in space but precesses in a helical fashion along a defined axis. In the smectic phases along with the orientational order, the molecules exhibit 1 dimensional (1D) translational order. This gives rise to a layered structure. In the layer plane, the arrangement of molecules is liquid like.

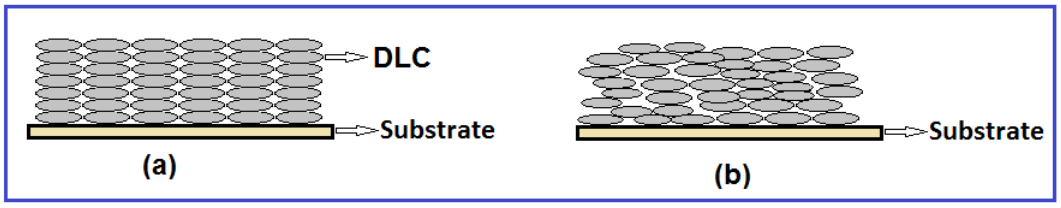

FIGURE 1.8: Schematic diagram of DLC in (a) columnar and (b) nematic phase .

LCs can be further classified based on the shape anisotropy as:

1. Discotic LCs (DLCs) made up of disc-like molecules,
2. Calamatic LCs made up of rod-like molecules,

3. Banana LCs made up of bent-core molecules.
4. Non traditional shapes e.g. H-type, hockey stick-type etc.

Some of the LC molecules, possessing a polar and a non-polar part, also form LM. Such mesogens are called amphotropic molecules. Table 1.2 shows examples of thermotropic LCs exhibiting different shape anisotropy forming stable LM. The LM of rod shaped 4-n-octyl-4-cyanobiphenyl (8CB) has been studied and it has been found that at collapse surface pressure (π_c) molecules tend to align themselves in smectic multilayer [55]. Recent studies have established that many compounds composed of disc-shaped molecules exhibit stable liquid crystalline phase. They are referred to as DLCs. Structurally, most of them fall into two distinct categories, columnar and discotic-nematic (Figure 1.8). The columnar phase, in its simplest form, has long-range translational periodicity in two dimensions and liquid-like disorder in the third, whereas the nematic phase is an orientationally ordered arrangement of discs without any long-range translational order [80]. Thin films of DLCs find potential industrial application in the fields of opto-electronics and photovoltaic devices such as light emitting diodes [81, 82], field-effect transistors [83], solar cells [84] and sensors [85].

Table 1.2: Thermotropic LCs forming stable LM

Shapes of thermotropic LCs	**Reference**
Disk	[51, 52]
Rod	[53–55]
Banana (bent core)	[56, 57]
Unconventional (like H type)	[58, 59]

There are numerous studies on the LM of the DLCs at the A-W interface. Such systems are known to exhibit monolayer phases where the disk-plane of the molecules are either planar to the water surface (face-on conformation) or it is perpendicular to the water surface (edge-on conformation) [52, 86–90].

1.3.1.2 Lyotropic LCs

Mesophases exhibited by organic molecules can also be obtained by the change in concentration, temperature, pH and ion contents. Such systems are termed as lyotropic LCs. Certain amphiphilic molecules dissolved in solvents like water form supramolecular assemblies which in turn exhibit mesophases. The lyotropic LCs exhibit cubic, hexagonal, lamellar, reverse hexagonal and micellar phases. Table 1.3 shows examples of lyotropic LCs forming stable LM. Stearic acid (SA) has

been the most commonly studied molecule. Monolayer of SA has shown great stability. Deposition of SA molecule at a different values of π on substrates has shown interesting results [44–46]. In 1964, Zisman [91] has substituted fluorine atoms in place of the hydrogen atoms on surfactants and obtained exquisitely fine control on the hydrophobicity of the monomolecular fluorinated surface. It was the most hydrophobic surfaces ever produced. The studies on LM of glycerides has lead to many interesting results. The existence of liquid crystalline phases in monolayers of glycerides was inferred from measurements of their densities, which were lower than those of the 3D crystalline phases and similar to those in lyotropic smectics [92].

TABLE 1.3: Lyotropic LCs forming stable LM

Lyotropic LCs	**Reference**
Fatty acids	[41–46]
Cholesterol	[47–50]
Glycerol	[92]
Octadecanethiol (ODT)	[93]

1.3.1.3 Nanomaterials and nanostructures

TABLE 1.4: Nanomaterials forming stable LM

Nanomaterials	**Reference**
Metal nanoparticles	[67–69]
Titanium dioxide (TiO_2)	[70]
Quantum dots (QDs)	[64–66]
Carbon nanotube (CNT)	[60–63]

Synthesis and processing of nanomaterials and nanostructures are the essential aspect of nanotechnology. Studies on new physical properties and applications of nanomaterials and nanostructures are possible only when nanostructured materials are made available with desired size, morphology, microstructure and chemical composition. Clusters of metallic atoms can be functionalized chemically with organic ligands to furnish it with an amphiphilic nature. Such functionalized nanoparticles when spread on the water surface yield a stable LM and show a variety of surface phases. Table 1.4 shows examples of nanomaterials and nanostructures forming stable LM.

1.3.1.4 Biological systems

Amphiphilic molecules are ubiquitous in biological systems. The lipids (e.g. fatty acids, phospholipids, cholesterol and cholesteryl esters) are the basic constituents

Table 1.5: Biological systems forming stable LM

Biological systems	**Reference**
Lipids	[74–76]
Proteins	[77–79]
Deoxy-ribonucleic acid (DNA)	[94–96]
Biopolymers	[97, 98]

of the cell membrane and are amphiphilic in nature. There are extensive studies on the LM and LB films of lipid molecules. Some polymers (including biopolymers) are also known to assemble on water surface to form a LM. Table 1.5 shows examples of biological systems forming stable LM.

DLCs at A-W and A-S interfaces show interesting properties. However, there are only a few studies on the LM and LB films of DLCs. In general, the conventional DLC molecules exhibit face-on or edge-on conformation at the A-W interface. The orientation of DLC at A-W interface is dependent on external parameters like surface density, temperature and molecular interaction. It can exhibit edge on configuration or face on configuration at A-W interface. The orientation of disc shaped molecule at an interface will be controlled by manipulating the intermolecular interaction and molecular substrate interaction. There is a large scope to observe new phases in the LM and molecular nucleation and aggregation at the A-S interface due to alteration of molecular interaction. In this thesis we report that due to weaker pi - pi interaction between the tricycloquinazoline (TCQ) core of the discotic molecules, a new phase in the LM and interesting patterns in the LB films of the TCQ based molecules with 6 ethelenoxy side chains (AmTCQ) molecules was observed. We found a stable LM of AmTCQ molecule. We found that AmTCQ monolayer exhibits gas phase, a L_1 phase with face-on molecular configuration, and L_{12} phase exhibiting both the face-on and edge-on conformations of the molecules. We have fabricated LB films of such molecules at different π_t and studied the nucleation and aggregation of the molecules using AFM. We found stable triangular nanostructures in the LB films deposited at $\pi_t \geq 5\ mN/m$. The LB films of AmTCQ molecule showed uniformly distributed triangular domains. The number of such triangles increases following a power law as a function of π_t of LB deposition. We demonstrated that the π_t to be a controlling parameter for altering the number of triangular domains in the LB films of AmTCQ molecules [52]. We extended our study on surface behavior of TCQ based DLC by altering the side chains of the AmTCQ molecules by covalently linking rod shaped cyanobiphenyl to the central disk shaped TCQ core. The TCQ based molecules with 6 cyanobiphenyl side chains (TCQCB) monolayer

exhibits gas phase, low density liquid (L_1), and high density liquid (L_2) phases. The molecular orientation in L_1 and L_2 phases were found to be edge-on. We found that AmTCQ molecule is fluorescent in nature and therefore it can be utilized for various photonic devices. We have carried out a systematic photophysical studies of the AmTCQ molecules and demonstrated that it can be employed as a molecular probe for fluorescence imaging of another DLC system.

A hybrid system consists of organic DLCs and metal oxide nanoparticles may find application in the field of photovolatics for the fabrication of high performance and efficient devices. We have studied LM and LB films of discotic hexa-alkoxy triphenylene molecule (HAT5) and HAT5+TiO_2 nanocomposite. Our study indicates that the energy gap of the LB films of HAT5 + TiO_2 nanocomposites can be controlled by altering the wt% of TiO_2 nanoparticles in the HAT5 matrix.

We found that LM can be employed as a template for the synthesis of nanoparticles at the A-W interface. Such nanoparticles can be transfered to the effective area of a device by a highly controlled LB deposition technique. In this thesis, we have employed LM for the fabrication of CdS nanoparticles at the A-W interface. Such nanoparticles were embedded into the LB films of a rod shaped liquid crystal, octacynobiphenyl (8CB). Such LB films were used as alignment layer during the fabrication of LC cell. We demonstrated that with the LB films of 8CB+CdS nanoparticles as alignment layer, the bulk LC in the cell can align planar. The presence of CdS nanoparticles in the LB film of 8CB matrix enhances the planar orientation in the bulk LC. It will be interesting to study the surface behavior of unconventional LC. Such LCs in which conventional mesogenic units are pre-organized in a classical shape can produce unusual phase structures and can exhibit unique physical properties. We have studied the LM and LB films of photosensitive H-Shaped LC molecules (HLC). The LB films of such molecule showed different patterns in bright light, UV light and dark state.

Bibliography

[1] R. K. Gupta and V. Manjuladevi, Molecular Interactions at Interfaces, InTech, Croatia, 2012

[2] V. Saxena , B. D. Malhotra, Curr. Appl. Phys, 3, 293, 2003.

[3] C. S. Cho, I. K. Park, J. W. Nah, et al., Macromol Res, 11, 2, 2003.

[4] P. M. S. Ferreira, A. B. Timmons, M. C. Neves, et al., Thin Solid Films, 389, 272, 2003.

[5] F. Babudri, G. M. Farinola, S. Giancane, et al., Mat. Sci. Eng. C-Bio S, 22, 445, 2002.

[6] Y. Kim, N. Minami, W. Zhu , et al., Synthetic Met, 135, 747, 2003.

[7] W. J. Ward III, W. R. Browell, R. M. Salemme, J. Membrane Sci., 1, 99, 1976.

[8] R. M. Metzger, J Solid State Chem., 168, 696, 2002.

[9] A. Riul Jr., D. S. Dos Santos Jr., K. Wohnrath, R. Di Tommazo, A. C. P. LF. Carvalho, F. J. Fonseca, O. N. Oliveira Jr., D. M. Taylor and L. H. C. Mattoso, Langmuir, 18, 239, 2002.

[10] J. N. Israelachvili, "Intermolecular and Surface Forces: With Applications to Colloidal and Biological Systems", Academic Press, London, 1992.

[11] G. L. Gaines, "Insoluble Monolayers at Gas—Liquid Interfaces", Wiley, New York, 1966.

[12] R. Lipowsky and E. Sackmann, "Handbook of Biological Physics", Elsevier Science, Amsterdam, 1995, Chapter 4.

[13] Dervichian, J. Chem. Phys., 7, 932, 1939.

[14] J. C. Huie, Smart Mater Struct., 12, 264, 2003.

[15] H. E. Ries, Nat. (London) 281, 287, 1979.

[16] H. M. A. McConnell, Rev. phys. Chem., 42, 171, 1991.

[17] C. M. Knobler , and R. C. Desai, A. Rev. phys. Chem., 43, 207, 1992.

[18] H. Schwickert, G. Strobl, Kimmig, J. chem. Phys., 95, 2800, 1991.

[19] Vladimir M. Kaganer, Helmuth Mohwald and Pulak Dutta, Rev. Mod. Phys., 71, 779, 1999.

[20] C. Ybert, W. Lu, G. Moller, C. M. Knobbler, J. Phys. Chem. B, 106, 2004, 2002.

[21] A. W. Adamson, Physical Chemistry of Surfaces, Wiley-Interscience, New York, 1990.

[22] D. Honig and D. Mobius, J. Phys. Chem., 95, 4590, 1991.

[23] S. Henon and J. Meunier, Rev. Sci. Instrum., 62, 936, 1991.

[24] S. Riviere, S. Henon, J. Meunier, D. K. Schwartz, M. W. Tsao, and C. M. Knobler, J. Chem. Phys. 101, 10045, 1994.

[25] V. Melzer, D. Vollhardt, G. Brezesinski, and H. Mohwald, J. Phys. Chem. B 102, 591 1998.

[26] G. Roberts, Langmuir-Blodgett Films, Plenum, New York, 1990.

[27] K. B. Blodgett, J. Am. Chem. Soc., 57, 1007, 1935.

[28] K. Graf, H. Riegler, Coll. surf. A: Physico. Eng. Asp., 131, 215, 1998.

[29] K. Graf, H. Riegler, Langmuir, 16, 5187, 2000.

[30] A. El Abed, M. C. Faure, E. Pouzet and O.Abillon, Phys. Rev. E, 65, 051603, 2002.

[31] C. S. Cho, I. K. Park, J. W. Nah, et al., Macromol Res, 11, 2, 2003.

[32] P. M. S. Ferreira, A. B. Timmons, M. C. Neves, et al., Thin Solid Films, 389, 272, 2003.

[33] F. Babudri, G. M. Farinola, S. Giancane, et al., Mat. Sci. Eng. C-Bio S, 22, 445, 2002.

[34] G. Binnig, H. Rohrer, Ch. Gerber, and E. Weibel, Phys. Rev. Lett., 50, 120, 1983.

[35] Q. Huo, S. Russev, T. Hasegawa, J. Nishijo, J. Umemura, G. Puccetti, K. C. Russell, R. M. Leblanc, J. Am. Chem. Soc., 122, 2002.

[36] P. Eyben, M. Xu, N. Duhayon, T. Clarysse, S. Callewaert, W. Vandervorst, J. Vacuum Sci. Tech. B, 20, 471, 2002.

[37] Hyunjoon Song, Franklin Kim, Stephen Connor, Gabor A. Somorjai, and Peidong Yang, J. Phys. Chem. B, 109, 188, 2005.

[38] Daniel K. Schwartz and Charles M. Knobler, J. Phys. Chem., 97, 8849, 1993.

[39] Z. L. Wang, J. Phys. Chem. B, 104, 1153, 2000.

[40] J. Pawley, Scanning, 19, 324, 1997.

[41] Peng, J. B., G. T. Barnes and I. R. Gentle, Adv. Coll. Inter. Sci., 91, 163, 2001.

[42] Kawai, Takeshi, Junzo Umemura and Tohru Takenaka, Langmuir, 5, 1378, 1989.

[43] Veale, G., I. R. Girling, and I. R. Peterson, Thin Solid Films, 127, 293, 1985.

[44] Shen Ye, Hiroyuki Noda, Shigeaki Morita, Kohei Uosaki and Masatoshi Osawa, Langmuir, 19, 2238, 2003.

[45] Fumiko Kimura, Junzo Umemura and Tohru Takenaka, Langmuir, 2, 96, 1986.

[46] Shen Ye, Hiroyuki Noda, Takuma Nishida, Shigeaki Morita and Masatoshi Osawa, Langmuir, 20, 357, 2004.

[47] R. K. Gupta and K. A. Suresh, Euro. Phys. J. E, 14, 35, 2004.

[48] Matharu, Zimple, G. Sumana, Sunil K. Arya, S. P. Singh, Vinay Gupta and B. D. Malhotra, Langmuir, 23, 13188, 2007.

[49] Ohnuki, Hitoshi, Rikimaru Honjo, Hideaki Endo, Tatsuro Imakubo and Mitsuru Izumi, Thin Solid Films, 518, 596, 2009.

[50] Michinobu, Tsuyoshi, Satoshi Shinoda, Takashi Nakanishi, Jonathan P. Hill, Kazuko Fujii, Tomoko N. Player, Hiroshi Tsukube and Katsuhiko Ariga, J. Ame. Chem. Soc., 128, 14478, 2006.

[51] M. F. Danier, O. C. Lettington, S. M. Small, Thin Solid Films, 99, 61, 1983.

[52] Raj Kumar Gupta, Manjuladevi V., C. Karthik, Sandeep Kumar, J. Phys.: conference series, 417, 012068, 2013.

[53] Y. Tabe, N. Shen, E. Mazur, and H. Yokoyama, Phys. Rev. Lett. 82, 759 (1999).

[54] F. Rondelez, D. Koppel, and B. K. Sadashiva, J. Phys. (Paris), 43, 1361, 1982.

[55] A. Bhattacharyya and K. A. Suresh, Europhys. Lett., 41, 641, 1998.

[56] J. Wabang, L. Zou, A. Jakli, W. Weissflog and E. K. Mann, Langmuir, 22, 3198, 2006.

[57] P. Garcia-Vazquez, O. G. Morales-Saavedra, G. Pelzl, J. Guadalupe Bañuelos and M. P. Carreón-Castro., Thin Solid Films, 517, 1770, 2009.

[58] C. Karthik, A. Gupta, A Joshi, V. Manjuladevi, R. K. Gupta, Mahesh Varia, AIP Conference Proceedings, 1591, 1036, 2014.

[59] B. Kumar, A. K. Prajapati, M. C. Varia and K. A. Suresh, Langmuir, 25, 839, 2008.

[60] M. Poonia, R. K. Gupta, Manjuladevi, V., S. K. Gupta and J. Akhtar, J. Nanopart. Res., 16, 1, 2014.

[61] Guo, Yinzhong, Nobutsugu Minami, Said Kazaoui, Junbiao Peng, Masaru Yoshida and Tokuji Miyashita, Physica B: Cond. Matt., 323, 235, 2002.

[62] Krstic, Vojislav, Georg S. Duesberg, Jorg Muster, Marko Burghard and Siegmar Roth, Chem. Mat., 10, 2338, 1998.

[63] Kim, Yeji, Nobutsugu Minami, Weihong Zhu, Said Kazaoui, Reiko Azumi and Mutsuyoshi Matsumoto. Jap. J. App. Phys., 42, 7629, 2003.

[64] Achermann, Marc, Melissa A. Petruska, Scott A. Crooker and Victor I. Klimov, J. Phys. Chem. B, 107, 13782, 2003.

[65] Dabbousi, B. O., C. B. Murray, M. F. Rubner and M. G. Bawendi, Chem. Mat., 6, 216, 1994.

[66] Milekhin, A., M. Friedrich, D. R. T. Zahn, L. Sveshnikova and S. Repinsky, App. Phys. A, 69, 97, 1999.

[67] R. K. Gupta, K. A. Suresh and S. Kumar, Phys. Rev. E, 78, 032601, 2008.

[68] Lu, Yu, Gang L. Liu and Luke P. Lee, Nano lett., 5, 5, 2005.

[69] Paul, Shashi, C. Pearson, A. Molloy, M. A. Cousins, M. Green, S. Kolliopoulou, P. Dimitrakis, P. Normand, D. Tsoukalas and M. C. Petty, Nano Lett., 3, 533, 2003.

[70] K. Choudhary, V. Manjuladevi, R. K. Gupta, P. Bhattacharyya, A. Hazra and S. Kumar, Langmuir, 2015.

[71] Li, Xiaolin, Guangyu Zhang, Xuedong Bai, Xiaoming Sun, Xinran Wang, Enge Wang and Hongjie Dai, Nat. Nanotech., 3, 538, 2008.

[72] Zheng, Qingbin, Wai Hing Ip, Xiuyi Lin, Nariman Yousefi, Kan Kan Yeung, Zhigang Li and Jang-Kyo Kim, ACS nano, 5, 6039, 2011.

[73] Kim, Jaemyung, Laura J. Cote, Franklin Kim, Wa Yuan, Kenneth R. Shull and Jiaxing Huang, J. Ame. Chem. Soc., 132, 8180, 2010.

[74] K. S. Birdi, Lipid and Biopolymer Monolayers at Liquid Interfaces, Plenum, New York, 1989.

[75] Okahata, Yoshio, Tomoya Tsuruta, Kuniharu Ijiro and Katsuhiko Ariga Langmuir, 4, 1373, 1998.

[76] Birdi, K. S., and D. T. Vu., Langmuir, 10, 623, 1994.

[77] Fujiwara, Ichiro, Michihiro Ohnishi, and Junetsu Seto, Langmuir, 8, 2219, 1992.

[78] Yasuda, Yoshiaki, Hiroaki Sugino, Hideki Toyotama, Yoshiki Hirata, Masayuki Hara and Jun Miyake, Bioelectrochem. bioenerg., 34, 135, 1994.

[79] Oh, Byung-Keun, Bum Suk Chun, Kwang-Won Park, Woochang Lee, Won Hong Lee and Jeong-Woo Choi, Mat. Sci. Eng. C, 24, 65, 2004.

[80] S. Chandrasekhar and G. S. Ranganath, Rep. Prog. Phys., 53, 57, 1990.

[81] G. Lussem and J. H. Wendroff, Polym. Adv. Technol., 9, 443, 1998.

[82] I. Seguy, P. Jolinat, P. Destruel, J. Farenc, R. Mamy, H. Bock, J. Ip and T. P. Nguyen, J. Appl. Phys., 89, 5442, 2001.

[83] N. Stutzmann, R. H. Friend and H. Sirringhaus, Sci., 299, 1881, 2003.

[84] L. Schmidt-Mende, A. Fechtenkotter, K. Mullen, E. Moons, R. H. Friend, and J. D. MacKenzie, Sci., 293, 1119, 2001.

[85] N. Boden, R. J. Bushby, J. Clements and B. Movaghar, J. Mater. Chem., 9, 81, 1999.

[86] A. Albrecht, W. Cumming, W. Kreuder, A. Laschewsky, and H. Ringsdorf, Col. Polym. Sci., 264, 659, 1986.

[87] N. C. Maliszewskyj, P. A. Heiney, J. K. Blasie, J. P. McCauley Jr. and A. B. Smith III, J. Phys. II (France), 2, 75, 1992.

[88] D. Gidalevitz, O. Y. Mindyuk, P. A. Heiney, B. M. Ocko, P. Henderson, H. Ringsdorf, N. Boden, R. J.Bushby, P. S. Martin, J. Strzalka, J. P. McCauley Jr. and A. B. Smith III, J. Phys. Chem. B, 101, 10870, 1997.

[89] N. C. Maliszewskyj, P. A. Heiney, J. Y. Josefowicz, J. P. McCauley Jr. and A. B. Smith III, Sci., 77, 264, 1994.

[90] A. Nayak, K. A. Suresh, S. K. Pal, and S. Kumar, J. Phys. Chem. B, 11, 11157, 2007.
F

[91] W. A. Zisman, Adv. Chem. Ser., 43, 1964.

[92] D. R. Merker and B. F. Daubert, J. Phys. Chem., 68, 2064, 1964.

[93] R. K. Gupta, et al., 568, 109, 2006.

[94] G. B. Sukhorukov, M. M. Montrel, A. I.Petrov, L. I. Shabarchina and B. I. Sukhorukov, 11, 913, 1996.

[95] Dai, Shuxi, Xingtang Zhang, Zuliang Du and Hongxin Dang, Mat. Lett., 59, 423, 2005.

[96] Okahata, Yoshio, Takuya Kobayashi and Kentaro Tanaka, Langmuir, 12, 1326, 1996.

[97] J. Kim and T. M. Swager, Nat. (London), 411, 1030, 2001.

[98] F. Monroy, H. M. Hilles, F. Ortega and R. G. Rubio, Phys. Rev. Lett., 91, 268302, 2003.

Chapter 2

Ultrathin films of Tricycloquinazoline (TCQ) based discotic liquid crystal molecules at different interfaces

2.1 Introduction

The study on molecular organization and structure formation at the nanometer length scale is important due to its application in the field of nanoscience and nanotechnology. The properties of materials can be maneuvered precisely by manipulating the nanostructures. Over the past few years, the supramolecular assembly leading to interesting nanostructures has drawn considerable amount of scientific attention because of its potential industrial applications [1]. The recent development in this area is due to technological advancement in the field of nanoscience. In bottom-up building mechanism of nanostructures, in addition to the molecular interaction, the molecular aggregation leading to supramolecular assemblies has been found to be dependent on external parameters such as temperature, pressure, external field and ion contents of the medium [2].

The surface can induce an ordering in the bulk, and hence the material properties can be varied by varying the structure of aggregates on the surface [3, 4]. The structure of the aggregates on a surface primarily depends on intermolecular and molecule–substrate interactions. Therefore it is relevant to study the surface

behaviour of the molecules which exhibit the possibilities of altering the phases due to the change in external parameter.

Over the past few years, the field of discotic liquid crystals (DLCs) has grown enormously because of the interesting electro-optical properties exhibited by the molecules [5]. Commonly, the DLC molecules are composed of a pi-conjugated central core with peripherally substituted flexible chains. It is generally believed that due to the strong pi - pi interaction of the cores, DLC assemble to yield various columnar mesophases [6]. The charge mobility along the length of the column has been found to be enormously high when compared to its perpendicular direction. This makes such columnar system to act as a semiconducting material with a very high value of anisotropy in the conductivity [7, 8]. The DLCs find potential industrial application in the fields of opto-electronics and photovoltaic devices such as light emitting diodes [9, 10], field-effect transistors [11], solar cells [12] and sensors [13].

There are several studies on the Langmuir monolayer (LM) of the disk-shaped molecules at the air-water (A–W) interface [14–17]. Such systems are known to exhibit monolayer phases where the disk-plane of the molecules are either planar to the water surface (face-on conformation) or it is perpendicular to the water surface (edge-on conformation). The supramolecular channels of the DLCs can be used for thin film field effect transistors, photocondutors and photovoltaics [18–20].

The cores of commonly studied discotic molecules are rich in pi-electrons, and such molecules are known to behave as p-type semiconductor with appropriate doping [8]. The TCQ based molecules are deficient in pi-electrons and are reported to behave as n-doped semiconducting materials [21-23]. TCQ is a biologically active molecule and it is found that it can intercalate with double stranded deoxyribonucleic acid (DNA). The nature of aggregation of the molecules on the surface is important for the device applications. There are several reports on the nanostructures in the Langmuir Blodgett (LB) films which are formed under the influence of various external parameters such as temperature, pressure, external field and ion contents in the medium [24–28]. Vickery et al. [24] have conducted direct observation of structural evolution in palmitic acid monolayers following LB deposition at different target surface pressure (π_t). Gupta et al. [25] have carried out atomic force microscopy (AFM) studies on LB films of cholesterol on different substrates. Hui et al. [27] observed that the defects in dilinoleoyl-phosphatidyl-ethanolamine monolayers is dependent on the pH of the aqueous environment.

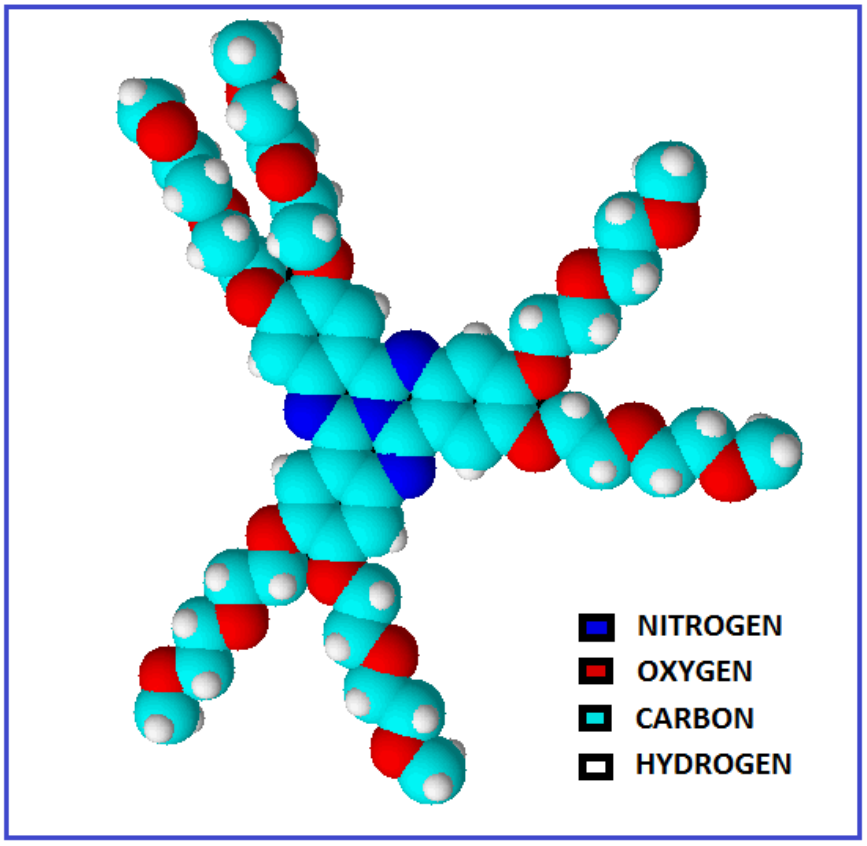

FIGURE 2.1: DLC molecule possessing TCQ core and six ethelenoxy side chains.

In this chapter, we discuss surface behavior of tricycloquinazoline based molecules with 6 ethelenoxy side chains (AmTCQ) by forming LM and LB films (Figure 2.1) at different interfaces. We find a stable monolayer of the molecules at the A–W interface. The monolayer exhibits gas, low density liquid (L_1), and high density liquid (L_{12}) phases. The conformation of the molecules in the L_1 phase was found to be face-on with interdigitated side chains whereas the molecules co-exist with the face-on and edge-on conformations in the L_{12} phase. The LB films of the AmTCQ molecules were deposited on solid substrates at different π_t and studied the nanostructures using the AFM technique. We have employed surface manometry, Brewster angle microscopy (BAM), AFM and infrared spectroscopy for our studies.

2.2 Experimental Methods

The AmTCQ molecule was synthesized by Prof. Sandeep Kumar of Raman Research Institute, Bengaluru [22]. The chemical structure of the molecule is shown in Figure 2.1. The molecule possesses six polar ethylenoxy side-chains

symmetrically attached to the TCQ core so that it retains its C3 fold symmetry. The diameter of the central TCQ core and the length of the ethylenoxy side-chain are approximately 1.0 nm each. It shows a hexagonal columnar phase in the temperature range of $77 - 233\,^{\circ}$C. The separation between the molecules in the column was found to be $\sim$ 0.35 nm [22, 29]. A solution of the sample was prepared in high performance liquid chromatography (HPLC) grade chloroform having a concentration of 9.7 x 10^{-5} M. The solution of the AmTCQ molecule appears yellowish-green. The yellowish-green color was observed even in the trough after the monolayer of the molecules was compressed completely to reach the collapse state. These observations indicate that molecule is fluorescent in nature and needs a systematic photophysical study. We have studied the photophysical properties of the molecules and presented in Chapter 4. The monolayer at A-W interface was formed by spreading the solution onto the ultrapure ion-free water. The surface pressure (π) - area per molecule (A_m) isotherms were obtained by compressing the monolayer symmetrically at the A-W interface in a Langmuir trough. The compression speed was maintained at 0.68 $(nm^2/molecule)/min$. The equilibrium spreading pressure (ESP) was determined by placing small crystallites of the molecules (3 mg) on the ion-free water in a teflon container (78.5 cm^2), and the π was recorded with time. The relaxation of the monolayer was studied by maintaining the monolayer at a given π, and monitoring the variation in the molecular area with time. The phases of the monolayer were observed using a BAM.

One layer of LB film was deposited on the silicon (Si(100)) substrates at different π_t by a single upstroke of the dipper. A LB film was deposited at zero π_t by holding the barriers at an A_m of 4.5 nm^2 and withdrawing the substrate slowly at the rate of 0.5 mm/min. The transfer ratio for this mechanism was zero as the deposition was done without the feedback and at a constant A_m of 4.5 nm^2. The molecules get deposited onto Si substrate due to substrate-molecular interaction. For the LB deposition at non-zero π_t, the π is maintained constant by a feedback mechanism during the deposition process. The change in the A_m during the deposition is recorded and the transfer ratio is calculated. We found the transfer ratio to be 1 ± 0.2 for depositions at non-zero π_t. The dipper speed was maintained at 5 mm/min during such depositions. The films were imaged by employing the AFM in semicontact mode. The piezo scanner of the AFM was calibrated using 1-D arrays of rectangular SiO_2 steps on a Si wafer (TGS1 series, NT-MDT). The spring constants and the resonance frequencies of the Si tips were in the ranges of 10-20 N/m and 180-270 KHz, respectively. The reported nanostructures in the

AFM images of the LB films were stable with respect to time. We scanned each of the LB films at an interval of about 24 hours and have observed the similar structures each time.

The monolayers were also transferred to freshly cleaved highly oriented pyrolytic graphite (HOPG) substrate at different π_t by Langmuir–Schaefer method [30]. A high resolution microscopy was done on the films deposited onto the HOPG substrate (ZYB, NT-MDT) by obtaining simultaneously topographic and tunneling current (I_t) images of the films in spreading resistance imaging (SRI) mode of an AFM.

The monolayers were also transferred onto gold deposited Si substrates by horizontal transfer technique and studied using reflection absorption infrared spectroscopy (RAIRS). The substrates were kept horizontally and immersed completely in the subphase prior to spreading of the molecules at the A–W interface in the trough. The monolayer was held at a π_t, and the water was siphoned out very slowly from the other side of the barriers. As the water level recedes, the monolayer at the given π_t gets adsorbed to the substrate. The reflection absorption IR spectra of such films on the gold deposited Si substrates were recorded using a FTIR spectrometer (Tensor 37, Bruker Optics). The experiments were carried out at the room temperature $\sim$22°C.

2.3 Results and discussion

The π - A_m isotherm of AmTCQ molecules is shown in Figure 2.2. The isotherm shows zero π at very large A_m. It shows a lift-off area per molecule (A_i) at around 3.5 nm^2. On decreasing the A_m, the π rises gradually and slowly. This was obtained corresponding to a region of the isotherm from a to b. at around 1.7 nm^2, the isotherm shows a large change in the slope. On further reduction in A_m, the π rises sharply. The steep rise in π corresponds to a region of the isotherm from b to c. The monolayer collapses at 1.0 nm^2 with a collapse surface pressure (π_c) of 24.3 mN/m. The extrapolation of the region of the isotherm between a and b to zero π yields an A_m value of around 3.3 nm^2 (=A_0^1). The extrapolation to the zero π of the steep region of the isotherm (i.e., b to c) yields a limiting area per molecule of around 1.6 nm^2 (=A_o).

The stability of a monolayer at A-W interface can be studied by maintaining the monolayer at a given π and monitoring the variation in molecular area with

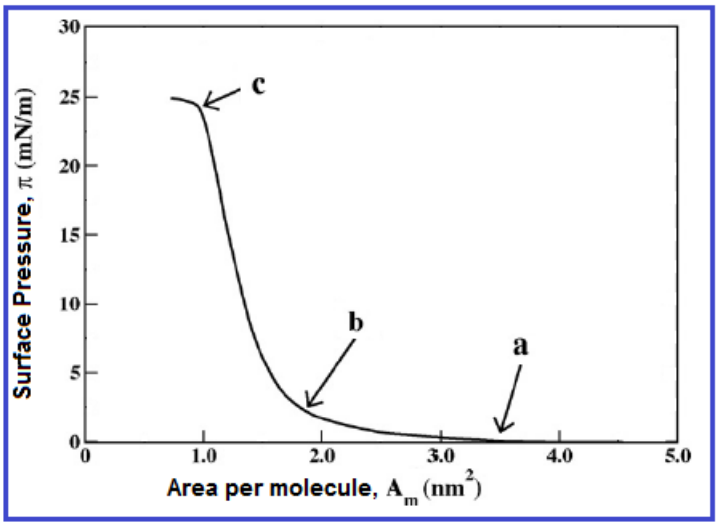

FIGURE 2.2: Surface pressure (π) - area per molecule (A_m) isotherm of the AmTCQ molecule. The arrows a, b and c are drawn to indicate the onset of low density liquid (L_1), high density liquid (L_{12}) phases and collapse during compression.

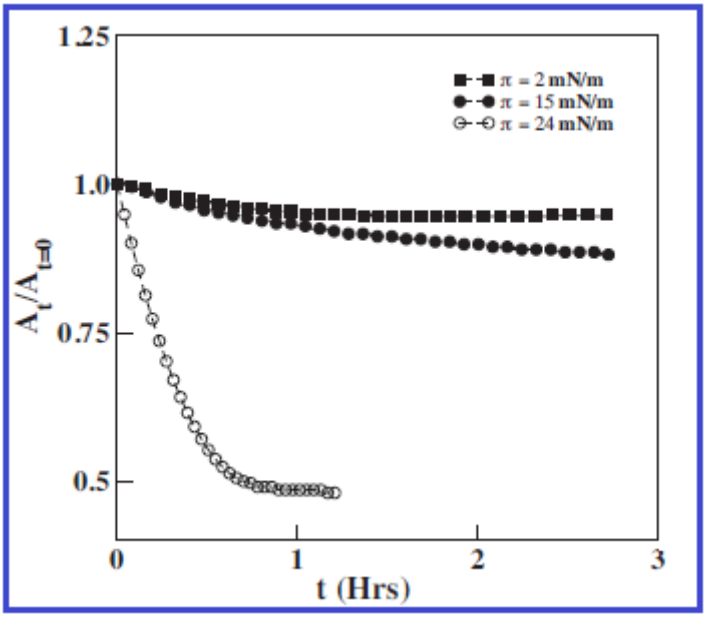

FIGURE 2.3: Variation of normalized area ($A_t/A_{t=0}$) with time (t) at different π. Here A_t is the A_m at a time t and $A_t = 0$ is the initial A_t.

time [31]. The variation of normalized area ($A_t/A_{t=0}$) of the AmTCQ monolayer at the A-W interface with time is shown in Figure 2.3. The variations indicate very small reduction in its values. Considering a linear dependence of the normalized area with time, we find rates of reduction of the area to be 0.05% and 0.09 % per minute at the π of 2 and 15 mN/m, respectively. The small reduction in area can be accounted for by the relaxation of the molecules in the monolayer. This suggests a stable monolayer of the AmTCQ molecule at the A-W interface. The decrease in normalized area at the π value of 24 mN/m is very rapid. This is due to the fact that at this π, the monolayer destabilizes and collapses. The ESP of a material is the π of its monolayer phase coexisting in equilibrium with its bulk phase [32]. It indicates qualitatively the spreading capability of the molecules at an interface, and the loss due to dissolution of the molecules into the subphase and its evaporation.

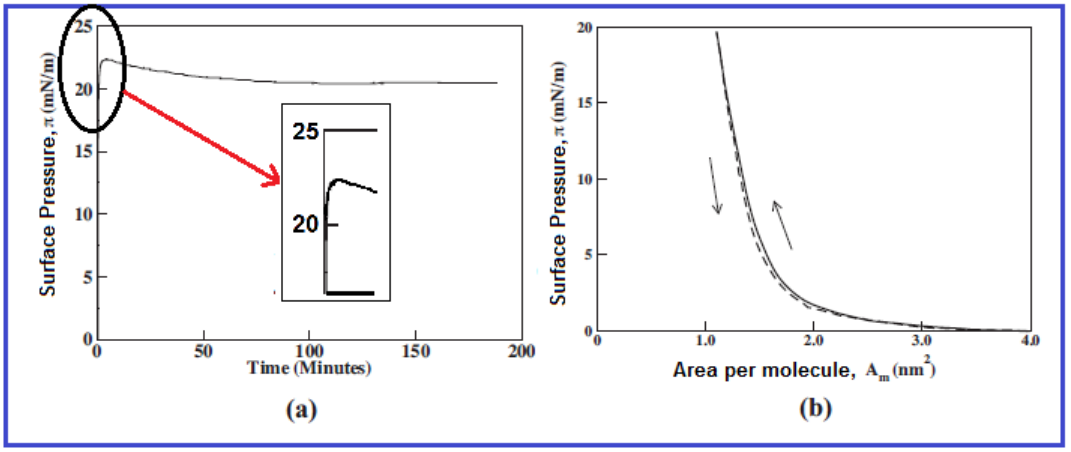

FIGURE 2.4: (a) Variation of π with time during the determination of the equilibrium spreading pressure (ESP) of AmTCQ molecules. (b) Isocycle by compression and expansion of the monolayer.

The result of the ESP measurement for AmTCQ molecules at the A-W interface is shown in Figure 2.4a. The π rises to a high value within a second. At a longer time, it showed a saturated value of π of 20.5 mN/m. This is the ESP value of the AmTCQ molecule. The kinetics during the ESP measurement suggests a very high degree of spreading capability of the molecule at the A-W interface. The saturated value of surface pressure for a longer duration may indicate a better stability of AmTCQ monolayer. A monolayer of amphiphilic molecules compressed to the π greater than its ESP is more prone to instability and tends to approach towards collapse [31]. The monolayer is subjected to isocycles (Figure 2.4b) by compressing and expanding it repeatedly. The isocycles showed negligible hysteresis, and the expansion curve approximately followed the compression curve. These surface

manometry results suggest that the LM of the AmTCQ molecules is stable at the A-W interface.

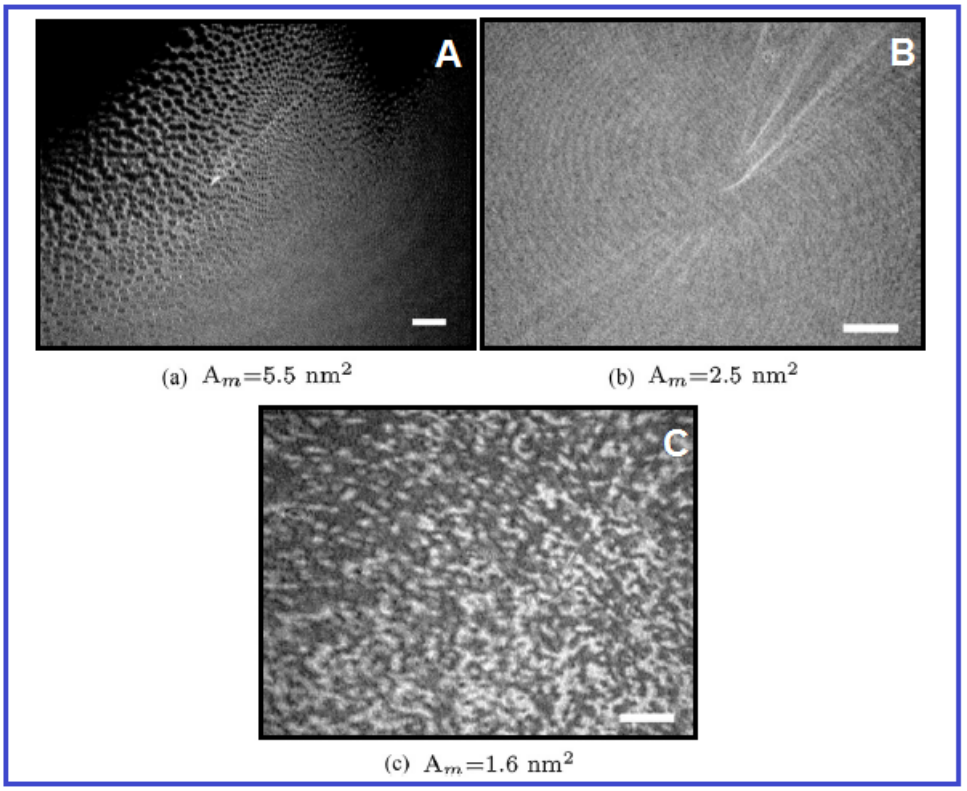

FIGURE 2.5: BAM images of the monolayer of AmTCQ molecules. The images were captured at an A_m shown below the respective images. (a) Coexistence of dark and gray domains. (b) Very uniform gray texture. (c) Coexistence of bright domains in the gray background. The scale bar represents a length of 500 μm.

The BAM images of the monolayer of AmTCQ molecules at different A_m are shown in Figure 2.5. The BAM image (Figure 2.5a) at a large A_m shows a coexistence of dark and gray regions. On compression, gray region grows at the expense of the dark region. We obtained a very uniform gray texture of the monolayer in the region of the isotherm between a and b. This is shown in Figure 2.5b. On further compression of the monolayer, the BAM image (Figure 2.5c) shows the presence of bright domains on the gray background. Interestingly, the coexistence of the bright domains on the gray background continues to exist till the monolayer collapses at 1.0 nm^2. This feature appears corresponding to the region from b to c of the isotherm. The bright domains and the gray regions appear fluidic and mobile under the microscope. The monolayer collapses on further compression, showing very bright 3D structures.

The intensity of the BAM images depends on the thickness of the film and the surface density of the molecules [33]. The dark region seen in the BAM images

at a very large A_m (Figure 2.5a) represents the gas phase whereas the gray region corresponds to L_1 phase. On compression, the gas phase disappears and a homogeneous gray texture representing the L_{12} phase was observed (Figure 2.5b). In the L_{12} phase, the coexistence of bright domains in the gray background (Figure 2.5c) were observed. The bright domain in the L_{12} phase might be thicker than the grey background. If the AmTCQ molecules orient planar to the water surface (face-on conformation) with the flexible ethylenoxy side-chains being interdigitated with the neighboring molecules, the molecular area is expected to be around 3.1 nm^2. If the molecules confine itself in an edge-on conformation, the molecular area could be around 1.0 nm^2. The value of A_0^1 in the L_1 phase was 3.3 nm^2.

The BAM images show a uniform gray texture in this phase (Figure 2.5b). Hence, the molecules are more likely expected to have the face-on conformation with interdigitated side-chain in the L_1 phase. The value of A_o in the L_{12} phase was found to be 1.6 nm^2 which is large for the edge-on and small for the face-on conformations. The BAM images in this phase (Figure 2.5c) reveal the coexistence of bright and gray regions. As the intensity level in the BAM images may depend on the thickness of the monolayer, the bright domains can be considered as thicker than that of gray regions. Therefore, the bright regions may correspond to the domains of the molecules with edge-on conformation, whereas the gray background may represent face-on conformation. The large value of A_o in the L_{12} phase is accounted by a coexistence of domains with face-on and edge-on conformations.

The monolayer of AmTCQ is transferred to HOPG substrate at different π_t by Langmuir-Schaefer method and scanned in SRI mode of AFM. Under such constant force state, a bias voltage is applied between the tip and the sample. Since the tip and sample are conducting, current tunnels between them. Such tunneling current (I_t) is measured at every pixel location during scanning. Therefore in SRI mode, a simultaneous imaging of the topographic map and I_t map is achieved. Such simultaneous measurement yields not only the surface topographic information but also local conducting properties of the films. The images captured in SRI mode of AFM for films deposited at different π_t are shown in Figure 2.6. Since the thickness of the films with face-on conformation of the molecules is small as compared to that of edge-on conformation, it is expected that the I_t for the face on conformation of the AmTCQ molecules on the HOPG surface is more as compared to that of their edge-on conformation. The value of I_t will be maximum for the HOPG surface without the presence of the organic layer over it.

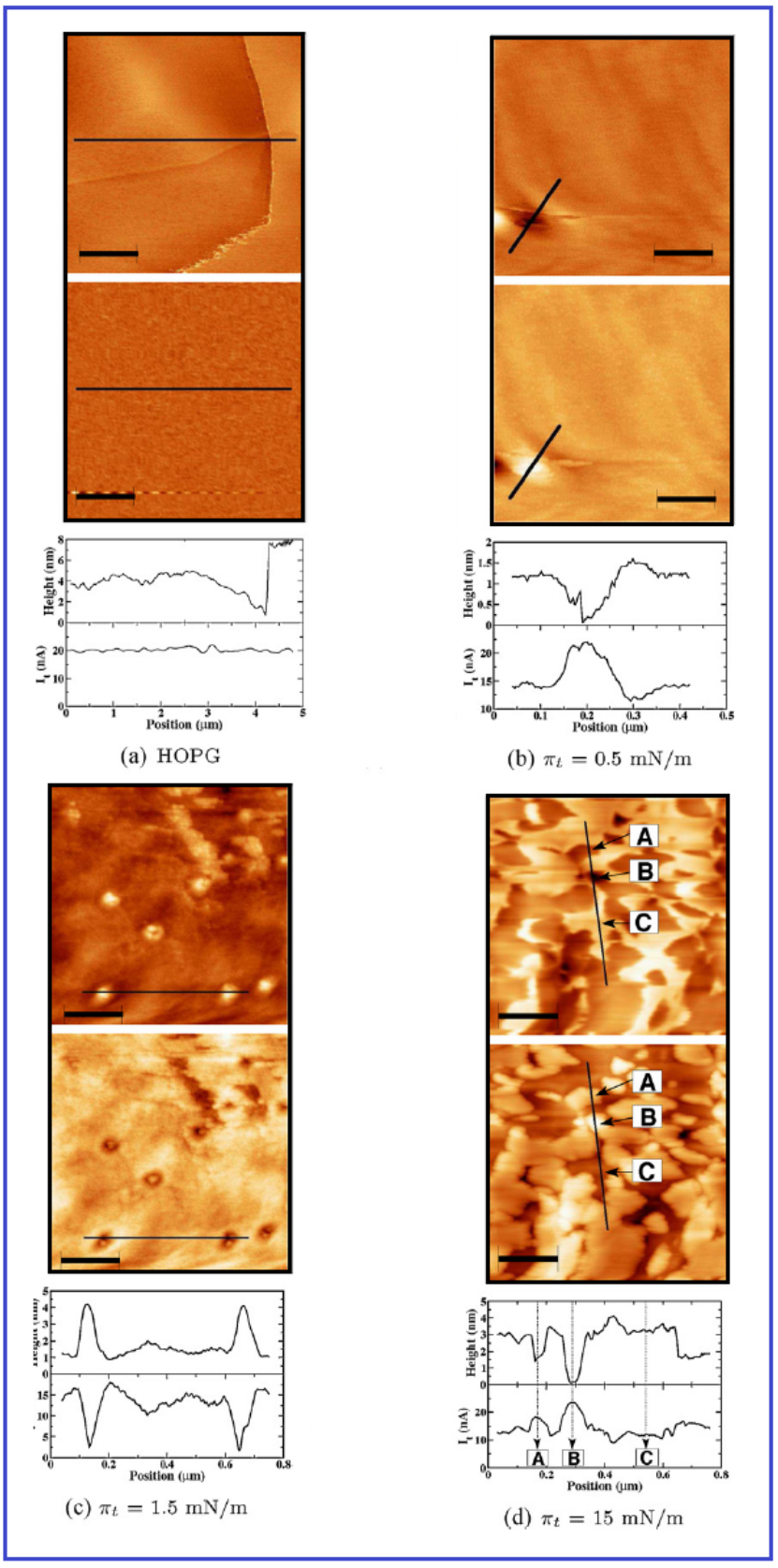

FIGURE 2.6: AFM images in SRI mode for the monolayer of AmTCQ molecules deposited at different π_t as indicated in the caption of the respective images. The top and bottom images are topographic and I_t map measured simultaneously in the SRI mode. The line profiles are drawn at the same location of both the maps and the corresponding graphs are shown below each images. The various features in the image (d) are labeled with A, B, and C. The corresponding points are indicated in the graphs by vertical lines. The scale bar in the image (a) and (b–d) represent lengths of 1 μm and 0.25 μm, respectively.

The topographic image of the HOPG surface shows very flat and uniform regions over the scan area of 5x5 μm^2. It also displays graphene terrace on the right side of the image (Figure 2.6a). Interestingly, the I_t image of the HOPG is uniform. The presence of terrace is not detectable as the I_t was constant throughout the region. When the tip is held at a constant force, the separation between the tip and surface features is also maintained constant. Therefore, the I_t remains uniform for the same material. The I_t will be different only for the materials with different conducting properties. The image for the film deposited at 0.5 mN/m (in L_1 phase) is shown in Figure 2.6b). The topographic image shows a very uniform film with a small defect at the left-bottom. The height profile data indicate that the average thickness of the uniform film to be 1.2 nm. This can be accounted for by the face-on conformation of the AmTCQ molecules. At the defect, the surface of the HOPG is exposed and therefore, the tunneling current at the defect site is higher as compared to the region where there are uniform deposition of the organic material. The topographic map of the film deposited at π_t equal to 1.5 mN/m shows the small bright domains grown over a uniform gray background (Figure 2.6c). The height variation data indicate the average height of bright domains and gray background to be around 3.5 and 1 nm, respectively. Thus, the bright regions can represent the domains with edge-on conformation of the molecules whereas the gray background represents the region with face-on conformation of the molecules. The I_t image shows lower values of I_t corresponding to the region with the edge-on conformation of the molecules as compared to the region with face-on conformation. Figure 2.6d shows the SRI mode images for the film deposited at the π_t equal to 15 mN/m. Such pressure corresponds to the L_{12} phase. The image reveal three different regions. These regions are labeled as A, B and C in the images and the corresponding points on the profile graphs are shown. The dark spots, gray background and the bright regions in the topographic image represent the HOPG surface, domains with face-on conformation and regions with edge-on conformation, respectively. The I_t values for the dark region representing the HOPG surface is the largest. Similarly the I_t values corresponding to the gray and bright region in the topographic images are high and low, respectively. Thus, the films deposited on HOPG substrate in L_1 phase reveal the molecules with face-on conformation and that deposited in L_{12} phase reveal both face-on and edge-on conformations. These results are consistent with the surface manometry and BAM.

A single layer of the AmTCQ molecule was transferred to the gold deposited Si substrates by the horizontal transfer technique. The reflection absorption infrared

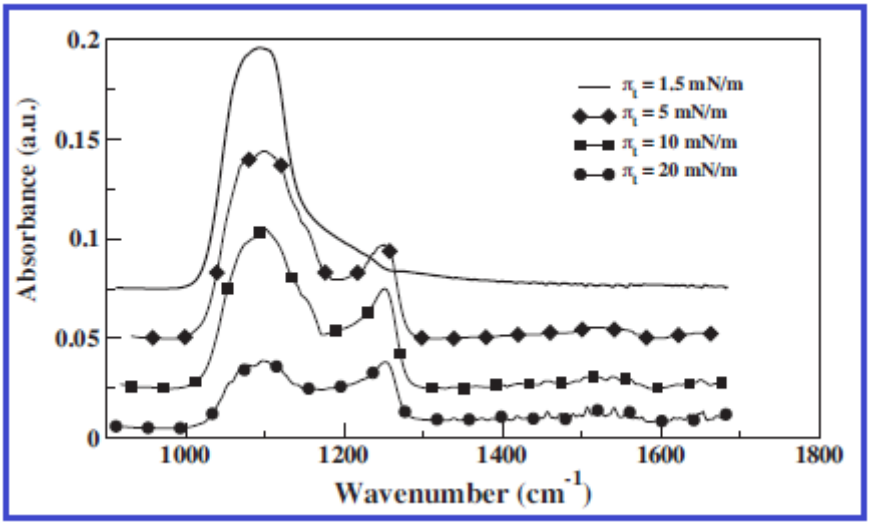

FIGURE 2.7: The RAIRS spectra of the films deposited at different π_t (π_t). The curves are relatively shifted vertically by absorbance value of 0.25 for visual clarity.

spectra are recorded and shown in Figure 2.7. The bands corresponding to the C-O-C alkyl (at 1100 cm^{-1}) and C-N aryl (at 1250 cm^{-1}) stretching are selected for the analysis. We simulated the infrared (IR) spectrum of the TCQ core using Gaussian 98 (B3LYP, 3-21G). We found that the transition dipole moment for C-N aryl stretch which is responsible for absorption at 1250 cm^{-1} is parallel to the disk plane of the TCQ core. Similarly, the transition dipole moment of C-O-C stretch which is responsible for the absorption at 1100 cm^{-1} is parallel along the side chain length of the AmTCQ molecule [34]. The absorbance values for the characteristic peaks and their ratio for the films deposited at different π_t are shown in Table 2.1. In the RAIRS setup, the IR beam is allowed to fall on the film at a grazing angle. At grazing angle, the state of polarization of the IR beam is predominantly parallel to the plane of incidence [34]. Therefore, the transition dipole moments associated with the molecules parallel to the surface causes the least absorption whereas the transition dipole moment perpendicular to the surface causes the large absorption of the IR radiation. The absorption curve from the film deposited at 1.5 mN/m shows a peak only at 1100 cm^{-1}. Therefore, the transition dipole moment corresponding to the absorption at 1100 cm^{-1} is perpendicular the surface. The signature of C-N stretch bond is not visible at this π_t. This indicate that the transition dipole moment corresponding to the absorption at 1250 cm^{-1} is planar to the surface and do not interact with the IR beam. Therefore, the disk plane of the AmTCQ molecule lies planar to the surface whereas the side chains of the molecule lie normal to the surface. Hence, the conformation of the AmTCQ molecules at π_t equal to 1.5 mN/m (i.e. L_1 phase)

can be face-on where the disk-plane lie planar to the surface and the interdigitated chain perpendicular to the surface. This model is shown in the Figure 2.8. The spectrum of the film corresponding to higher π_t show the signature of the peak at 1250 cm^{-1}. This continues to exist till the π_t equal to 20 mN/m. The height of the peak at 1100 cm^{-1} decreases whereas that at 1250 cm^{-1} increases with increase in π_t. This indicate that due to increase in π_t, more number of transition dipole moment corresponding to 1250 cm^{-1} absorption align perpendicular to the surface and on the other hand the transition dipole moment corresponding to 1100 cm^{-1} absorption align parallel to the surface. Such alignment corresponds to the edge-on conformation of the AmTCQ molecule.

TABLE 2.1: The absorbance values and relative comparison (A/B) as obtained from RAIRS spectra for the AmTCQ monolayer deposited at different π_t on the gold deposited Si substrate. The value of absorbance (Abs.) at a characteristic peak is estimated after baseline correction with a linear fit.

S.N.	π_t (mN/m)	**Abs. at 1100** cm^{-1} **(A)**	**Abs. at 1250** cm^{-1} **(B)**	**A/B**
1	0.5	0.12	NA	NA
2	5.0	0.094	0.0467	2.01
3	10	0.082	0.0510	1.61
4	20	0.033	0.0304	1.08

It can be pointed out that if all the molecules make a transition to edge-on due to increase in π, the IR spectra would have revealed a constant value of absorbance independent of π_t. However in the present case, we observe a relative change in the height of absorbance values (A/B in Table 1) with the change in π_t. This can be interpreted as in the L_{12} phase, the number of AmTCQ molecules which align themselves to edge-on conformation increases with the increase in π.

Therefore, the molecular conformations above π equal to 1.5 mN/m are both edge-on and face-on. The RAIRS study also indicates the face-on conformation of the molecules in the L_1 phase and face-on and edge-on coexistence in L_{12} phase. Based on the results from surface manometry, microscopy and spectroscopy, we propose a model for the molecular orientation in different phases of Langmuir monolayer of AmTCQ molecule. This is shown in Figure 2.8a and Figure 2.8b. Figure 2.8a shows the face-on conformation of the disk-shaped molecules with the interdigitated side-chain in the L_1 phase. Figure 2.8b shows the both face-on and edge-on conformations in the L_{12} phase.

There are numerous reports on the stable LM of discotic molecules. The reports have indicated the monolayers to exhibit gas and liquid phases. The molecular conformations in the liquid states were reported to be either face-on or edge-on.

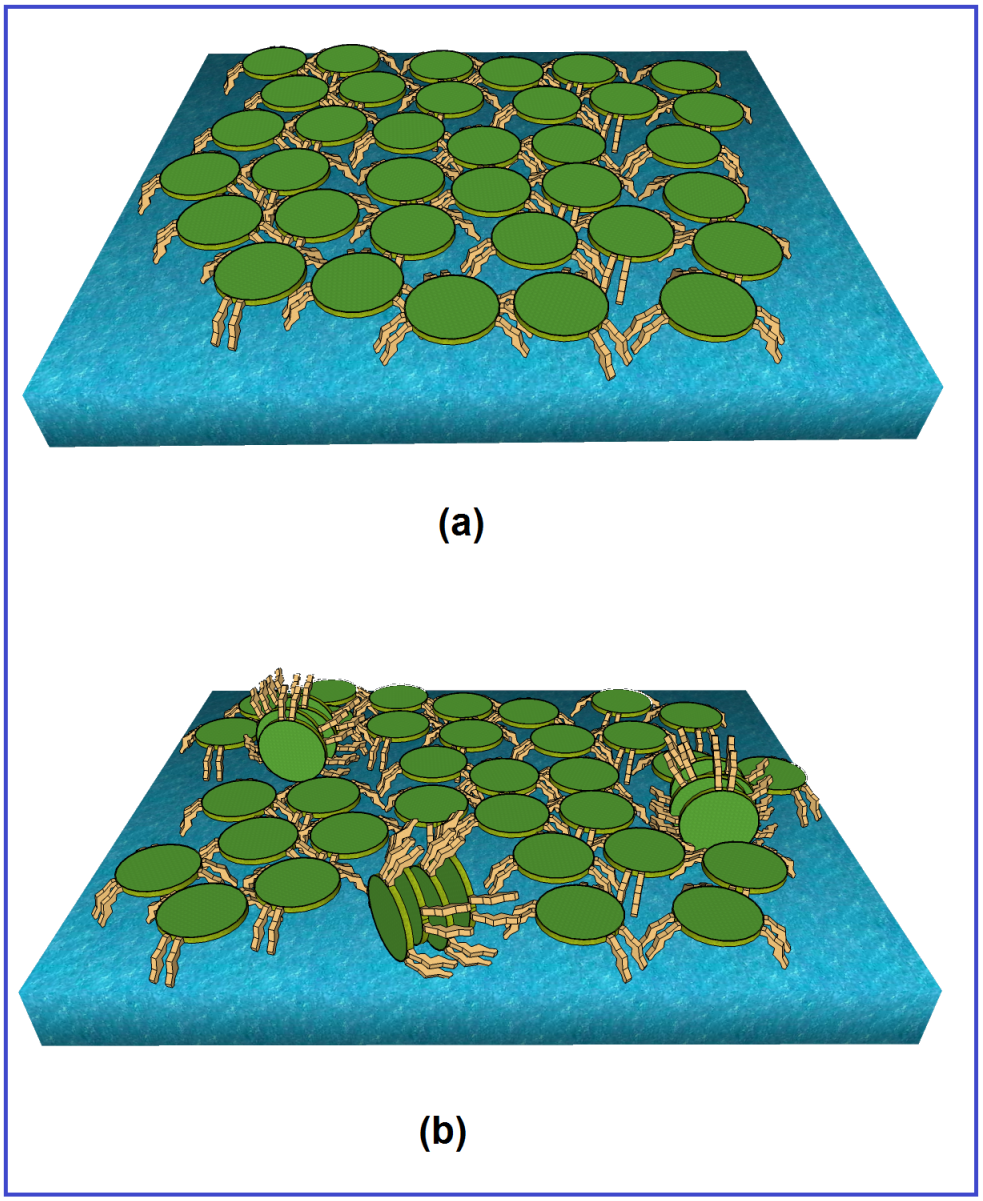

FIGURE 2.8: (a) The possible molecular conformation of AmTCQ molecules at the A-W interface in L_1 phase. (b) The possible molecular conformation of AmTCQ molecules at the A-W interface in L_{12} phase.

Our study indicates the new phase, L_{12} where the discotic molecules co-exist in both face-on and edge-on conformation. The nature of conformation of the discotic molecules on the surface is believed to be dependent on intermolecular and molecule-substrate interactions [3, 4]. If the intermolecular interaction is greater than the molecule-substrate interaction, the molecules prefer the edge-on over face-on conformation. The DLCs rich in pi-electrons have stronger core-core interaction leading to the condensed liquid state with edge-on conformation of the molecules. In the present case, the molecules are deficient in pi-electrons resulting in weaker intermolecular interaction. Such weak intermolecular interaction may

be responsible for the L_{12} phase where the molecules exhibit edge-on and face-on conformations.

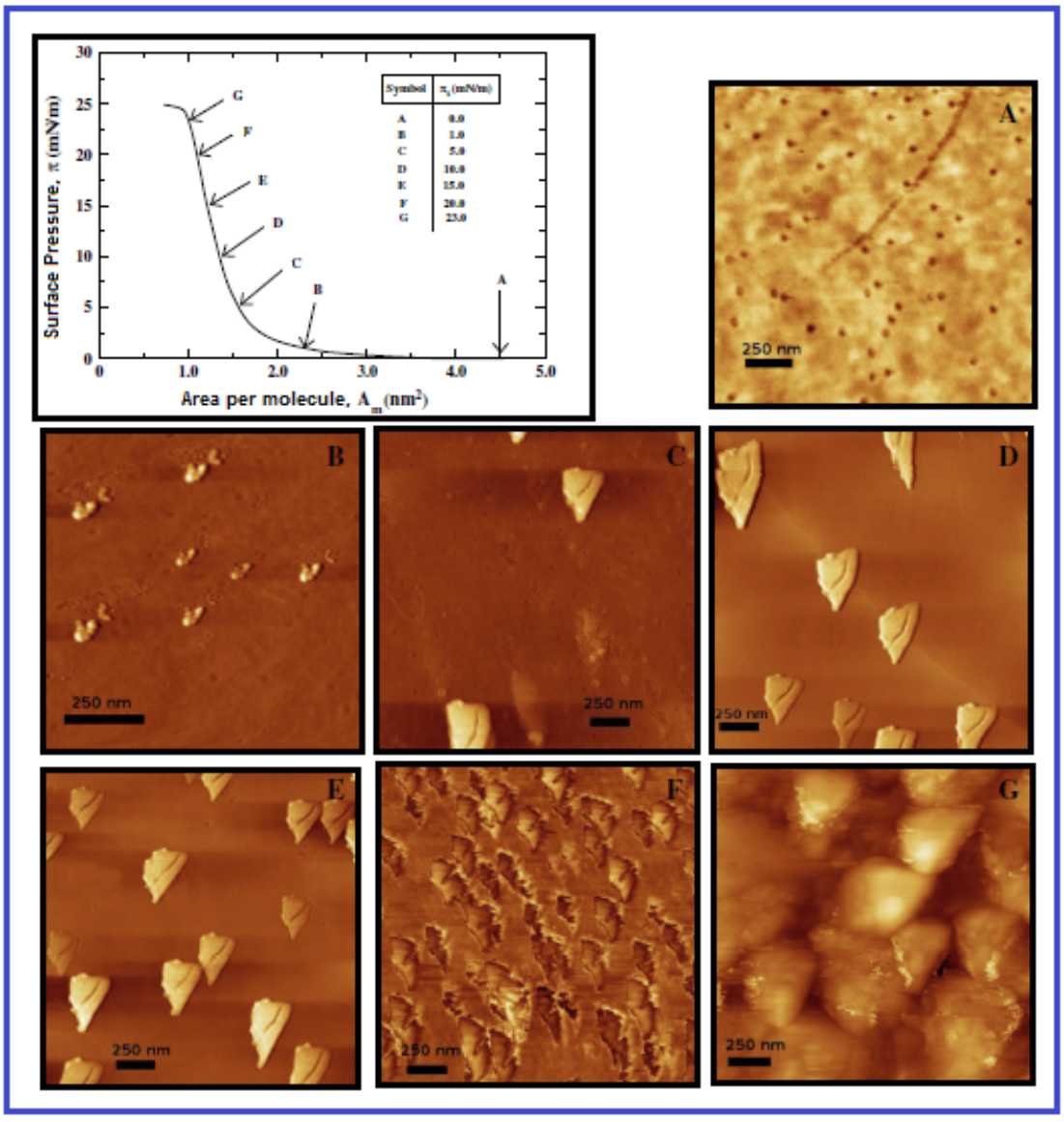

FIGURE 2.9: $\pi - A_m$ isotherm of the AmTCQ molecule. The AFM images of the LB film on Si substrate deposited at the target surface pressure (π_t) as indicated by the arrows in the isotherm.

It will be interesting to study the molecular aggregation and nanostructure formation at different thermodynamical state. Hence, we transferred the monolayer of AmTCQ molecule onto a solid surface using the highly controlled LB technique and studied the morphology of the molecular aggregation using AFM. The AFM images of the LB films of AmTCQ molecules transferred onto Si (100) substrates at different target π are shown in the Figures 2.9A to 2.9G. Figure 2.9A shows the AFM image of the LB film at zero π_t. The image reveals

bright background with some dark regions. At a π_t of 0.5 mN/m, such dark regions vanish and a uniform texture was obtained. The AFM image at 1 mN/m (Figure 2.9B) shows small droplet-like domains in the uniform background. Since 1 mN/m is close to $L_1 - L_{12}$ transition π, the AFM images of the LB films deposited at such π_t indicate the traces of L_{12} phase as the droplet-like domains. At a higher π (5 mN/m), the droplet-like domains transformed to triangular structures. Interestingly, the triangle like structure appears to exist in the LB films deposited in the π_t range from 5 to 15 mN/m (Figures 2.9C to 2.9E). This triangular structure exhibits similar geometrical properties like shape, size and defects. However, there is an overall increase in the number of such triangles with the increase in π_t. A close observation of the internal feature of the triangle reveals a crack-line defect through the middle of each of the triangles. At a π_t of 20 mN/m (Figure 2.9F), the triangles get deformed and the crack-line of the triangles appears to widen up.

The AFM image of the LB film at 23 mN/m reveals very thick domains (Figure 2.9G) which is the due to the collapse instability of the monolayer on the water surface at such π_t. The AFM images of the LB films of AmTCQ molecules with corresponding height profiles are shown in Figure 2.10. The height profiles are drawn on various parts of the AFM images and average thickness of the surface features are estimated there in. The bright region in Figure 2.10A corresponds to the film of average thickness of 0.7±0.2 nm. Such thickness of the film can be accounted for by a planar orientation of the molecules wherein the disc plane is parallel to the substrate plane (i.e. face-on conformation). The dark regions in the image represent the Si surface. The droplet-like domains in the Figure 2.10B are observed at a π_t of 1 mN/m. The average height of the droplet-like domains is found to be 3.2±0.3 nm. This can be accounted for by the vertical orientation of the molecules in such domains. In such thick domains, the molecules tend to orient with its disc plane perpendicular to the substrate plane (i.e. edge-on conformation). These domains can act as nucleation sites for the growth of triangular structure at higher π_t. The triangular shaped domains are observed at surface pressures greater or equal to 5 mN/m. Figure 2.10C shows a single triangular domain. The average thickness of the triangular domains is found to be 3.2 nm which can be accounted for by a vertical or edge-on conformation of the molecules in such domains. The domain possesses a crack-line. At higher π_t the number of such triangular domains increases. This can be observed in Figure 2.10D. It is noteworthy that each triangular domain possesses a crack-line defect. The area occupied by a triangular domain is around 60,000 nm^2. We have

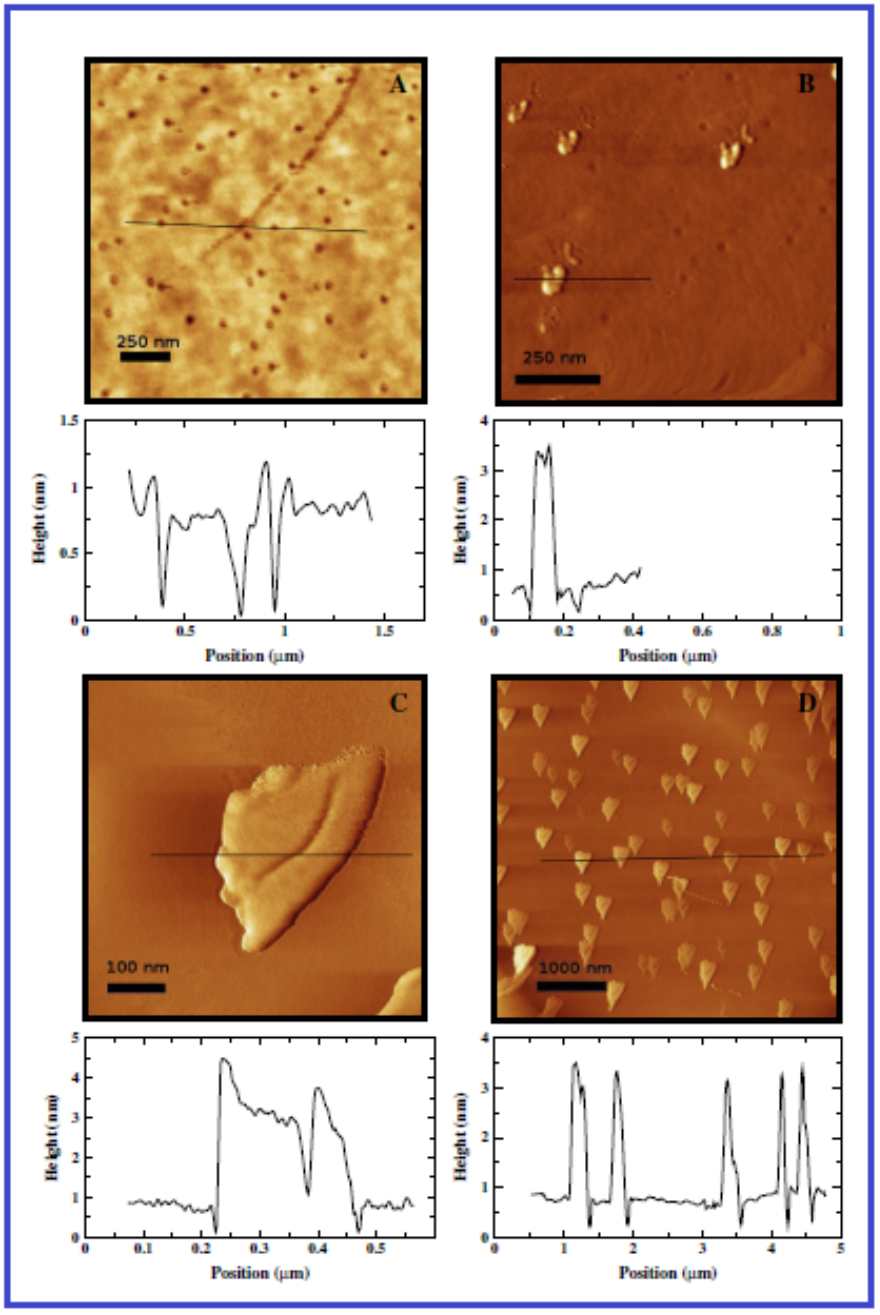

FIGURE 2.10: AFM images of LB film of AmTCQ molecules deposited at π_t of (A) 0 mN/m, (B) 1 mN/m, (C) 10 mN/m and (D) 15 mN/m. The height profile corresponding to the black line drawn over each image is shown below respective images.

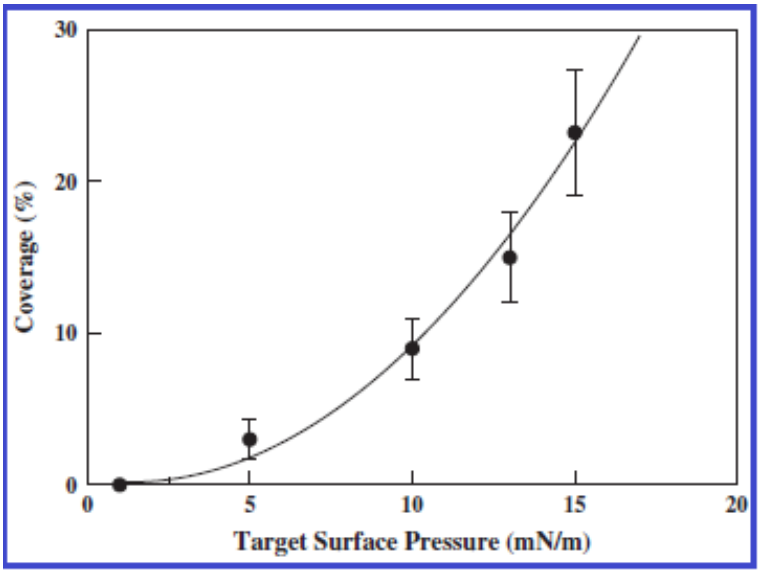

FIGURE 2.11: Percentage area coverage (c) of triangular domains in the LB films deposited at different target surface pressure (π_t). The dark circles are the experimental data points. The solid line is a fit polynomial curve: $c = 0.4 - 0.32\pi_t + 0.12\pi_t^2$.

estimated percentage of area coverage of the triangular domains in the LB films deposited at different π_t. This is shown in Figure 2.11. We find an increasing trend in the coverage with the increase in π_t. The variation of the coverage as a function of π_t is fit to a polynomial curve.

We found that the molecular conformations in the L_1 phase of the LM of AmTCQ molecules is face-on whereas in the L_{12} phase, the molecules are found to coexist in both the face-on and edge-on conformations at the A-W interface. Interestingly, the molecular aggregation in the edge-on domains leads to a steady state triangular structure. The LB films deposited on Si (100) can experience some strain due to lattice mismatch between the substrate and the films [28, 35]. The strain increases with the increase in π_t. The strain in the LB film deposited at 1 mN/m gets relaxed with the formation of droplet-like domains at the localized sites (Figure 2.9B). With increasing π_t, the droplets transformed to triangular domains. The triangular structure is found to be stable in the π_t range of 5 to 15 mN/m. With the increase in π_t (in the range 5 to 15 mN/m), the strained LB films get relaxed by increasing the number of triangular domains. The percentage area coverage of the triangular domains as a function of target π_t exhibits a polynomial variation. The triangular domains exhibit crack-line defect. The appearance of crack line in the triangles might be due to such relaxation of the strained film to its thermodynamical equilibrium state. The triangular domains in the LB films become unstable if the π_t greater or equal to 20 mN/m. The ESP of the AmTCQ molecule was found to be around 20 mN/m. Therefore, the AFM images of the

LB films of AmTCQ molecules deposited at π_t greater or equal to 20 mN/m reveal instability in form of the deformation of the triangular domains. It can clearly be observed from the AFM images of LB films at the surface pressures of 20 and 23 mN/m (Figure 2.9F and Figure 2.9G). In a report, the triangular domains have been observed in the ultrathin polystyrene films adsorbed on a mica substrate in the presence of aqueous surfactant medium. Such triangular structure are dependent on polymerization time. The triangular structure was suggested to be formed under the influence of lattice structure of the mica substrate [36].

2.4 Conclusion

We found a stable LM of AmTCQ molecules at the A-W interface. The monolayer exhibits gas phase, L_1 phase with face-on molecular configuration, and L_{12} phase exhibiting both the face-on and edge-on conformations of the molecules. In the proposed model for face-on conformation, the core of the molecules lie planar to the water surface where the flexible ethylenoxy side-chains being interdigitated with the neighboring molecules. The appearance of both face-on and edge-on conformations in the L_{12} phase might be due to the weak intermolecular interaction. We transferred the LB films of the AmTCQ molecules onto the Si substrate at different π_t. The LB films deposited in the gas phase (zero π_t) shows the flat domains with face-on conformation of the molecules. At a low π_t of 1 mN/m), we obtained nucleation sites for the growth of triangular domains. As the π_t increases, we obtained triangular domains. The shape and size of such domains appear to be stable with respect to the π_t provided if the π_t is less than the ESP of the AmTCQ molecules (i.e. greater than 20 mN/m). As the π_t increases, the number of triangular domains increases. The triangular domains deform as the π_t increases above ESP of the AmTCQ molecules indicating instability. Such instability arises as the monolayer approaches collapse above the ESP. The triangular domains may be formed due to the relaxation of strained LB films of the AmTCQ molecules. The strain in the LB films develops due to the lattice mismatch of the films and Si(100) substrate. The role of mica substrate on the formation of triangular domains in polystyrene films have been reported [36]. The ability to understand and control the molecular organization in the thin films is very challenging, and some efforts are been invested in this field [37, 38]. Our study also demonstrates the π_t to be a controlling parameter for altering the number of triangular domains. Further, it will be interesting to understand the role of molecular interactions on nanostructure formation in the

LB films. Hence, we extended our study on surface behavior by altering the side chains of the AmTCQ molecules. Novel liquid crystalline molecules has been synthesized by covalently linking rod shaped cyanobiphenyl to the central disk shaped TCQ core. The presence of rod shaped cyanobiphenyls at the periphery provides additional polarity to the discotic molecules. The surface behavior of such molecules is presented in the next chapter.

Bibliography

[1] K. Ariga, K. Sakakibara, G. J. Richards and J. P. Hill, Supramolecular Chem.,23, 183, 2011.

[2] Y. Qiu, P. Chen, and M. Liu, J. Am. Chem. Soc., 132, 9644, 2010.

[3] P. Ruffieux, O. Groning, M. Bielmann, C. Simpson, K. Mullen, L. Schlapbach, P. Groning, Phys. Rev. B, 66, 073409, 2002.

[4] R. Friedlein, X. Crispin, C. D. Simpson, M. D. Watson, F. Jackel, W. Osikowicz, S. Marciniak, M. P. de Jong, P. Samori, S. K. M. Jonsson, M. Fahlman, K. Mullen, J. P. Rabe, W. R. Salaneck, Phys. Rev. B, 68, 195414, 2003.

[5] S. Kumar, Chem. Soc. Rev., 35, 83, 2006.

[6] S. Chandrasekhar, G. S. Ranganath, Rep. Prog. Phys., 53, 57, 1990.

[7] L. Y. Chiang, J. P. Stokes, C. R. Safinya, A. N. Bloch, Mol. Cryst. Liq. Cryst., 125, 279, 1985.

[8] P. G. Schouten, J. M. Warman, M. P. de Haas, M. A. Fox, H. L. Pan, Nat., 353, 736, 1991.

[9] G. Lussem, J. H. Wendroff, Polym. Adv. Technol., 9, 443, 1998.

[10] I. Seguy, P. Jolinat, P. Destruel, J. Farenc, R. Mamy, H. Bock, J. Ip, T. P. Nguyen, J. Appl. Phys., 89, 5442, 2001.

[11] N. Stutzmann, R. H. Friend, H. Sirringhaus, Sci., 299, 1881, 2003.

[12] L. Schmidt-Mende, A. Fechtenkotter, K. Mullen, E. Moons, R. H. Friend, J. D. MacKenzie, Sci., 293, 1119, 2001.

[13] N. Boden, R. J. Bushby, J. Clements, B. Movaghar, J. Mater. Chem., 9, 2081, 1999.

[14] A. Albrecht, W. Cumming, W. Kreuder, A. Laschewsky, H. Ringsdorf, Col. Polym. Sci., 264, 659, 1986.

[15] N. C. Maliszewskyj, P. A. Heiney, J. K. Blasie, J. P. McCauley Jr., A. B. Smith III, J. Phys. II (France), 2, 75, 1992.

[16] D. Gidalevitz, O. Y. Mindyuk, P. A. Heiney, B. M. Ocko, P. Henderson, H. Ringsdorf, N. Boden, R. J. Bushby, P. S. Martin, J. Strzalka, J. P. McCauley Jr., A. B. Smith III, J. Phys. Chem. B, 101, 10870, 1997.

[17] A. Nayak, K. A. Suresh, S. K. Pal, S. Kumar, J. Phys. Chem. B, 111, 11157, 2007.

[18] S. Sergeyev, W. Pisula, Y. H. Geerts, Chem. Soc. Rev., 36, 1902, 2007.

[19] S. Laschat, A. Baro, N. Steinke, F. Giesselmann, C. Hagele, G. Scalia, R. Judele, E. Kapatsina, S. Sauer, A. Schreivogel, M. Tosoni, Angew. Chem. Int. Ed., 46, 4832, 2007.

[20] T. Kato, N. Mizoshita, K. Kishimoto, Angew. Chem. Int. Ed., 45, 38, 2006.

[21] N. Boden, R. C. Borner, R. J. Bushby, J. Clements, J. Am. Chem. Soc., 116, 10807, 1994.

[22] S. Kumar, D. S. S. Rao, S. K. Prasad, J. Mater. Chem., 9, 2751, 1999.

[23] R. Hiesgen, H. Schonherr, S. Kumar, H. Ringsdorf, D. Meissner, Thin Solid Films, 358, 241, 2000.

[24] S. A. Vickery, R. C. Dunn, Langmuir, 17, 8204, 2001.

[25] R. K. Gupta, K. A. Suresh, Euro. Phys. J. E, 14, 35, 2004.

[26] D. Whang, S. Jin, Y. Wu, C. M. Lieber, Nano Lett. 3, 1225, 2003.

[27] S. W. Hui, R. Viswanathan, J. A. Zasadzinski, Israelachvili, Biophys. J., 68, 171, 1995.

[28] J. A. Zasadzinski, R. Viswanathan, L. Madsen, J. Garnaes, D. K. Schwartz, Sci., 263, 1726, 1994.

[29] N. Boden, R. J. Bushby, K. Donovan, Q. Liu, Z. Lu, T. Kreouzis, A. Wood, Liq. Crys., 28, 1739, 2001.

[30] K. Lambert, R. K. Capek, M. I. Bodnarchuk, M. V. Kovalenko, D.V.Thourhout, W. Heiss, and Z. Hens, Langmuir, 26, 7732, 2010.

[31] R. D. Smith, J. C. Berg, J. Col. Int. Sci., 74, 273, 1980.

[32] G.L. Gaines Jr., Insoluble Monolayers at Liquid-Gas Interfaces, WileyInterscience, New York, 1966.

[33] S. Riviere, S. Henon, J. Meunier, D. K. Schwartz, M. W. Tsao, C. M. Knobler, J. Chem. Phys., 101, 10045, 1994.

[34] R. G. Greenler, J. Chem. Phys., 44, 310, 1966.

[35] R. E. Caflisch, J. Sci. Comput., 37, 3, 2008.

[36] H. Nakamura, H. Sakai, S. Aoshima, M. Abe, J. Oleo. Sci., 51, 781, 2002.

[37] F. Zaera, Chem. Rev., 112, 2920, 2012

[38] R. Verma, A. Sharma, K. Kargupta, J. Bhaumik, Langmuir, 21, 3710, 2005.

Chapter 3

Effect of modification of side chains of TCQ based discotic molecules on its surface behavior at different interfaces

3.1 Introduction

Discotic liquid crytals (DLCs) are known to exhibit monolayer phases where the disk-plane of the molecules are either planar to the water surface (face-on conformation) or it is perpendicular to the water surface (edge-on conformation) [1–5]. The nature of conformation of the discotic molecules on the surface is believed to be dependent on intermolecular and molecule-substrate interactions [6, 7]. If the intermolecular interaction in the layer is greater than the molecule-substrate interaction with respect to Gibbs free energy, the molecules prefer the edge-on conformation. If the molecule-substrate interaction is greater than the intermolecular interaction then the molecules prefer face-on conformation.

Tricycloquinazoline (TCQ) based molecules with 6 ethelenoxy side chains (AmTCQ) molecules are deficient in pi-electrons resulting in weaker intermolecular interaction. Due to such weaker intermolecular interaction, the Langmuir monolayer (LM) of AmTCQ molecule exhibit novel L_{12} phase, where it prefers both face-on and edge-on conformation. The molecular aggregation of AmTCQ molecules at the air-solid (A-S) interface was found to be the co-existence of face-on and edge-on conformation. Interestingly, the Langmuir Blodgett (LB)

film of AmTCQ molecules deposited in L_{12} phase shows uniformly distributed and structurally similar triangular domains. The number of such triangular domains increase on increasing the target surface pressure (π_t) of LB deposition [8].

In this chapter, we have studied the role of molecular interaction on the surface behavior by changing the chemical nature of the molecules. We have altered chemically the side chains of TCQ core by substituting rod shaped cyanobiphenyl groups in place of ketone groups. The substitution of rod shaped cyanobiphenyl groups provides additional polarity and may result in different entropy in different environment. Here, the surface behavior of TCQ based molecules with 6 cyanobiphenyl side chains (TCQCB) molecule at air-water (A-W) and A-S interface was investigated.

The study reveals that the LM of the TCQCB molecule at A-W interface exhibits a low density and a high density liquid phases. The TCQCB molecules prefer edge-on conformation. The atomic force microscopy (AFM) images reveal a structural transformation from elongated domains to very compact grainy texture for the LB films deposited in the low and high density liquid phases, respectively.

3.2 Experimental Methods

The TCQCB molecule was synthesized in the laboratory by Prof. Sandeep Kumar of Raman Research Institute, Bengaluru [9, 10]. The chemical structure of the molecule is shown in Figure 3.1. The molecule possesses six polar cyano-alkyloxybiphenyl side-group symmetrically attached to the TCQ core so that it retains its C_3 fold point group symmetry. The diameter of the TCQCB molecule is found to be around 5.3 nm. A solution of the sample was prepared in HPLC grade chloroform having a concentration of 1.7×10^{-5} M. The monolayer at the A-W interface was formed by spreading the solution onto the ultrapure ion-free water. The surface pressure (π) - area per molecule (A_m) isotherms were obtained by compressing the monolayer at a speed of 0.5 $(\mathrm{nm}^2/molecule)/min$. A high resolution microscopy was done by transferring the monolayer onto very clean solid (glass coverslip) substrates, and obtaining the topographic images of the films using AFM. Prior to deposition, the glass coverslip substrates were treated hydrophilically by boiling them in piranha solution (3:1, conc H_2SO_4:H_2O_2) for 1 minute, and then rinsed successively with ion-free water, absolute alcohol and acetone solvents. The substrates were then dried by blowing hot air at 70 °C. We deposited a single layer of LB films on these substrates at different π_t by a single

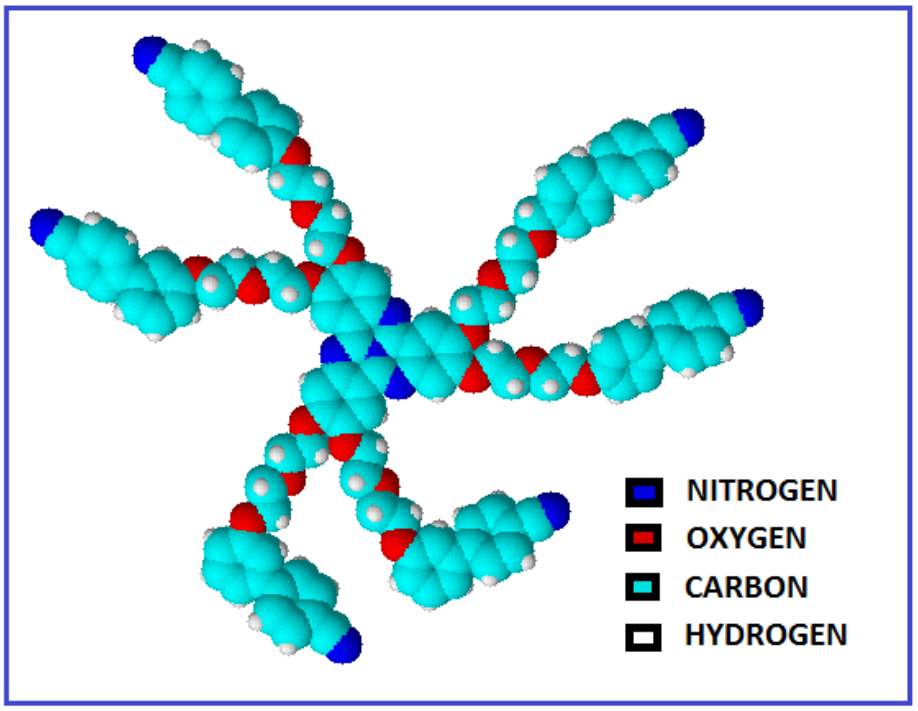

FIGURE 3.1: The chemical structure of the TCQCB molecule.

upstroke of the dipper. The AFM imaging were done in semi-contact mode in ambient. The spring constants and the resonance frequencies of the Si tips were in the ranges of 10-20 N/m and 180-270 KHz, respectively. The experiments were carried out at room temperature (∼22 °C).

3.3 Results and Discussion

The π - A_m isotherm of TCQCB molecules is shown in Figure 3.2. The isotherm shows zero π at very large A_m. It shows a A_i at around 7 nm^2. On decreasing the A_m, the isotherm indicates a change in the slope and then followed by a gradual rise in π. This region of the isotherm corresponds to L_1 phase. On further decreasing the A_m another slope change is obtained at 30 mN/m. The π rises rapidly till the monolayer collapses at around collapse surface pressure (π_c) of 58 mN/m. This region of the isotherm corresponds to L_2 phase. The extrapolation of the region of the isotherm between 6 to 2.2 nm^2 to zero π yields an A_m value of around 5.6 nm^2 (=A_o^1). The extrapolation to the zero π of the rapidly increasing π region of the isotherm yields a limiting area per molecule of around 3.0 nm^2 (=A_o).

The maximum value of E in the L_1 and L_2 phases were obtained as 46 and 61 mN/m, respectively. The values are relatively smaller as compared to a commonly

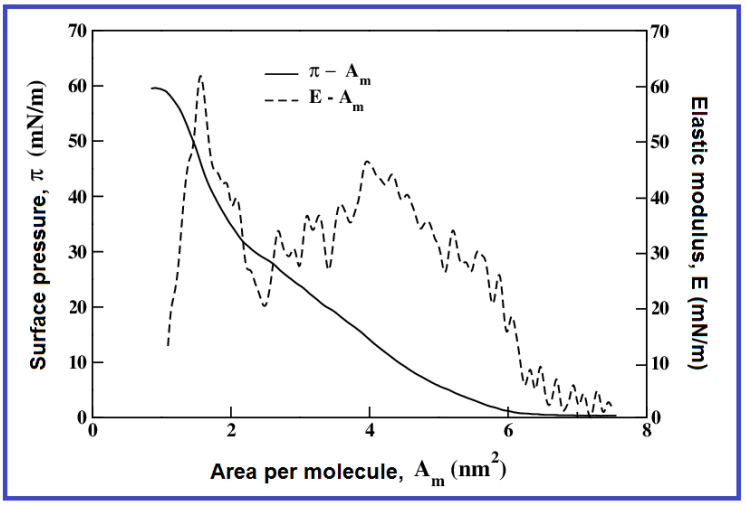

FIGURE 3.2: Surface pressure (π) - area per molecule (A_m) isotherm (solid line) and in-plane elastic modulus (E) - A_m of the TCQCB molecule (dashed line).

studied molecule, octadecanoic acid. The maximum values of E of octadecanoic acid in the L_1 and L_2 phases were found to be 100 and 400 mN/m, respectively. This indicates that the observed L_1 and L_2 phases are more fluidic as compared to that of L_1 phase of octadecanoic acid. For a face-on conformation of the TCQCB molecules on the water surface, the average molecular area value is estimated to be around 22 nm^2. However, the π - A_m isotherm of the TCQCB molecule indicates the average molecular areas in L_1 and L_2 phases to be around 5.6 and 3.0 nm^2, respectively. Such smaller average molecular areas in the different phases can be accounted for by the edge-on conformation of the molecules. Therefore, the L_1 and L_2 phases are low density and high density liquid phases wherein the TCQCB molecules exhibits edge-on conformation.

The isocycles show small hysteresis; however the compression and expansion curves are retraceable. There are no shift in A_m of the isocycles relative to each other. This indicates a better stability of TCQCB monolayer at the A-W interface.

Figure 3.4 shows the AFM image of a bare glass coverslip. The average root mean square roughness of glass coverslip substrates were found to be $\sim$ 0.1 nm for a scan range of 2.0×2.0 μm^2. This indicate a reasonably smooth surface of the glass coverslip [11]. The LB films of the TCQCB molecules are deposited on glass coverslip at different π_t, and scanned using AFM. The AFM images of such film are shown in Figure 3.5.

The AFM image of the LB films deposited at 10 mN/m (Figure 3.5A) shows the bright domains grown over a less bright background. The average height of such bright domains is 5.2±0.3 nm. This height corresponds to a vertical orientation

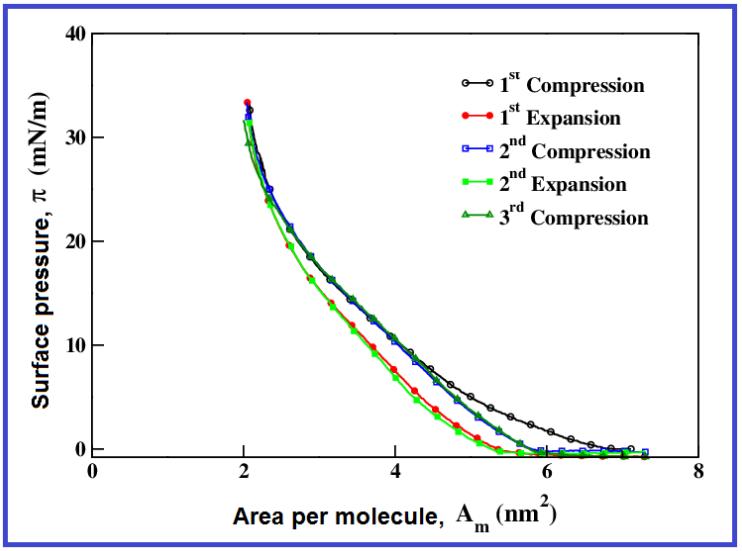

FIGURE 3.3: Isocycles obtained during repeated compression and expansion of the TCQCB monolayer at A-W interface.

of TCQCB molecules. The average height of the less bright region is around 3 nm. This can be accounted for by a tilt of the molecules. The bright domains do not show any preferential growth direction, and are found to be grown randomly. The morphology of the domains are found to be changed with the increase in π_t. The less bright region appear to vanish whereas the randomly grown bright domains assemble to yield interesting pattern. The AFM image of LB films of TCQCB molecules at 20 mN/m (Figure 3.5B) shows the domains to be elongated and oriented in a preferential direction. The height variation data also reveal that the average height of such elongated domains to be around 5.5 nm. With the further increase in π_t ($=$ 30 mN/m), the elongated domains appear to be vanishing. This can be observed from the Figure 3.5C. The AFM image at π_t of 35 mN/m (Figure 3.5D) reveal grainy texture wherein the elongated domains as observed in Figures 3.5B and 3.5C have completely transformed to isotropic small grain-like domains. The π_t of 30 mN/m is close to the L_1-L_2 phase transition. Therefore, the elongated domains as observed in the L_1 phase undergo a structural transformation to very compact grainy and isotropic texture in the L_2 phase.

The π-A_m isotherm of TCQCB molecules indicate the low density L_1 phase where the molecules exhibit edge-on conformation. Because of the low density of L_1 phase, when the LB films were deposited at the low π_t ($\leq$10 mN/m), two regions were obtained: region with vertically oriented molecules and region with tilted molecules. With the increasing π_t, the titled region vanishes and the AmTCQ molecules prefer vertical orientation. The LB films deposited in L_1 phase at a

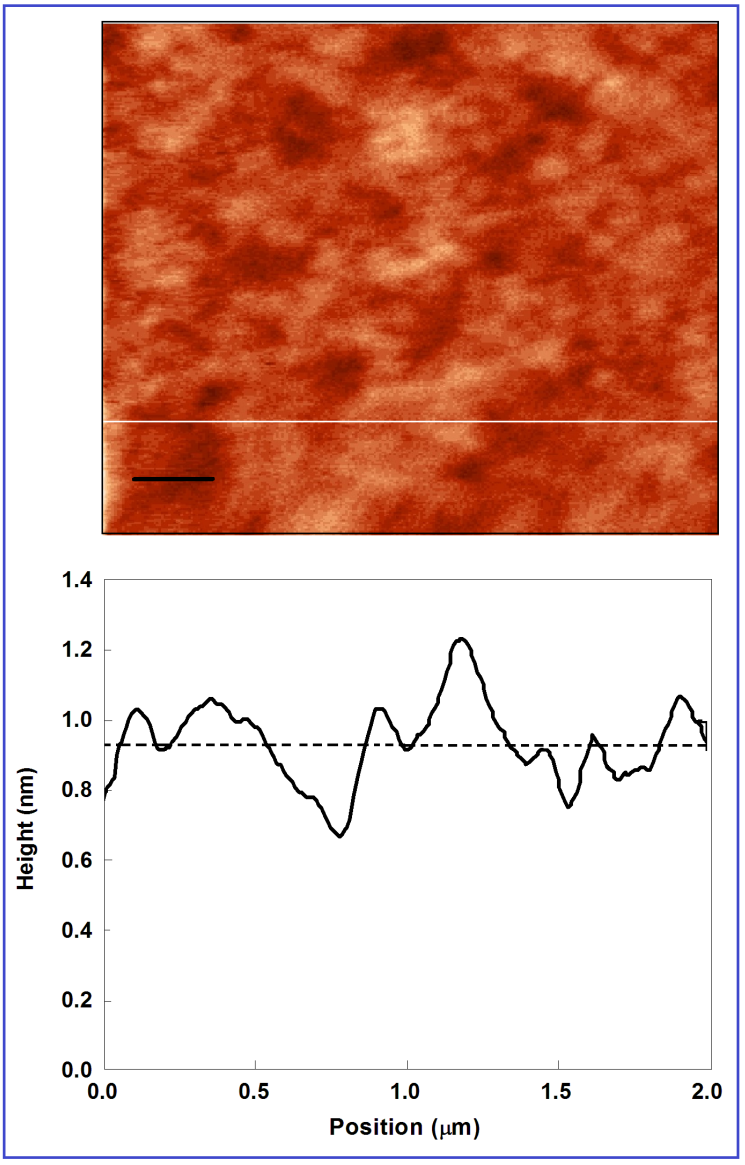

FIGURE 3.4: (Top) AFM image of a bare glass coverslip. (Below) Height profile is drawn along the white line on the AFM image. The scale bar represent a length of 0.25 μm. Dashed line represent the average height of the image.

higher π_t (>10 mN/m) exhibited elongated domains. Such domains undergo a structural transformation to a compact grainy texture in the LB films deposited in L_2 phase.

Based on our studies, we propose a model for the molecular orientation in L_1 and L_2 phase of LM of TCQCB molecules. Figure 3.6a shows the possible molecular conformation of TCQCB molecules at the A-W interface in L_1 phase. In this phase, the molecules may prefer edge on conformation with a tilt. In order to consider the cancellation of the dipole moment, the molecules were shifted relatively with respect to each other. The molecular conformation in L_2 phase is

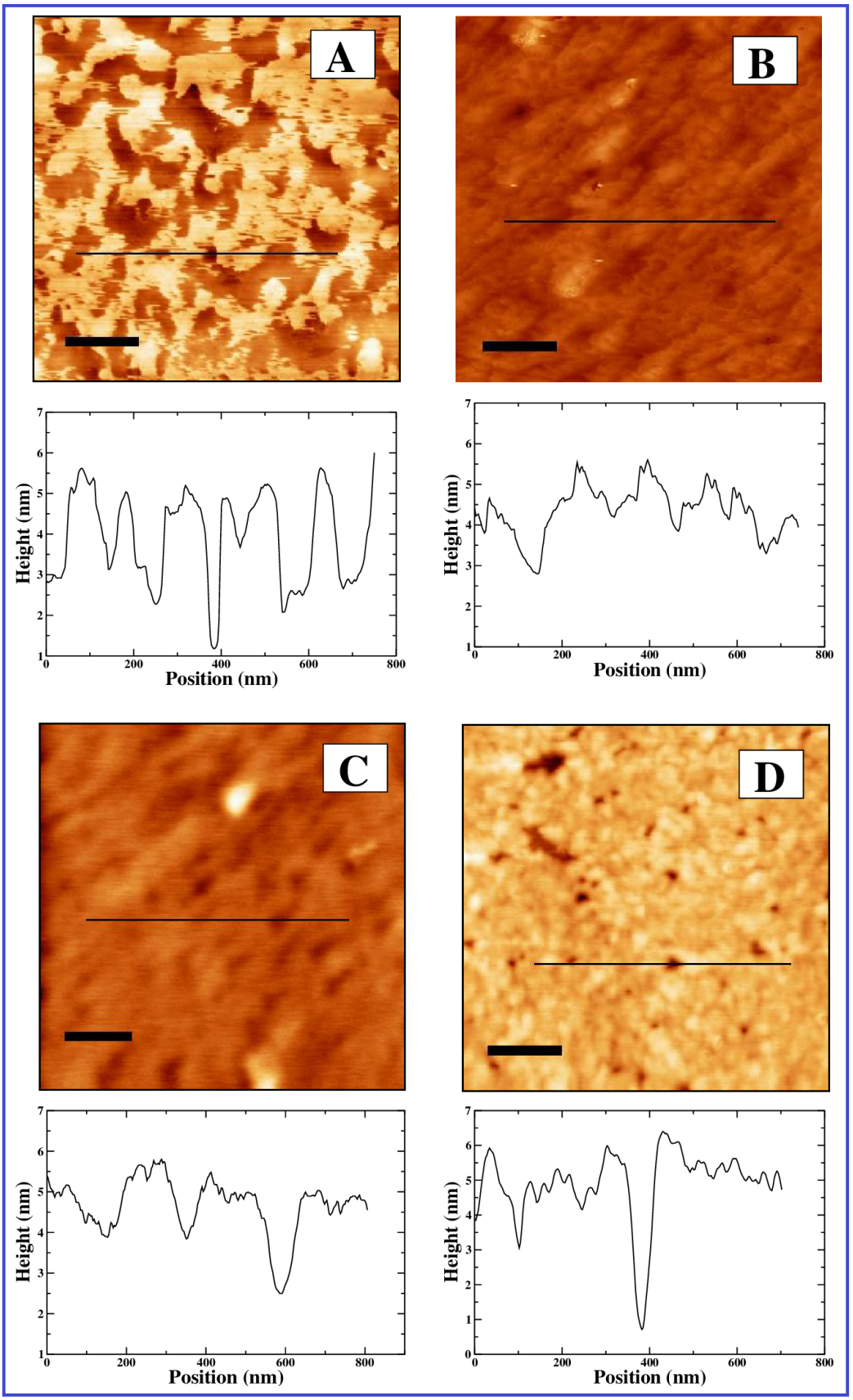

FIGURE 3.5: AFM images of LB films of TCQCB molecule. The target surface pressure (π_t) for LB films deposition corresponding to the images A, B, C and D are 10, 20, 30 and 35 mN/m, respectively. The height profile along the dark line drawn on the images are shown below the respective images. The scale bar represent a length of 200 nm.

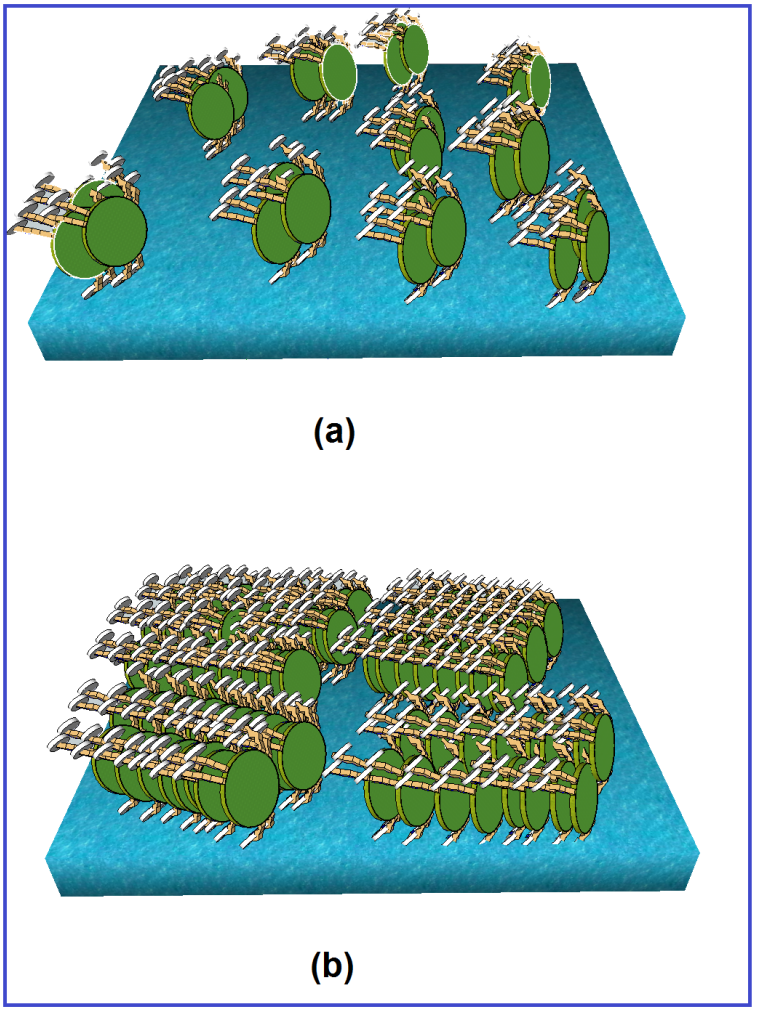

FIGURE 3.6: (a) The possible molecular conformation of TCQCB molecules at the A-W interface in L_1 phase. (b) The possible molecular conformation of TCQCB molecules at the A-W interface in L_2 phase.

shown in Figure 3.6b. In the L_2 phase, the molecules are shown to exhibit edge-on conformation in a highly dense surface layer. The molecules may form a compact layer by cancelling the intermolecular dipolar repulsion. Therefore, the side chains of the molecules are shown interdigitated with the side chains of the neighbouring molecules.

3.4 Conclusions

We found a stable LM of TCQCB molecules. The monolayer exhibits gas phase, L_1 and L_2 phases. The molecular orientation in L_1 and L_2 phases were found to be edge-on. The AFM images of the LB films deposited at $\pi_t \leq 10\ mN/m$ reveal the domains with vertical and tilted orientation of molecules. With increasing π_t,

the elongated domains were observed. The elongated domains as observed in L_1 phase undergoes a structural transformation to form a dense grainy texture in L_2 phase.

Bibliography

[1] A. Albrecht, W. Cumming, W. Kreuder, A. Laschewsky, and H. Ringsdorf, Col. Polym. Sci., 264, 659, 1986.

[2] N. C. Maliszewskyj, P. A. Heiney, J. K. Blasie, J. P. McCauley Jr., and A. B. Smith III, J. Phys. II (France), 2, 75, 1992.

[3] D. Gidalevitz, O. Y. Mindyuk, P. A. Heiney, B. M. Ocko, P. Henderson, H. Ringsdorf, N. Boden, R. J. Bushby, P. S. Martin, J. Strzalka, J. P. McCauley Jr., and A. B. Smith III, J. Phys. Chem. B, 101, 10870, 1997.

[4] N. C. Maliszewskyj, P. A. Heiney, J. Y.Josefowicz, J. P. McCauley Jr., and A. B. Smith III, Sci., 264, 77, 1994.

[5] A. Nayak, K. A. Suresh, S. K. Pal, and S. Kumar, J. Phys. Chem. B, 11, 11157, 2007.

[6] P. Ruffieux, O. Groning, M. Bielmann, C. Simpson, K. Mullen, L. Schlapbach, P. Groning, Phys. Rev. B, 66, 073409, 2002.

[7] R. Friedlein, X. Crispin, C. D. Simpson, M. D. Watson, F. Jackel, W. Osikowicz, S. Marciniak, M. P. de Jong, P. Samori, S. K. M. Jonsson, M. Fahlman, K. Mullen, J. P. Rabe, W. R. Salaneck, Phys. Rev. B, 68, 195414, 2003.

[8] C. Karthik, Manjuladevi V., Raj Kumar Gupta, and Sandeep Kumar, J. Mol. Struct., 1070, 52, 2014.

[9] S. Kumar, D. S. S. Rao and S. K. Prasad, J. Mater. Chem., 9, 2751, 1999.

[10] S. Kumar, Chemistry of discotic liquid crystals: From monomers to polymers, CRC Press, New York, 2010.

[11] R. K. Gupta and Manjuladevi V., Int. J. Nanosci. Nanotech., 101, 171, 2011.

Chapter 4

Fluorescence behavior of AmTCQ discotic LC molecules and its application for imaging in bulk and Langmuir monolayer

4.1 Introduction

The optical imaging of liquid crystals (LCs) provide vital physical insights related to molecular organization and the phase transitions [1, 2]. Various microscopy techniques like near-field scanning optical (NSOM), fluorescence, fluorescence confocal polarizing, two photon and third harmonic generation microscopy have been employed for such studies [3–12]. Using NSOM, Higgins et al. [3] have studied the local optical and electrooptical properties of boron-dipyrromethene dye doped polymer dispersed LC. Held et al. [6] have studied the textural transitions in a polymer stabilized cholesteric LC using confocal microscopy. Salter et al. [8] investigated LC director dynamics of nematic LC using two photon fluorescence microscopy. In all these microscopy techniques, the LC systems have been doped with some fluorescent probe molecules. Incorporation of additives may lead to either phase seperation or complex formation with the host molecules and thereby may alter the physical properties of the mixed system. So, it is preferable to employ some fluorescent probe with liquid crystalline nature which can be doped into a similar LC host. Several LC molecules with intrinsic fluorescence nature have been sythesized and are reported in literature [13–18]. For example,

Benning et al. [14] have shown 3, 4, 9, 10-tetra-(n-alkoxycarbonyl)-perylene to exhibit fluorescent behavior. Kim et al. [15] have synthesized highly fluorescent LCs containing benzoxazole moiety, and have investigated their photo-physical properties. Benjamin et al. [16] reported functional phasmidic LC with intrinsic luminescence properties. Salamonczyk et al. [17] reported LC with benzothiophene moiety to be fluorescent in nature.

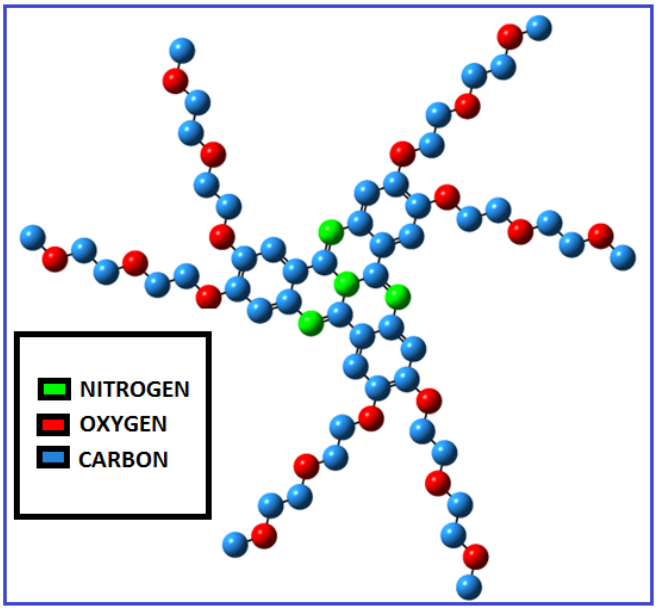

FIGURE 4.1: Ball and stick model of AmTCQ molecule

Solvatochromatism is one of the tools for quantifying the fluorescence response of dye molecules [19]. Several dye doped LC systems have been studied through solvatochromatism [20–22]. Marrucci et al. [20] investigated the role of dye structure in photoinduced reorientation of dye-doped LCs. They measured optical nonlinearity associated with photoinduced molecular reorientation of dye-doped nematic LCs for a homologous set of dyes belonging to the anthraquinone family, dissolved both in a polar and in a nonpolar LC host. Iwanaga et al. [21] showed that oligothiophene dyes show good solvatochromatic behavior in LCs and find its application in LC displays. Gilani et al. [22] showed solvatochromatism of fluorinated azoquinolin-8-ol dyes in LC solutions. In all such reported systems, LCs are doped with some dye molecules. The doping of dye molecules may give rise to impurity in LC system therfore, it is worth to study the solvatochromatic behavior of pure LC molecules exhibiting intrinsic fluorescence behavior. Such studies will provide valuable information for LC imaging and display applications. To our best of knowledge, there are no such studies on pure LC molecules. Disoctic liquid crystals (DLCs) possessing tricycloquinazoline (TCQ) core have been reported to be fluorescent [23]. In this chapter, for the first time we report

solvatochromatic studies on TCQ based molecules with 6 ethelenoxy side chains (AmTCQ) molecule without the aid of any dye. We have doped AmTCQ molecule into structurally similar DLC, hexa-alkoxy triphenylene (HAT5) molecule and have done fluroescence imaging. The fluorescene microscope images reveal the potential of AmTCQ molecules as a probe to study the optical properties of another DLC system. Epifluorescence microscopy technique can be used to visualize Langmuir monolayer (LM) at the A-W interface [24]. So, we further extended our studies by performing epifluorescence imaging of the LM of pure AmTCQ molecules. We found reasonable contrast for identifying phases in the LM of the AmTCQ molecules.

We recorded ultraviolet-visible (UV-VIS) and fluorescence spectra for the AmTCQ molecule in various solvents. The solvatochromatic shifts were estimated. The ground state and excited state dipole moment of AmTCQ molecule were determined using Lippert's [25], Bakhshiev's [26] and Kawski–Chamma–Viallet's [27, 28] equations. Using density functional theory (DFT) approach, the ground state dipole moment of the AmTCQ molecule was computed employing Gaussian 03 programme package. The computed value of the dipole moment was found to be in agreement with that estimated through experimental data. Calculations were performed to find the parameters like angular difference between the ground and excited state dipole moments, oscillator strength, transition dipole moment and relative quantum yields of the AmTCQ molecules in various solvents.

4.2 Materials and methods

4.2.1 Materials

Hexa-alkoxy triphenylene (HAT5) (Figure 5.1) was synthesized by Prof. Sandeep Kumar, Raman Research Institute, Bengaluru [29]. Spectroscopic grade chloroform ($CHCl_3$), ethanol, acetone, dimethylformamide (DMF), acetonitrile, dimethylsulfide (DMS), methanol, toluene, benzene, butanol, carbontetrachloride (CCl_4), cyclohexane, dichloromethane (DCM), diethylether, tetrahydrofuran (THF) were used as procured from Sigma Aldrich and Merck. Optical quality quartz plate (roughness$\sim$1 nm) was used for fluorescence imaging of the bulk LC doped with AmTCQ.

4.2.1 Experimental methods

The solutions of AmTCQ in various solvents were prepared at a fixed solute concentration of 0.26 mg/ml (Figure 4.2). The luminescence spectra measurements were done using Shimadzu spectrofluorimeter at excitation wavelength of 390 nm.

FIGURE 4.2: Solution of AmTCQ molecule prepared in $CHCl_3$ (0.26 mg/ml). The color of the solution appears to be yellowish-green.

The mixture of chloroform solution of HAT5 doped with 1, 5 and 10 mole percent of AmTCQ was spread on to the quartz plate. The solvent was allowed to evaporate for 60 minutes. The samples prepared were imaged using a fluorescence microscope (BX43 Olympus). All the experiments were carried out at 20 $\pm$ 0.3 °C. The LM of AmTCQ was observed under an epifluorescence microscope (Leitz Metallux 3). The gas phase appears dark and the liquid like phase appears bright in the epifluorescence images of LM of AmTCQ.

4.2.2 Computational methods

First principles electronic structure investigation was done on AmTCQ molecule using Gaussian 03 program package. The geometry optimization of AmTCQ molecule (Figure 8.1) was carried out within DFT framework. This was followed

with the evaluation of vibrational frequency analysis at the B3LYP level of theory. Ground state dipole moment of AmTCQ was calculated by exchange correlation functional as hybrid B3LYP with full electron 6-311 G basis set. It is one of the suitable and tested combination of theory in DFT for organic molecules [30–32].

4.2.3 Theoretical methods

The ground state and the excited state dipole moment values of AmTCQ molecule were estimated using the following equations.

Lippert's Equation :

$$v_a - v_f = mF(k,n) + c \tag{4.1}$$

Bakshiev's Equation :

$$v_a - v_f = m_1 F_1(k,n) + c \tag{4.2}$$

Kawski-Chamma-Viallet's Equation :

$$(v_a + v_f)/2 = -m_2 F_2(k,n) + c \tag{4.3}$$

Here v_a and v_f are the absorption and luminescence wavenumbers respectively, and c is a constant. The difference between v_a and v_f is Stoke's shift. F(k,n), F_1(k,n) and F_2(k,n) are Lippert's, Bakshiev's and Kawski-Chamma-Viallet's polarity functions given by equations 4.4, 4.5 and 4.6 in terms of dielectric constant (k) and refractive index (n) of the solvents used :-

Lippert's polarity function :

$$F(k,n) = \frac{k-1}{2k+1} - \frac{n^2-1}{2n^2+1} \tag{4.4}$$

Bakshiev's polarity function :

$$F_1(k,n) = \frac{2n^2+1}{n^2+2}\left(\frac{k-1}{k+2} - \frac{n^2-1}{n^2+2})\right) \tag{4.5}$$

Kawski-Chamma-Viallet's polarity function :

$$F_2(k,n) = \frac{2n^2+1}{2(n^2+2)}\left(\frac{k-1}{k+2} - \frac{n^2-1}{n^2+2}\right) + \frac{3n^4-1}{2(n^2-1)^2} \tag{4.6}$$

Slopes m and m_1 are estimated from the plots between F(k,n), $F_1(k,n)$ versus Stokes shift respectively. The slope m_2 is estimated from the plot of $F_2(k,n)$ vs. arithmetic mean of absorption and fluorescence wavenumber [25–28]. The values of slopes m, m_1 and m_2 can be further related to the ground state dipole moment (p_g), excited state dipole moment (p_e), Onsager radius cavity (a), Planck constant (h) and speed of light in vacuum (c) given by following equations :-

$$m = \frac{2(p_e - p_g)^2}{hca^3} \tag{4.7}$$

$$m_1 = \frac{2(p_e - p_g)^2}{hca^3} \tag{4.8}$$

$$m_2 = \frac{2({p_e}^2 - {p_g}^2)}{hca^3} \tag{4.9}$$

These equations are based on the Onsager's reaction field theory, which assumes that the fluoropore is a point dipole residing in the center of a spherical cavity in a homogeneous and isotropic dielectric with relative permittivity (k). The cavity radius chosen for our study is the radius of the TCQ core of AmTCQ molecule. The estimated value is 0.5 nm [23, 33].

Further the ground state and excited state dipole moments can also be calculated using the following equations :-

$$p_g = \frac{m_2 - m_1}{2}\left(\frac{hca^3}{2m_1}\right)^{\frac{1}{2}} \tag{4.10}$$

$$p_e = \frac{m_2 + m_1}{2}\left(\frac{hca^3}{2m_1}\right)^{\frac{1}{2}} \tag{4.11}$$

From equations[4.10 and 4.11] we get :-

$$p_e = \frac{|m_2 + m_1|}{|m_2 - m_1|}p_g \tag{4.12}$$

Generally excited state dipole moment and ground state dipole moment are not parallel to each other. So, the angular separation (ϕ) between them is estimated by the following relation [34, 35]

$$\cos\phi = \frac{1}{2p_g p_e}[({p_g}^2 + {p_e}^2) - \frac{m_1}{m_2}({p_e}^2 - {p_g}^2)] \tag{4.13}$$

Further from the fluorescence spectra, relative quantum yield, oscillator strength and transition dipole moment of the AmTCQ molecule are estimated. In the fluorescence spectra, maximum intensity was observed in case of AmTCQ in dichloromethane (DCM). So, relative quantum yield ($\frac{\phi_1}{\phi_2}$) can be calculated from the quantum yield of AmTCQ in various solvents (ϕ_1) with respect to AmTCQ in DCM (ϕ_2) using the following equation [36] :-

$$\frac{\phi_1}{\phi_2} = \frac{\left(1 - 10^{-A_2^*}\right) n_1^2 \alpha_1}{\left(1 - 10^{-A_1^*}\right) n_2^2 \alpha_2} \tag{4.14}$$

where subscript 1 refers to the various AmTCQ solutions and subscript 2 refers to the reference solution. A* is the absorbance at 390 nm which is the excitation wavelength. Here α is the area under the fluorescence curve for AmTCQ in a particular solvent and n is the refractive index of different solvents used.

The oscillator strength (f) of AmTCQ molecule in various solvents is computed using the following equation [37] :-

$$f = 4.32 \times 10^{-9} \epsilon_{max} \nu_{1/2} \tag{4.15}$$

The transition dipole moment of the AmTCQ molecule is obtained using the approximated equation below [38] :-

$$\mu = 0.0958 \left[\epsilon_{max} \times \frac{\nu_{1/2}}{\nu_{max}} \right] \tag{4.16}$$

where ϵ_{max} is the molar absorbance at the maximum, ν_{max} is wavenumber for maximum absorption and $\nu_{1/2}$ is band width at half maxima.

4.3 Results and Discussion

The absorption and the corresponding fluorescence spectra for AmTCQ in solvents with different polarity are shown in Figure 4.3. Values of absorption and fluorescence maxima wavenumbers have been calculated from the spectra. The UV-VIS spectroscopic measurements shows average absorption maxima at 402 nm. The luminescence spectra were recorded at excitation wavelength of 390 nm.

Figure 4.3 shows that the solvent-induced shift of the emission spectrum is higher than the shift in the absorption spectrum. The shift observed in spectral band

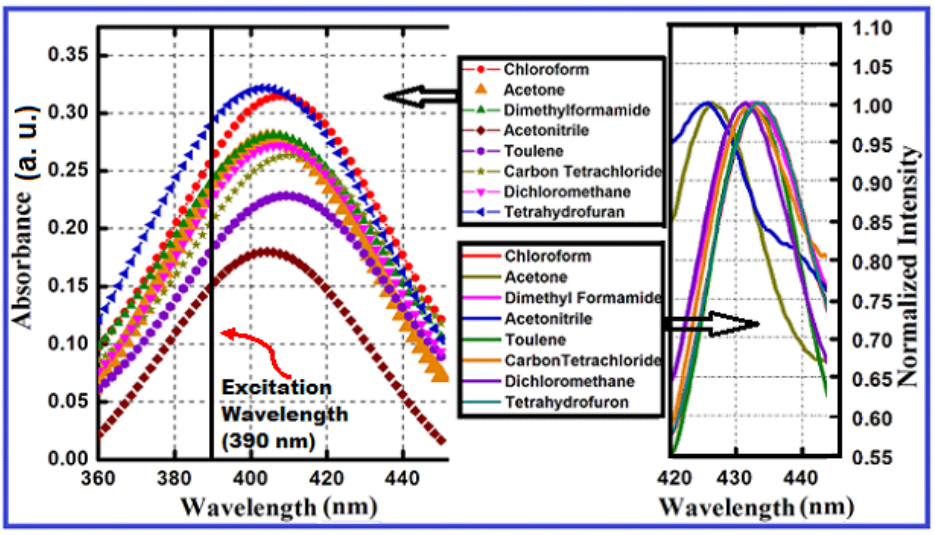

FIGURE 4.3: The UV-VIS (left side) and fluorescence (right side) curves of AmTCQ in various solvents.

arises from the large reaction field which a solute molecule experiences due to the polarization of the surrounding solvent molecules [39]. This is due to the larger excited-state permanent dipole moment of AmTCQ when compared to its ground state. The shifts observed are dependent on the nature of solvent (polar or non-polar), dielectric constant etc. This is evident from the fact that, in certain cases the shift in fluorescence spectrum of AmTCQ in various solvents is not necessarily accompanied by a shift in the absorption spectra; if exists, it need not be in proportion to the one observed in fluorescence [40]. Since in our case the excited state of a molecule is much different from its ground state, it may be more or less depending upon the transition involved, the ground state dipole moment may slightly change from solvent to solvent, but the excited state may be much different. Thus it is expected that little changes in absorption, while large change in the fluorescence spectrum with change in solvent.

TABLE 4.1: Spectral data: emission wavenumbers (v_f), absorption wavenumbers (v_a), Stoke's shift (v_f - v_a) and arithmetic mean of Stoke's shift ((v_f + v_a)/2)

Solvents used	v_f (cm^{-1})	v_a (cm^{-1})	v_f - v_a (cm^{-1})	(v_f + v_a)/**2** (cm^{-1})
Chloroform	23073.37	24517.01	1443.64	23795.19
Acetone	23397.29	24738.39	1341.11	24067.84
Acetonitrile	23408.24	24738.39	1330.15	24073.32
Dimethylformamide	23105.36	24738.39	1633.03	23921.88
Toluene	23126.73	24517.01	1390.28	23821.87
Dichloromethane	23126.73	24517.01	1390.28	23821.87
Carbontetrachloride	23141.18	24517.01	1375.83	23829.1
Tetrahydrofuran	22786.31	24738.39	1952.08	23762.35

Table 4.1 shows the absorption wavenumbers (v_a), emission wavenumbers (v_f), Stoke's shift (v_f - v_a) and arthermetic mean of emission and absorption wavenumbers ((v_f + v_a)/2) of AmTCQ in different solvents. Stoke's shift is an indicator about the change from ground state to excited state structure of AmTCQ molecule. They can be attributed to factors such as dipole-dipole interaction between solvent and solute, change in the nature of emitting state induced by solvent and specific solvent-solute interactions such as H-bonding [41]. They also define change in energies of levels of a solute due to change in the solvent medium. Emission states arise out of energy of more relaxed excited states and hence are more informative than absorption spectra. The parameters found using these shifts are vital for describing the intramolecular charge transfer in molecular excited states [42–47] and inter-molecular charge transfer in excited complex [48, 49].

In our present study, we have used non-polar (k<5), borderline polar aprotic (k ranges from 5-20) and polar aprotic solvents (k>20) for our calculations. We observed bathochromic shift (red shift) from ground to excited state of AmTCQ in solvents of different polarity. Due to the efficiency of vibrational relaxation there is loss of energy before fluorescent emission. This loss of energy results from several dynamic processes, including dissipation of vibrational energy, reorientation of the solvent molecules around the excited state dipole, redistribution of electrons in the solvent molecules as a result of the altered dipole moment of the excited fluorophore, and fluorophore-solvent interactions (such as hydrogen bonding). The shifts in the AmTCQ molecule in various solvents indicate that the transition involved is from a pi-bonding orbital to an antibonding (pi*) orbital (pi$\rightarrow$pi* transition) and lowest lying state of AmTCQ is pi$\rightarrow$pi*.

TABLE 4.2: Dielectric constants (k), refractive index (n) of the solvents, Lippert ($F(k,n)$), Bakhshiev ($F_1(k,n)$), Kawski Chamma Viallet ($F_2(k,n)$) solvent polarity function

Solvents used	k	n	$F(k,n)$	$F_1(k,n)$	$F_2(k,n)$
Chloroform	4.81	1.442	0.147	0.371	0.487
Acetone	21.09	1.359	0.289	0.791	0.641
Acetonitrile	36.64	1.344	0.312	0.863	0.665
Dimethylformamide	36.7	1.431	0.274	0.835	0.709
Toluene	2.38	1.497	0.012	0.033	0.351
Dichloromethane	8.93	1.424	0.218	0.589	0.582
Carbon tetrachloride	2.24	1.459	0.014	0.015	0.318
Tetrahydrofuran	7.58	1.407	0.209	0.549	0.551

Using equations [4.4-4.6], Lippert's, Bakshiev's and Kawski-Chamma-Viallet's polarity function for various solvents (Table 4.2) are calculated. The k and n values were taken from the literature [50]. In Figure 4.4, the plot (a) is Stokes

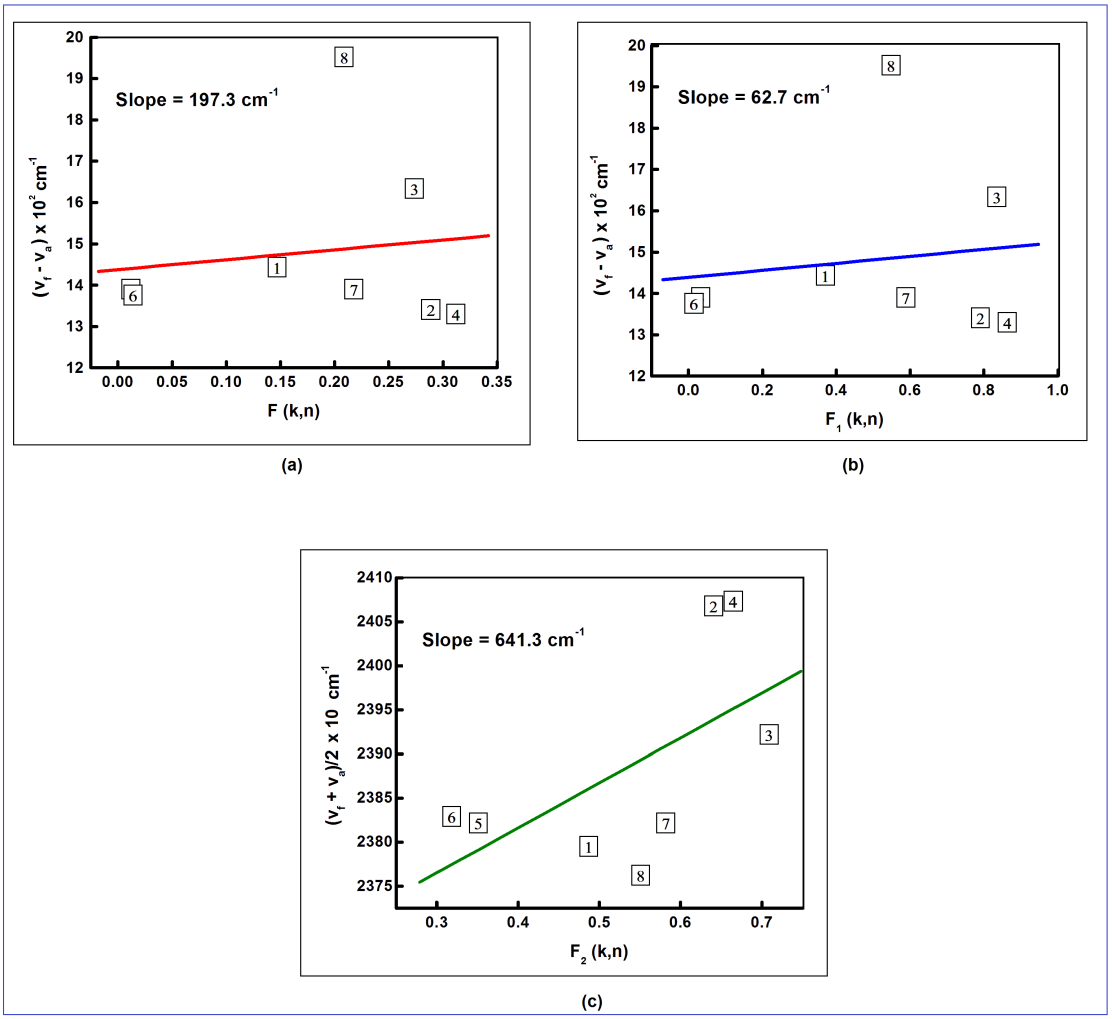

FIGURE 4.4: The plot (a) is stokes shift versus Lippert polarity function (F(k, n)), (b) is stokes shift versus Bakshiev polarity function ($F_1(k,n)$) and (c) is arithmetic mean of emission/absorption wavenumbers versus Kawski Chamma Vallet polarity function ($F_2(k,n)$) of AmTCQ in various solvents: (1) chloroform, (2) acetone, (3) acetonitrile, (4) Dimethyl formamide, (5) toluene, (6) Dichloromethane, (7) Carbon tetrachloride, (8) THF. (———Linear fit)

shift versus $F(k,n)$; (b) is Stokes shift versus $F_1(k,n)$; and (c) is arithmetic mean of emission and absorption wavenumbers versus $F_2(k,n)$ of AmTCQ molecule in various solvents. The linear dependence of spectral shifts on polarity functions (Figure 4.4) exhibits a good correlation. It can be seen that, a majority of solvents obey the linear plots. Deviation of few solvents from linearity may be due to specific solute-solvent interactions.

From Figure 4.4, slopes m, m_1 and m_2 were estimated to be 239.23, 84.85 and 509.29 cm^{-1} respectively. The ground state dipole moment (p_g) value of AmTCQ molecule was calculated to be 2.56 D using Equation 4.10. The excited dipole moment (p_e) of the AmTCQ molecule was found to be 3.59 D (Table 4.3). The

TABLE 4.3: Estimated values of ground state p_g and excited state p_e dipole moment

Calculations	p_g **(D)**	p_e **(D)**	p_e / p_g	ϕ
Estimated	2.56	3.59	1.40	0 °
Gaussian'03	3.20			
Lippert's Theory		4.28		
Bakshhiev's Theory		3.85		
Kawski Chamma Vallet's Theory		3.85		

higher value of excited state dipole moment compared to that of ground state of the AmTCQ might be due to an increase in charge separation in the excited state. The change in the excited state dipole moment with reference to ground state dipole moment (δp) i.e p_e - p_g and the ratio of ground state and excited state dipole moment ($\frac{p_e}{p_g}$) of the AmTCQ molecule was found to be 1.03 and 1.40 respectively. It can be seen that the p_e value obtained for AmTCQ molecule by Lippert method is large as compared to values obtained by all other methods. It is due to the fact that this method does not take into account the polarizability of the solute. It is observed that the shift of emission peak with change in solvent polarity are more pronounced than the shift of absorption peak, indicating $p_e > p_g$; i.e. the dipole moment of the molecules increase on excitation. Therefore, the excited state of AmTCQ is more polar than the ground state.

Using Gaussian 03, the ground state dipole moment value of the AmTCQ molecule was computed to be 3.2 D. The inconsistency in the estimated and computed values of dipole moment is due to the fact that the molecule is considered as an isolated system (as in gas phase) during computation, whereas the experimentally obtained values are in solution phase, where the solvent (matrix) introduces strong perturbation. Further it is evident from Table 4.3 that the changes in the dipole moments of the AmTCQ molecule on electronic excitation is rather small. This suggests that the emission of the AmTCQ molecule originates from a state, which although more polar than ground state, is probably a locally excited intramolecular charge transfer (ICT) state. Charge transfer accompanying excitation to lowest excited singlet state usually results in the excited molecule having a greater dipole moment than the ground state [51]. Usually while estimation of these parameters, many authors [52–55] assumed that excited state dipole moment is almost parallel with the ground state. Accordingly using Equation 4.13, no angular separation was found between the excited and ground state dipole moment of the AmTCQ molecule (0 °). Hence, the dipole moments in both the states were found to be collinear.

The polarity of a solvent generally influences the fluorescence-emission spectra

of fluorophores. Changes in quantum yields and shifts in spectra are valuable parameters of fluorophore sensitivity to the solvent polarity. Quantum yield is the ratio of total number of emitted photons (number of emitted photons is represented by the area under a fluorescence emission-spectrum) to the total number of photons absorbed. The sensitivity of fluorophores to solvent polarity has practical applications in the field of physical biochemistry. When fluorophores are bound to proteins, nucleic acids, membranes, or macromolecules, in general, the fluorescence-emission spectra change. These changes can be employed to detect binding sites on macromolecules or to determine the polarity of binding sites [56].

TABLE 4.4: Absorbance (A), Absorbance at excitation wavelength (390 nm) (A*), Polarity (P), Quantum Yield (ϕ_1/ϕ_2)

Solvents used	**A**	**A*(390 nm)**	**P**	ϕ_1/ϕ_2
Chloroform	0.27	0.22	4.1	0.2
Acetone	0.26	0.22	5.1	0.1
Acetonitrile	0.21	0.18	5.8	0.014
Dimethylformamide	0.24	0.2	6.4	0.084
Toluene	0.21	0.16	2.4	0.754
Dichloromethane	0.25	0.21	3.1	1
Carbontetrachloride	0.22	0.17	1.6	0.29

The estimation of relative quantum yield of AmTCQ in various solvents to AmTCQ in dichloromethane has been summarized in Table 4.4. The estimated values indicated maximum quantum yield for AmTCQ in toluene with respect to AmTCQ in dichloromethane and minimum quantum yield for AmTCQ in acetonitrile with respect to AmTCQ in dichloromethane. The hydrogen-bonded solvents generally show a greater red shift than those which do not form hydrogen bond. Hence, larger quantum yields are observed in solvents with no hydrogen bonding. The estimated relative quantum yield value of AmTCQ in acetonitrile is very low which could be due to emissionless deactivation processes during the transition from the excited state to ground state.

TABLE 4.5: Molar absorbance (ϵ), Band shift at half maxima (Δv_a), oscilator strength (f), transition dipole moment (μ_t)

Solvents used	ϵ **max**	Δv_a (cm^{-1})	f	μ_t**(D)**
Chloroform	864	144508.7	0.539	6.84
Acetone	832	152671.8	0.548	6.86
DMF	672	152671.8	0.443	6.17
Acetonitrile	768	137362.6	0.455	6.26
Toluene	672	152671.8	0.443	6.2
Carbontetrachloride	800	137362.6	0.474	6.41
Dichloromethane	704	144508.7	0.439	6.17
Tetrahydrofuran	896	144508.7	0.559	6.93

Oscillator strength (f) which is a measure of the integrated intensity of the charge transfer complex and transition dipole moment (μ_t) of AmTCQ in various solvents have been summarized in Table 4.5. The values of the calculated oscillator strength indicate a strong interaction between the donor – acceptor pair with relative high probability transitions in AmTCQ. The maximum strength of the AmTCQ molecule was found out to be in tetrahydrofuran.

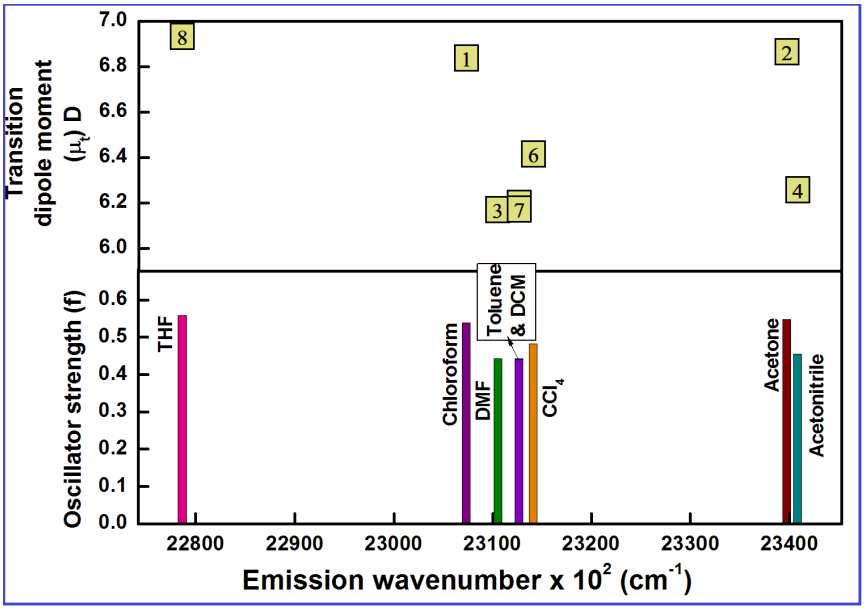

FIGURE 4.5: The plot shows variation of transition dipole moment (Top) and Oscillator strength (Below) as the function of emission wavenumber for AmTCQ in various solvents: (1) chloroform, (2) acetone, (3) Dimethyl formamide, (4) acetonitrile, (5) toluene, (6) Carbon tetrachloride,(7) Dichloromethane, (8) THF.

The transition dipole lengths of AmTCQ molecule in various solvents from absorption data is listed in Table 4.5. They are based on the assumption of complete transfer of one unit charge in the transition. It is reasonable to assume that this represents a maximum in the amount of charge that might be separated, and therefore a minimum length for the charge separation [38, 57]. The estimated values ranged from 6.17-6.93 D. However, oscillator strength values for AmTCQ in toluene, DMF and DCM was found to be same. The transition dipole moment values for AmTCQ in DMF and DCM was found to be same (Figure 4.5).

In our study, we found the solvatochromatic shifts without the aid of any inorganic or organic dye. This is an indicator of the AmTCQ molecule acting as a fluoropore itself, hence does not require any dye to aid solvatochromatism. In order to employ AmTCQ molecules for fluorescence imaging, we doped another DLC system, HAT5 with 1, 5 and 10 mole percent of AmTCQ molecule. The fluorescence image of pure AmTCQ molecule reveals bright green uniform region (Figure 4.6a). However

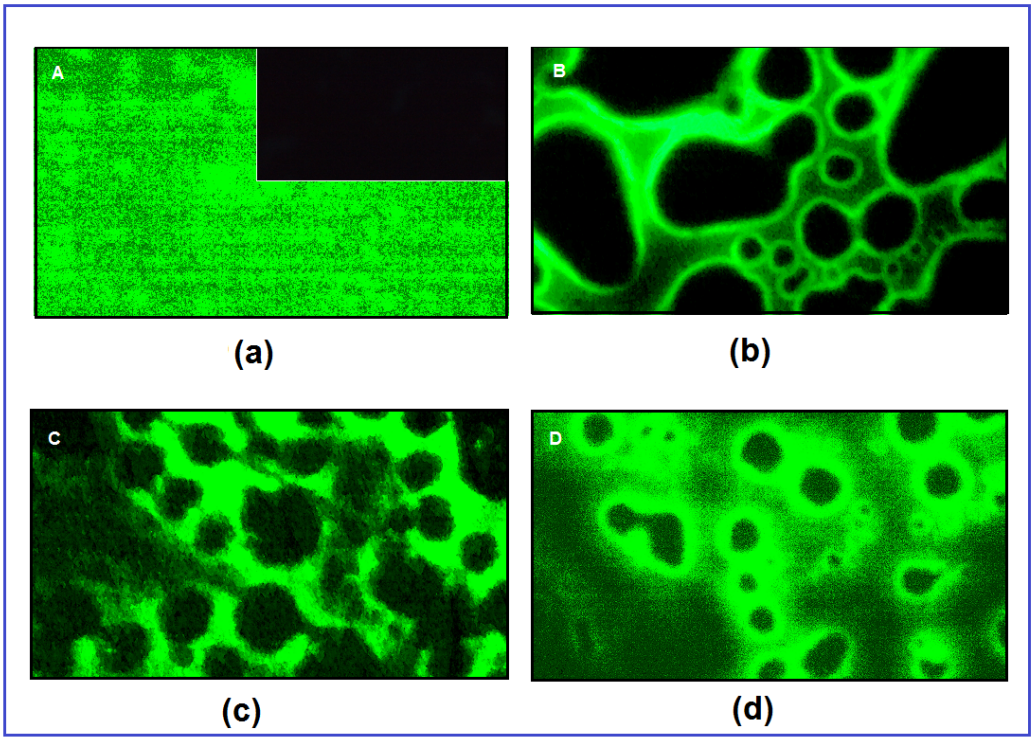

FIGURE 4.6: The fluorescence microscopy images of (a) AmTCQ molecue (Bright green region) (Inset shows fluorescence microscopy image of HAT5 (Dark region)) and HAT5 doped with (b) 1 (c) 5 (d) 10 mole percent of AmTCQ.

the fluorescence image of pure HAT5 shows complete dark region indicating no signature of fluorescence (inset in (Figure 4.6a) The image corresponding to 1 % of AmTCQ in HAT5 (Figure 4.6b) shows bright green texture. The brightness increases with the increase in the concentration of AmTCQ in HAT5 (Figure 4.6c and Figure 4.6d). This indicates that even with 1 mole percent of AmTCQ in HAT5 the imaging of a LC system can be obtained.

In order to observe the LM of AmTCQ molecules at the A-W interface, we have carried out the epifluorescence microscopy [58] without the aid of any fluoropore. The epifluorescence images were captured at the points A abd B as indicated in the isotherm of the AmTCQ monolayer (Figure 4.7a) and they are shown in Figure 4.7b. Both the figures shows bright region indicating the fluorescent feature of the AmTCQ molecules. Figure 4.7b(A) shows bright region and darks regions. The bright region is due to the liquid like phase of the AmTCQ molecules whereas the dark voids indicate the gas phase. On compression the dark region disappears leading to a uniform bright region. This indicates that on compression of the monolayer, the gas phase disappears and a uniform liquid-like phase appears (Figure 4.7b(B)). Such observation further confirms that AmTCQ molecules can be employed for various fluorescence studies.

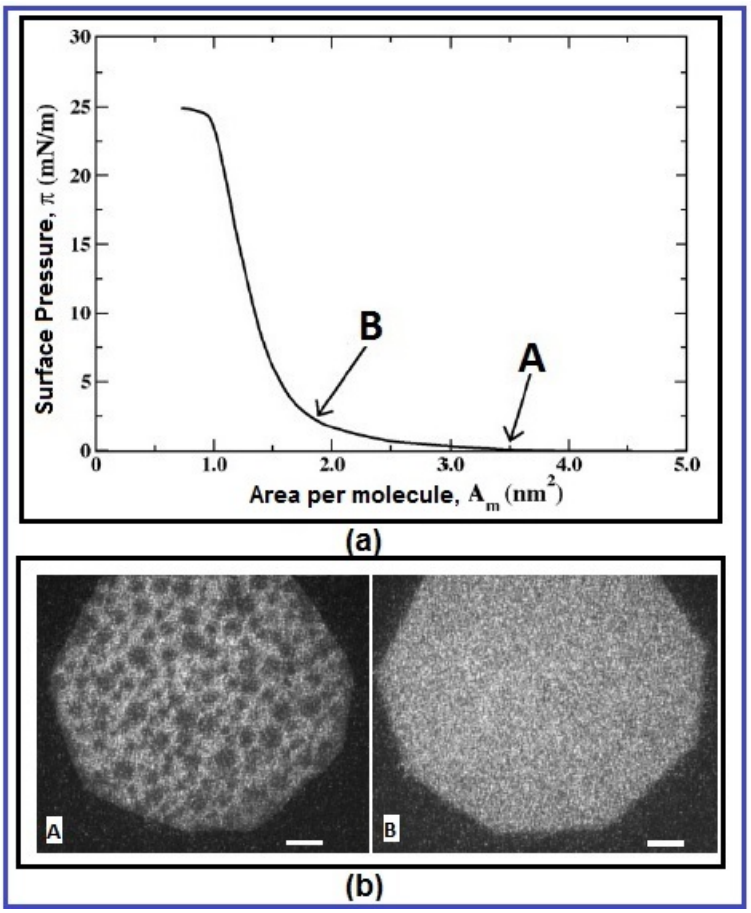

FIGURE 4.7: (a) Isotherm of LM of AmTCQ molecule at A-W interface. The arrows on the isotherm indicate the position at which the epifluorescence images were captured. (b) The epifluorescence images of LM of AmTCQ captured at A and B as indicated in the isotherm. Image A shows gas-liquid like coexistence phase and Image B shows liquid like phase. The scale bar is 500 μm in length.

4.4 Conclusions

The effect of various solvents of different polarity on photophysical properties of AmTCQ molecule was studied. We observed red shift in the emission spectra with increase in polarity of the solvent. The Stoke's shift, Lippert's, Bakshiev's, and Kawski–Chamma–Viallet's polarity function were estimated from the experimental data. We found the ground and excited state dipole moment value of the molecule to be 2.56 D and 3.59 D respectively. Computationally, the ground state dipole moment value was calculated to be 3.20 D using Gaussian 03 package. Angular separation predicted the excited and ground state dipole moment to be parallel to each other.

Our study indicates that AmTCQ can be employed for imaging another non-fluorescent DLC. It will be interesting to study the photophysical properties

of such molecules in a confined geometry formed by different mesophases of LCs. The potential of TCQ based LC should be used for imaging using confocal and two-photon microscopy. Figure 4.8 shows a schematic diagram of an application of AmTCQ in the fluorescence imaging of another DLC.

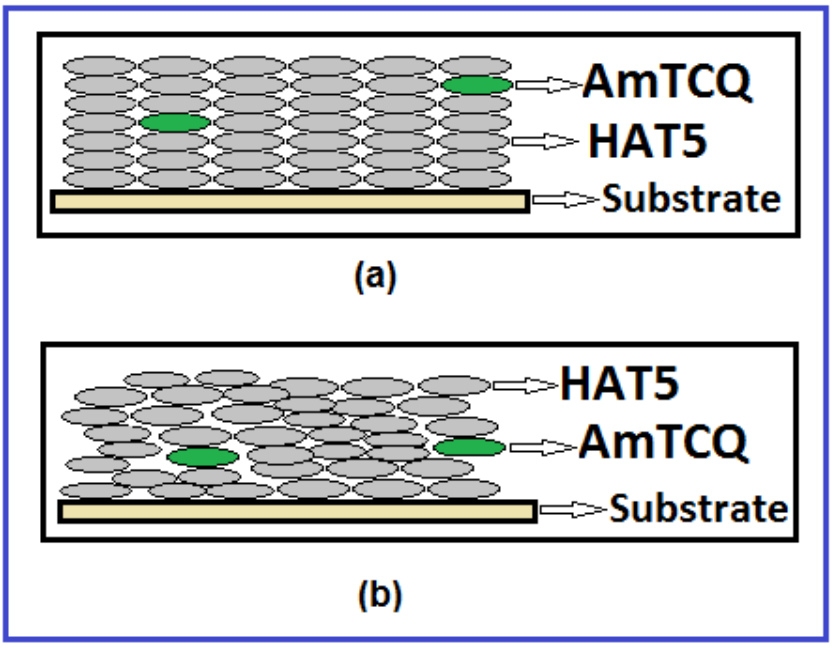

FIGURE 4.8: Schematic view of fluorescence imaging on HAT5 with the aid of fluorescent AmTCQ molecule in a) columnar phase b) nematic phase.

Bibliography

[1] Feringa, Ben L., Ed., Molecular switches, Weinheim, Wiley-vch, 2001.

[2] Michael C. Petty, Martin R. Bryce and David Bloor, An introduction to molecular electronics, Oxford University Press, USA, 1995.

[3] Higgins, A. Daniel , et al., J. Phys. Chem. B, 105, 5874, 2001.

[4] K. Amundson, A. van Blaaderen and P. Wiltzius, Phys. Rev. E, Stat. Phys. Plasmas Fluids Relat. Interdiscip. Topics, 55, 1646, 1997.

[5] M. Ofuji, Y. Takano, Y. Houkawa, Y. Takanishi, K. Ishikawa, H. Takezoe, T. Mori, M. Goh, S. Guo and K. Akagi, Jpn. J. Appl. Phys., 45, 1710, 2006.

[6] G. A. Held, L. L. Kosbar, I. Dierking, A. C. Lowe, G. Grinstein, V. Lee and R. D. Miller, Phys. rev. lett., 79, 3443, 1997.

[7] Lavrentovich and O. D., Pramana, 61, 373, 2003.

[8] P. S. Salter, G. Carbone, E. J. Botcherby, T. Wilson, S. J. Elston and E. P. Raynes, Phys. rev. lett., 103, 257803, 2009.

[9] W. Denk, J. H. Strickler and W. W. Webb, Sci., 248, 73, 1990.

[10] R. S. Pillai, M. OhE, H. Yokoyama, G. J. Brakenhoff and M. Muller, Opt. Express, 14, 12976, 2006.

[11] lin, Y. Silberberg, Y. Barad and J. S. Patel, Appl. Phys. Lett., 74, 3107, 1999.

[12] D. Yelin, Y. Silberberg, Y. Barad, and J. S. Patel, Phys. Rev. Lett., 82, 3046, 1999.

[13] Larrabee, Robert Dean, U.S. Patent No. 3, 960, 753, 1976.

[14] S. Benning, , et al., Liq. Crys., 27, 901, 2000.

[15] Kim, Sehoon and Soo Young Park, Mol. Crys. Liq. Crys., 337, 405, 1999.

[16] Hoag, P. Benjamin and L. Gin. Douglas , Adv. Mat., 10, 1546, 1998.

[17] M. Salamonczyk, et al., App. Phys. Lett., 95, 171901, 2009.

[18] A. C. Sentman and D. L. Gin., Adv. Mat., 13, 1398, 2001.

[19] C. Reichardt and T. Welton, Solvents and solvent effects in organic chemistry, John Wiley Sons., New York, 2011

[20] L. Marrucci, D. Paparo, M. Vetrano, M. Colicchio, E. Santamato and G. Viscardi, J. Chem. Phys., 113, 10361, 2000.

[21] H. Iwanaga, K. Naito and F. Effenberger, Liq. crys., 27, 115, 2000.

[22] A. Ghanadzadeh Gilani, M. Yazdanbakhsh, N. Mahmoodi, M. Moghadam and E. Moradi, J. Mol. Liq., 139, 72, 2008.

[23] E. Keinan, S. Kumar, S. Singh, R. Ghirlando and E. J. Wachtel, Liq. crys., 11, 157, 1992.

[24] V. von Tscharner and H. M. McConnell, Biophys. J. 36, 409, 1981.

[25] E. Lippert, Bull. Chem. Soc. Jpn, 29, 465, 1956.

[26] N. Bakshiev, O. Girin and V. Libov, Opt Spectrosc, 14, 395, 1963.

[27] A. Kawski, Zeitschrift Fur Naturforschung A, 57, 255, 2002.

[28] A. Chamma and P. Viallet, Acad Sci Ser C, 1901, 1970.

[29] S. Kumar, Chemistry Of DLCs: From Monomers To Polymers, Taylor and Francis, US, 2010.

[30] J. Montgomery Jr, M. Frisch, J. Ochterski and G. Petersson, J. Chem. Phys., 110, 2822, 1999.

[31] P. Cimino, L. Gomez-Paloma, D. Duca, R. Riccio and G. Bifulco, Mag. Res. Chem., 42, S26, 2004.

[32] R. Jain, T. Bally and P. R. Rablen, J. Org. Chem., 74, 4017, 2009.

[33] R. K. Gupta, V. Manjuladevi, C. Karthik, S. Kumar and K. Suresh, Coll. Surf. A, 410, 91, 2012.

[34] P. Suppan, Chem. Phys. Lett., 94, 272, 1983.

[35] Y. H. Zhao, M. H. Abraham and A. M. Zissimos, J. Org. Chem., 68, 7368, 2003.

[36] Morris, John V., Mary A. Mahaney and J. Robert Huber, J. Phys. Chem., 80, 969, 1976.

[37] H. Tsubomura and R. P. Lang, J. Ame. Chem. Soc., 83, 2085, 1961.

[38] P. Venuvaanlingan, U.C. Singh, N.R. Subbaratnam, Spect. Act., 37, 505, 1981.

[39] J.R. Lombardi, J. Phys. Chem. A, 102, 2817, 1998.

[40] A. J. Pesce, C.G. Rosen, T. Pasby, Fluorescence Spectroscopy, Marcel Dekker, New York, 1971.

[41] George, Gisha, Photochemical and photophysical studies of a few bischromophoric systems, 2010.

[42] M. B. Ledger, P. Suppan. Spectrochim. Acta, 23A, 641, 1967.

[43] P. Suppan. J. Chem. Soc., 4, 3125, 1968.

[44] M. Ito, K. Inuzuka, M. Imanishi, J. Am. Chem. Soc., 82, 1317, 1960.

[45] P. Suppan, C. Tsiams, Spectrochim. Acta, 36A, 364, 1980.

[46] D.K. Deshpande, M.A. Shashidhar, K. Suryanarayana Rao, Z. Phy. Chem., Leipzig, 262, 588, 1981.

[47] L. S. Prabhumirashi, D. K. Narayan Kutty, A. S. Bhide, Spectrochim. Acta, 39A, 663, 1983; L. S. Prabhumirashi, Spectrochim. Acta, 39A, 91, 1983.

[48] Z. R. Crabowski, K. Rothiewicz, A. Siemiarezuk, D. J. Cowley, W. Baumann, Nouv. J. Chem., 3, 443, 1979.

[49] H. Beans, H. Knibbe, A. Weller, J. Chem. Phys., 47, 1183, 1967.

[50] A. Chamma and P. Viallet, Acad Sci Ser C, 1901, 1970

[51] V. K. Sharma, P. D. Saharo, N. Sharma, R. C. Rastogi, D. Mohan, Spectrochim. Acta A, 59, 1161, 2003.

[52] B. Siddlingeshwar, S. M. Hanagodimath, Spectrochim. Acta Part A: Mol. Bio. Spect., 72, 490, 2009.

[53] Janina Kabatac, Borys Osmialowski, Jerzy Paczkowski, Spectrochim. Acta Part A: Mol. Bio. Spect., 63, 524, 2006.

[54] D. S. Biradar, B. Siddlingeshwar, S. M. Hanagodimath, J. Mol. Struct., 875, 108, 2008.

[55] J. Thipperudrappa, D. S. Biradar, S. R. Manohara, S. M. Hanagodimath, S. R. Inamadar, R. J. Manekutla, Spectrochim. Acta Part A: Mol. Bio. Spect., 69, 991, 2008.

[56] Lakowicz, J. R. Principles of Fluorescence Spectroscopy, Plenum Press, New York, 1986.

[57] Paley, M. S., Harris, J. M., Looser, H., Baumert, J. C., Bjorklund, G. C., Jundt, D. and Twieg, R. J., J. Org. Chem., 54, 3174, 1989.

[58] V. von Tscharner and H. M. McConnell, Biophys. J. 36, 409, 1981.

Chapter 5

Studies on thin films of discotic liquid crystal, hexa-alkoxy triphenylene (HAT5) doped with TiO_2 nanoparticles

5.1 Introduction

In our previous chapters, we reported our studies on tricycloquinazoline (TCQ) based discotic liquid crystals (DLCs) [1, 2]. On altering the molecular interaction by altering the side chain, we found interesting molecular states in the different surface phases exhibited by the Langmuir monolayer (LM) of TCQ based DLC.

DLC act as semiconducting material on its alignment with proper doping. Since most DLC materials possess characteristics of an acceptor and exhibit high mobility due to their columnar arrangement, they may become a potential candidate for photovoltaic devices [3]. When DLC is doped with p-type or n-type material, it finds application in light emitting diodes [4] and organic solar cells [5]. It has been observed that the Langmuir Blodgett (LB) films of a polymer possessing triphenylene moieties in the side groups show in plane conductivity [6]. The efficiency and sensitivity of a device increases manifold, if the functional material is spread to form ultrathin films. Such enhancement occurs due to increase in surface-to-volume ratio of the material. There are some studies on the ultrathin films of DLC materials [2, 7–10].

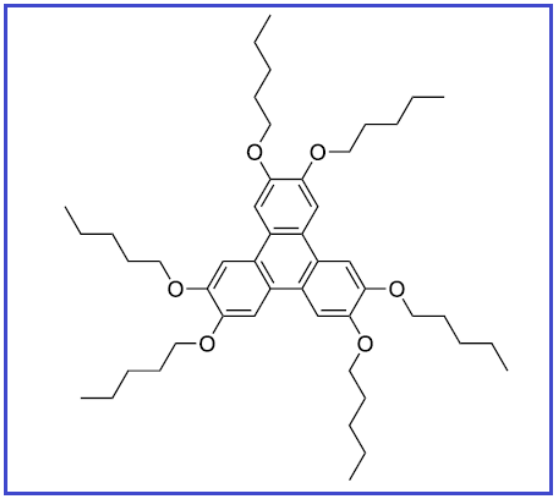

FIGURE 5.1: Chemical structure of hexalkoxytriphenylene (HAT5).

In this chapter, we have doped a commonly studied DLC, hexa-alkoxy triphenylene (HAT5) with TiO_2 nanoparticles and studied the properties at interfaces. HAT5 (Figure 5.1) forms a stable LM at the air water interface [11, 12]. HAT5 acts as acceptor molecule (p-type) having high charge mobility. The TiO_2 nanoparticles act as n-type dopant [13] to the HAT5 monolayer.

The monolayers of HAT5 as well as HAT5+TiO_2 nanocomposites at the A-W interface are found to be stable. The LM of HAT5 nanocomposites when compared to that of pure HAT5 condenses due to TiO_2 doping. We found that the high density liquid phase of HAT5 appears unperturbed qualitatively even on doping of TiO_2 nanoparticles. We deposited the LB films of HAT5 and HAT5+TiO_2 nanocomposites at different target surface pressure (π_t). The LB films were characterized using ultraviolet-visible (UV-VIS) spectroscopy and atmoic force microscopy (AFM).

We found that the energy gap decreases due to doping of TiO_2 nanoparticles in HAT5 and it reduces rapidly for the LB films of HAT5 and HAT5+TiO_2 deposited at the higher π_t. The surface morphology of the LB films deposited in the low density liquid (L_1) and high density liquid (L_2) phase of HAT5 and HAT5+TiO_2 nanocomposites show increase in density and size of clusters of TiO_2 nanoparticles with the increase in wt.% of the TiO_2 nanoparticles in the HAT5 matrix.

5.2 Experimental Methods

HAT5 molecule was synthesized by Prof. Sandeep Kumar, Raman Research Institute, Bengaluru [1]. TiO_2 nanoparticles were procured from Sigma Aldrich. The solutions of both TiO_2 and HAT5 were prepared in chloroform (HPLC grade) with a concentration of 1 mg/ml. The solutions were mixed appropriately so as to obtain HAT5+TiO_2 nanocomposites of 5, 10, 15 and 20 wt.% of TiO_2 nanoparticles in HAT5. The spreading volume was kept at 300 μl. All the experiments were done at room temperature ($\sim$22°C). We recorded surface pressure (π) - area per molecule (A_m) isotherms for pure HAT5 and as well as for HAT5 nanocomposites using the LB trough. The barrier speed during compression was kept at 20 mm/min.

The LB films of pure HAT5 and HAT5 + TiO_2 nanocomposites with 5 and 20 wt.% of TiO_2 in L_1 (π_t = 2 mN/m) and L_2 phase (π_t = 20 mN/m) were deposited on to the coverslips. The dipper speed was maintained at 5 mm/min. The LB films were characterized using UV-VIS spectroscopy. The UV-VIS spectra was recorded for the LB films in transmission mode. The energy gap [14] was calculated as :-

$$E = \frac{hc}{\lambda} \tag{5.1}$$

where E is the energy gap, h is Planck's constant, c is the velocity of light in vacuum and λ is the absorption wavelength at which the peak is observed. Topographic images of the LB films were obtained by using AFM. The films were scanned using Si tips having spring constants between 1 to 10 N/m in contact mode.

5.3 Results and Discussion

Figure 5.2 shows π - A_m isotherms of the LM of pure HAT5 and HAT5+TiO_2 nanocomposites with 5, 10, 15 and 20 wt % of TiO_2 nanoparticles. The isotherm of the pure HAT5 (inset of Figure 5.2) shows a lift-off area (A_i) to be around 800 cm^2.

Initially, the π rises slowly on decreasing the area. There is a rapid increase in surface pressure at area less than 700 cm^2 till the monolayer collapses at around collapse surface pressure (π_c) of 30 mN/m. The region of the isotherm corresponding to the sharp rise in π indicates L_2 phase. The slope change in the isotherm at around π of 30 mN/m is due to collapse of the monolayer. Unlike a

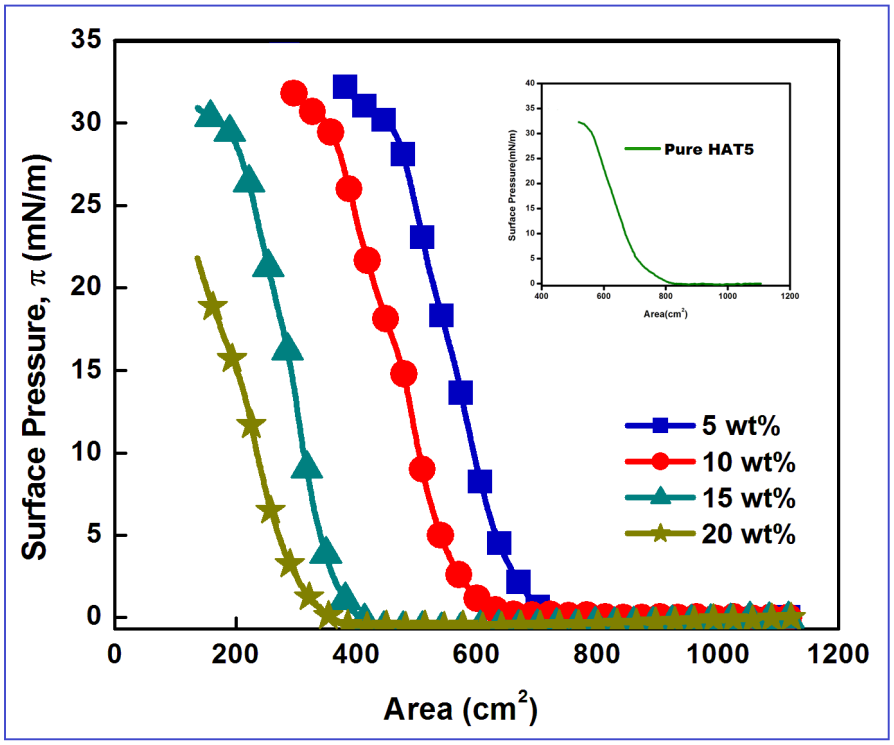

FIGURE 5.2: Surface pressure (π)- Area (A) isotherms of Langmuir monolayer of the pure HAT5 (inset) and HAT5+TiO_2 nanocomposite with TiO_2 nanoparticles at different wt.% at the air-water interface.

sharp drop in π as observed in the case of stearic acid, here the collapse is slow. In case of HAT5+TiO_2 nanocomposites, due to the presence of TiO_2 nanoparticles, the isotherms shift towards the lower area indicating a condensation effect on the monolayer. The A_i decreases on increasing the wt.% of TiO_2 in the LM of HAT5+TiO_2 nanocomposites. The A_i obtained were as 750, 620, 425 and 370 cm^2 for the HAT5 nanocomposites with 5, 10, 15 and 20 wt.% of TiO_2 nanoparticles, respectively. Figure 5.3 shows the variation of A_i as a function of wt.% of TiO_2 nanoparticles. It can be noted that the variation is non-linear. Therefore, the TiO_2 nanoparticles interact significantly with the HAT5 molecules at the interface and thereby introducing condensation effect on the monolayer. The π_c appears to remains unchanged for the HAT5+TiO_2 nanocomposites. The overall nature of the isotherms of the HAT5+TiO_2 nanocomposites also remains similar to that of pure HAT5. Therefore, the L_2 phase of the HAT5+TiO_2 nanocomposites appear similar to that of the isotherm of pure HAT5.

The LB films, HAT5 and HAT5+TiO_2 nanocomposites (5 and 20 wt.%) are deposited onto glass coverslips at the π_t of 2 and 20 mN/m. The average transfer ratios for the LB deposition of HAT5 and HAT5 doped with 5 and 20 wt % TiO_2 are found to be 0.74, 0.81, 0.92 at 2 mN/m and 0.86, 0.91, 0.95 at 20 mN/m,

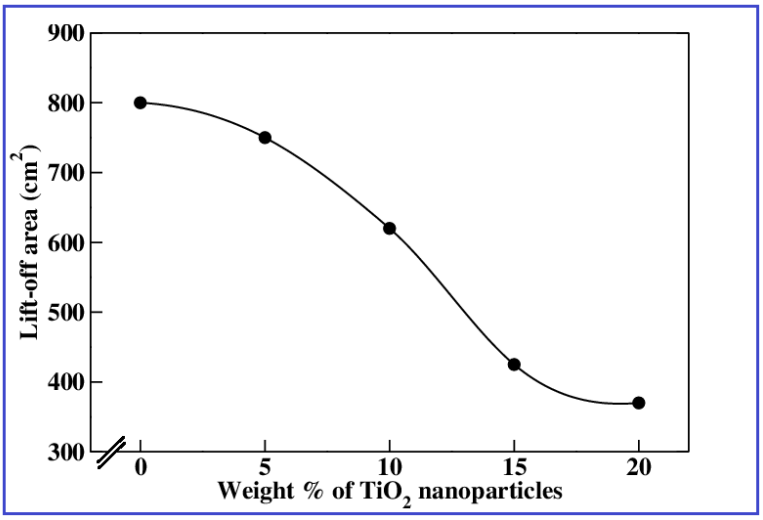

FIGURE 5.3: The variation of lift-off area (A_i) as a function of wt.% of TiO_2 nanoparticles in the HAT5 monolayer. The continuous line is to indicate the non-linear behavior of the variation.

respectively. The transfer efficiency is found to be better not only at the higher π_t but also for the higher wt.% of the TiO_2 nanoparticles in the HAT5.

We observe red shift in the spectrum as the concentration of TiO_2 in HAT5 increases for LB films deposited at π_t of 2 mN/m (Figure 5.4a) as well as for π_t of 20 mN/m (Figure 5.4b). For the LB film deposited at π_t of 2 mN/m, we obtain energy gap value for the pure HAT5 as 3.43 eV. Similarly, the LB film of the pure HAT5 at π_t of 20 mN/m indicate the energy gap to be 3.25 eV (Figure 5.5).

These values of energy gap are comparable to energy gap for bulk HAT5 i.e. 3.2 eV [15]. The TiO_2 nanoparticles are n-type semi-conducting material and it is expected that doping these nanoparticles into HAT5 may reduce the energy gap. Hence, it is observed that as the concentration of the TiO_2 nanoparticles is varied from 5 to 20 wt %, energy gap value decreases systematically from 3.3 to 3.18 eV for the film deposited at π_t of 2 mN/m and 3.09 to 2.81 eV for the film deposited at 20 mN/m. Further the reduction in energy gap is larger for the LB film deposited at π_t of 20 mN/m than compared to the one deposited at π_t of 2 mN/m. Decrease in the energy gap value indicates better charge mobility which is an important factor in improving the power efficiency of the bulk heterojunction photovoltaic cells [3].

The AFM images of the LB films of HAT5 and HAT5+TiO_2 nanocomposites (5 and 20 wt.%) deposited in the L_1 and L_2 phase are shown in Figure 5.6 and 5.7. The AFM image (Figure 5.6a and Figure 5.7a) of the LB film of pure HAT5

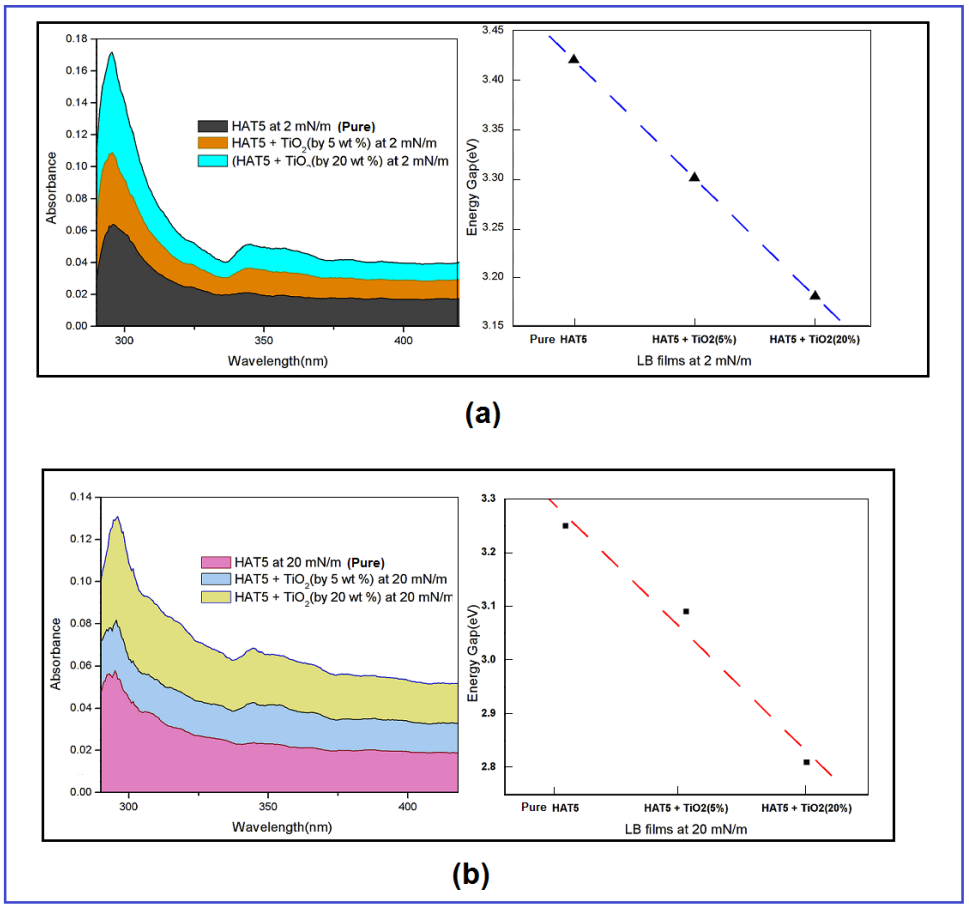

FIGURE 5.4: UV-VIS (a) (Left side) UV-Vis absorption spectra measurements for LB films of HAT5, HAT5+TiO_2 nanocomposites with 5 and 20 wt % of TiO_2 deposited on the glass coverslips at a target surface pressure (π_t) of 2 mN/m. (Right side) Plot indicating decrease in energy gap (eV) value on increasing the dopant concentration. (b) (Left side) Absorption spectra measurements for LB films of HAT5, HAT5+TiO_2 nanocomposites with 5 and 20 wt % of TiO_2 nanoparticles deposited on the coverslips at π_t of 20 mN/m. (Right side) Plot indicating decrease in energy gap (eV) value on increasing the dopant concentration.

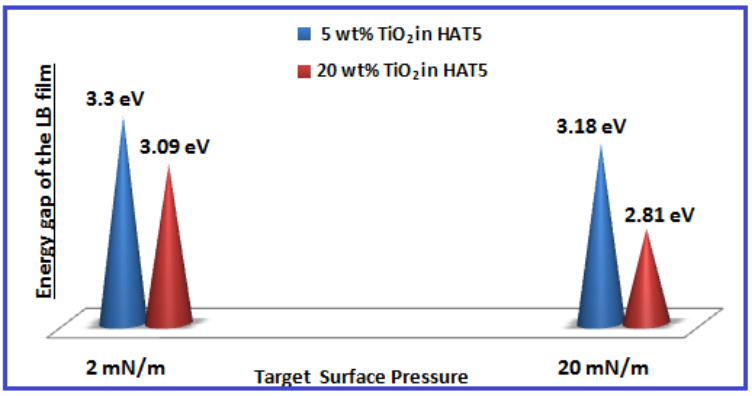

FIGURE 5.5: Variation of energy band gap of the LB films deposited at π_t of 2 mN/m and 20 mN/m for 5 and 20 wt.% of TiO_2 in HAT5.

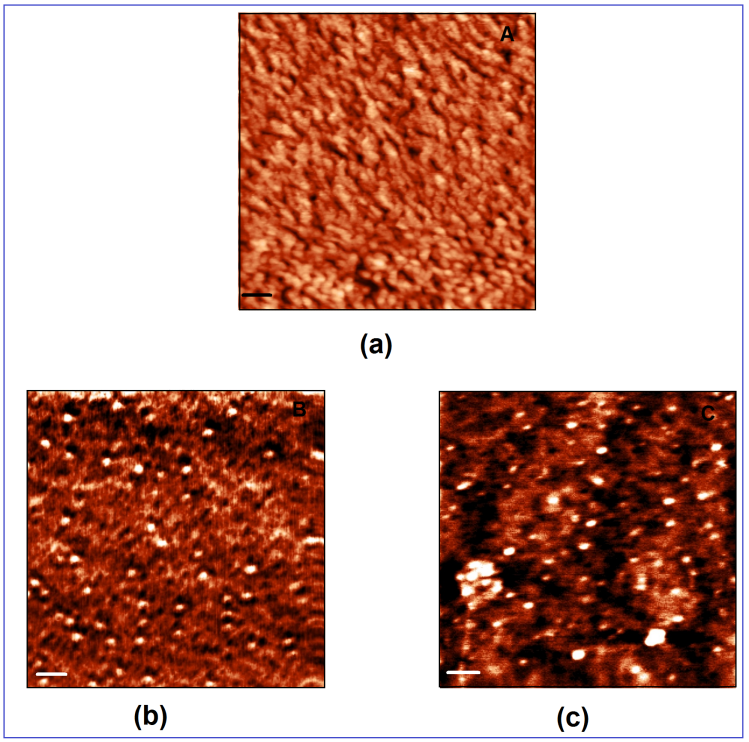

FIGURE 5.6: The AFM images of LB films of (a) HAT5 (b) HAT5+TiO_2 nanocomposite with 5 wt.% of TiO_2 nanoparticles and (c) HAT5+TiO_2 nanocomposite with 20 wt.% of TiO_2 nanoparticles. The films were deposited at the $\pi_t = 2\ mN/m$. The scale bar for image A is 0.5 μm in length and the scale bar for image B and C is 0.2 μm in length.

deposited in the L_1 phase and L_2 phase show uniform texture. There are only a few defects and the image appear homogeneous over the scan area of 5×5 μm^2. Interestingly, the AFM images (Figure 5.6b, 5.6c, 5.7b and 5.7c) of the LB films of HAT5 + TiO_2 nanocomposites show bright dots on the uniform background. The bright dots represents clusters of TiO_2 nanoparticles embedded in the uniform layer of HAT5. As the wt.% of TiO_2 nanoparticles increases, the cluster size of TiO_2 nanoparticles also increase from 40 to 50 nm at 2 mN/m and 70 to 85 nm at 20 mN/m (Figure 5.8). As the wt.% of TiO_2 nanoparticles increases, the density and the area of uniformly sized clusters of TiO_2 nanoparticles increases (Figure 5.6 and Figure 5.7). The density of clusters of TiO_2 nanoparticles embedded in the matrix of HAT5 layer, therefore can be related to the spectral properties of the LB films of the nanocomposite. With the increase in the density and the size of clusters of the nanoparticles, the energy gap may reduce.

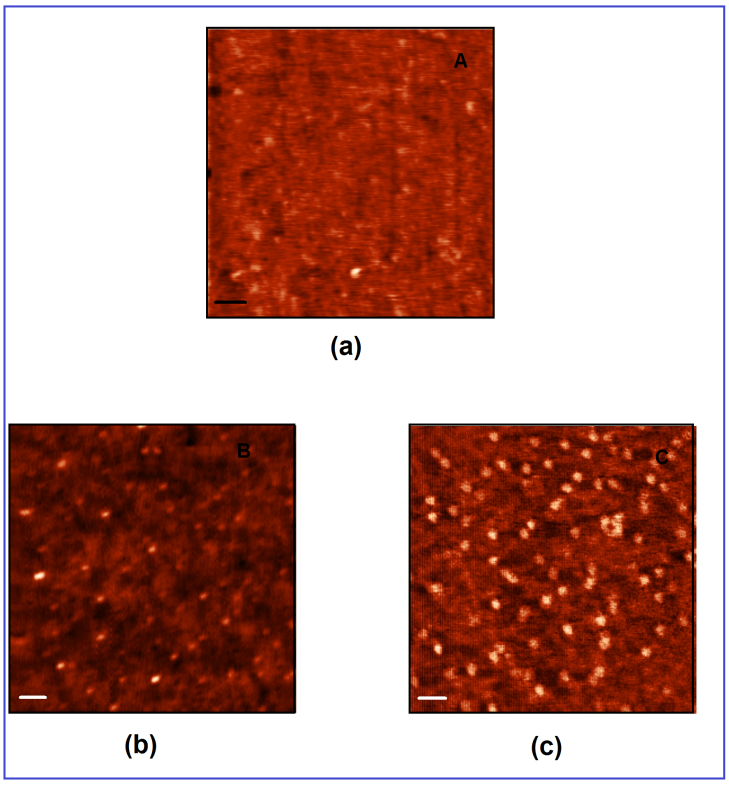

FIGURE 5.7: The AFM images of LB films of (a) HAT5, (b) HAT5+TiO_2 nanoparticles, 5 wt.% and (c) HAT5+TiO_2 nanoparticles, 20 wt.%. The films were deposited in the L_2 phase at the $\pi_t = 20\ mN/m$. The scale bar for image A is 0.5 μm in length and the scale bar for image B and C is 0.2 μm in length.

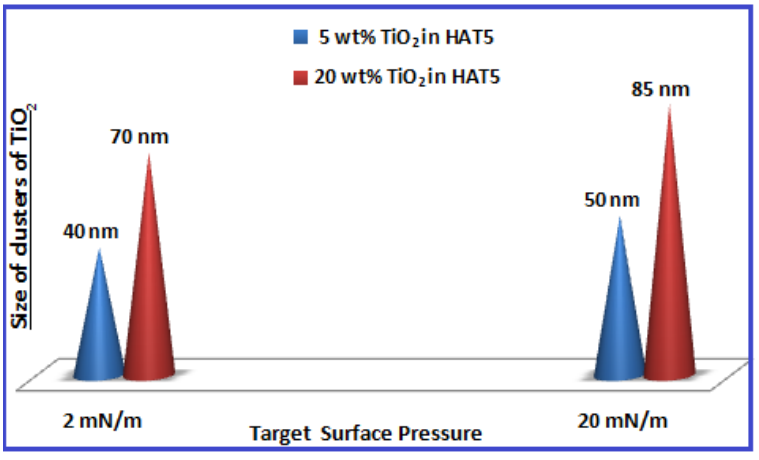

FIGURE 5.8: Variation of size of clusters of TiO_2 nanoparticles of the LB films deposited at π_t of 2 mN/m and 20 mN/m for 5 and 20 wt.% of TiO_2 in HAT5.

5.4 Conclusions

The LB films of pure HAT5 and HAT5+TiO_2 nanocomposites show very interesting results which may be useful for applications in the field of photovoltaics. The LM of pure HAT5 and HAT5+TiO_2 nanocomposites with different wt.% of TiO_2 nanoparticles are studied. We found condensation effect on the monolayer of HAT5+TiO_2 nanocomposites due to the presence of TiO_2 nanoparticles. The LB films of HAT5 and HAT5+TiO_2 nanocomposites with 5 and 20 wt.% of TiO_2 nanoparticles are deposited at π_t of 2 and 20 mN/m. The UV spectroscopy results indicate the reduction in energy gap with the increase in concentration of TiO_2. The reduction is found to be significant for the LB films deposited at higher surface pressures. The surface morphology of the LB films of pure HAT5 and HAT5+TiO_2 nanocomposites was obtained using AFM. We found increase in density of clusters of TiO_2 nanoparticles with the increase in wt.% of the nanoparticles in HAT5 matrix. We observed reduction in the energy gap of the HAT5 system in a controlled manner on appropriately doping the system with TiO_2 nanoparticles. Our study indicates a control over the energy gap of the LB films of HAT5 + TiO_2 nanocomposites by altering the wt.% of TiO_2 nanoparticles in the HAT5 matrix.

Bibliography

[1] S. Kumar, Chemistry Of Discotic Liquid Crystals: From Monomers To Polymers, Taylor and Francis, US, 2010.

[2] R. K. Gupta, V. Manjuladevi, C. Karthik, S. Kumar and K. Suresh, Coll. Surf. A, 410, 91, 2012,

[3] A. Facchetti, Y. Deng, A. Wang, Y. Koide, H. Sirringhaus, T. J. Marks and R. H. Friend, Ang. Chemie International Edition, 39, 4547, 2000.

[4] M. Pope and C. E. Swenberg, Ann. Rev. Phys. Chem., 35, 613, 1984.

[5] C. Y. Liu, H. L. Pan, M. A. Fox and A. J. Bard, Science, 261, 897, 1993.

[6] C. Catry, M. V. der Auweraer, F. C. De Schryver, H. Bengs, L. Haussling, O. Karthaus and H. Ringsdorf, Mac. Chem. Phy., 194, 2985, 1993.

[7] O. Albrecht, W. Cumming, W. Kreuder, A. Laschewsky and H. Ringsdorf, Coll. Polym. Sci., 264, 659, 1986.

[8] N. C. Maliszewskyj, P. A. Heiney, J. K. Blasie, J. P. McCauley Jr, and A. B. Smith III, J. de Phys. II, 2, 75, 1992.

[9] A. Nayak, K. Suresh, S. Kumar Pal, and S. Kumar, J. Phys. Chem. B, 111, 11157, 2007.

[10] D. Gidalevitz, O. Y. Mindyuk, P. A. Heiney, B. M. Ocko, P. Henderson, H. Ringsdorf, N. Boden, R. J. Bushby, P. S. Martin and J. Strzalka, J. Phys. Chem. B, 101, 10870, 1997.

[11] A. Hardouin and M. Levelut, J. Chim. phys, 80, 53, 1983.

[12] A. Skoulios and D. Guillon, Mol. Crys. Liq. Crys., 165, 317, 1988.

[13] C. Di Valentin, G. Pacchioni and A. Selloni, J. Phys. Chem. C, 113, 20543, 2009.

[14] Murov, L. Steven and Hug, L. Gordon and Carmichael, Ian Handbook of photochemistry, CRC Press, US, 1963.

[15] C. Karthik, K. Choudhary, A. Joshi, A. Gupta, Manjuladevi V., R. K. Gupta and S. Kumar, Adv. Sci. Lett., 20, 1138, 2014.

Chapter 6

Langmuir monolayer assisted fabrication of cadmium sulfide (CdS) nanoparticles and its role in surface manometry and alignment of rod shaped liquid crystal

6.1 Introduction

The field of photonics is enriched by cadmium sulfide (CdS) quantum dots (QDs) [1, 2]. The extraordinary properties of CdS QDs can be employed for biological imaging [3, 4], microelectronics and optoelectrochemistry [5–7]. The properties of CdS QDs are dependent on its size and shape [8–13]. Murray et al. [8] have shown that the band-gap of QDs increases as their size decreases, resulting in shorter wavelengths emission. Frenzel et al. [13] have investigated optical excitations in different structures of CdS QDs. CdS nanoparticles can be synthesized by micorwave irradiation, double-hydrophylic block copolymers, fusarium oxysporum, reverse micellar system etc [14–17]. We employed Langmuir monolayer (LM) as a template for the synthesis of CdS nanoparticles at the air-water (A-W) interface. Such nanoparticles can be transfered to the effective area of a device by a highly controlled Langmuir-Blodgett (LB) deposition technique. The LB technique can control the film thickness and gap between the charge carriers of the semiconductor nanoparticles which in turn can govern

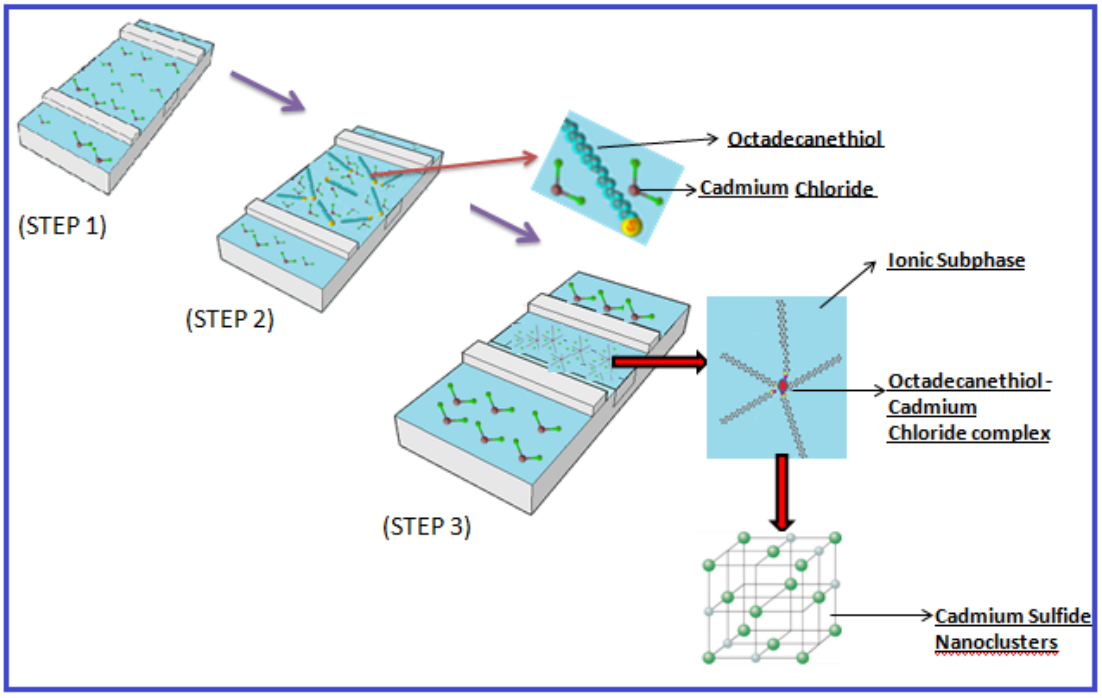

FIGURE 6.1: Schematic diagram of formation of cadmium sulfide (CdS) nanoparticles.

the electronic and optical properties of the film [18]. In this chapter, we report the formation of CdS nanoparticles as a result of interaction between octadecanethiol (ODT) and cadmium divalent ion (Cd^{2+}) at the A-W interface (Figure 6.1). The aqueous subphase is made ionic by adding a salt, cadmium chloride ($CdCl_2$) in ultrapure ion free water. A LM of ODT molecules is formed on the surface of such subphase. The hydrophilic SH group of the ODT molecule interacts with the metal ion dissolved in the aqueous subphase resulting in formation of CdS nanoparticles [19]. The fabrication of nanoparticles is confirmed using ultraviolet-visible (UV-VIS) spectroscopy, atomic force microscopy (AFM), X-ray diffraction (XRD) and field emission scanning electron microscopy (FESEM). The absorption spectra revealed the signature of CdS nanoparticles. The XRD results indicate the crystalline structure of CdS nanoparticles to be zinc blend type (cubic). We have estimated size of the nanoparticles using AFM, XRD and FESEM. The experimental results showed the size of the nanoparticles to be around 25 nm. We observed that there was no significant change in radius of the nanoparticles on varying surface pressure and ionic concentration. Zetapotential measurements were carried out on the colloidal solution of nanoparticles to confirm their stability in ethanol solvent.

Fabrication of liquid crystal (LC) based devices require the film of liquid crystalline material to be uniform and defectless. We found that LB film deposition

of monolayer of 4-n-octyl-cyanobiphenyl (8CB) on different solid substrates is difficult. This is due to the fact that 8CB molecules exhibit a large dipole moment due to the presence of cyano group (-CN). Therefore, due to strong intermolecular dipolar repulsion, the anchoring strength of the 8CB monolayer onto solid substrate is very weak. There are few reports in the literature wherein 8CB monolayer is transferred to solid substrate by horizontal deposition or Schaeffer method [20–22]. Here, we intended to increase the anchoring strength of the monolayer of 8CB by incorporating CdS nanoparticles at the different sites of the monolayer matrix. The incorporation of the nanoparticles were done in-situ by adopting the surface chemistry of the fabrication of CdS nanoparticles as discussed above. The CdS doped LB film of 8CB were employed for observing alignment of a LC.

6.2 Experimental Methods

6.2.1 Materials

The materials octadecanethiol (ODT), chloroform (HPLC grade), cadmium chloride (98%) ($CdCl_2$) were procurred from Sigma Aldrich, Merck and Hinedia respectively. All the above chemicals were utilized as procured. The ultrapure ion free water was used for the experiments. All experiments were done at 20 $\pm$ 0.3°C.

6.2.2 Methods

6.2.2.1 Surface manometry measurements

A chloroform solution of ODT at a concentration of 3.48 mM was prepared. The Cd^{2+} divalent ion was formed by adding $CdCl_2$ in ion free water. The solution of ODT was uniformly spread over the ionic subphase of $CdCl_2$ salt solution. The barrier speed was maintained at 20 mm/min. The surface pressure (π) - area per molecule (A_m) isotherms were recorded for three different concentration (10^{-4}, 10^{-5} and 10^{-6} M) of $CdCl_2$ in the ion free water. The solution of 8CB was prepared in chloroform at a concentration of 3.48 mM. The 8CB solution was then mixed with 10 and 20 mole percent of ODT solution. The mixed solution of 8CB and ODT was spread over the ultrapure subphase and also over the aqueous subphase having 10^{-4} M concentration of $CdCl_2$. The π - A_m isotherms were

obtained by compressing the monolayer symmetrically at the A-W interface in a Langmuir trough.

6.2.2.2 Langmuir Blodgett deposition

The LB films were deposited on to the optical quality quartz plates. The LB deposition was done at four different target surface pressure (π_t) (5, 20, 30 and 40 mN/m) and for three different concentration (10^{-4}, 10^{-5} and 10^{-6} M) of $CdCl_2$ in the ion free water. The LB films of 8CB mixed with 10 mole percent of ODT on both the ultrapure and ionic subphase were deposited on Si wafer and glass slides. The dipping speed of the substrate was maintained at 5 mm/min during both upstroke and downstroke of the dipper.

6.2.2.3 UV-VIS Spectroscopic Measurements

UV-VIS spectra of the LB films deposited on quartz plates were recorded. In addition, LB film of ODT-Cd^{2+} complex was dissolved in chloroform by ultra-sonicating the film on quartz substrate for half an hour. The obtained chloroform solutuion of ODT-Cd^{2+} complex was scanned using the spectrometer.

6.2.2.4 Field Emission Scanning Electron Microscopy

The LB film deposited on silicon substrates were scanned using FESEM. The extra high tension value was kept at 5.00 kV and the width of the aperture was set at 4.2 mm. The images were captured at the magnification of 300 KX.

6.2.2.5 Atomic Force Microscopy

AFM measurements were done on the LB film deposited onto quartz substrate at π_t of 5 and 30 mN/m. The concentration of $CdCl_2$ in the subphase was 10^{-5} M. Topographic images were obtained by scanning the films using Silicon tips having resonant frequencies in the ranges of 180-270 KHz and spring constants between 10 to 20 N/m in semicontact mode.

6.2.2.6 X-Ray Diffraction

The LB film deposited at π_t of 30 mN/m from the subphase of 10^{-4} M of $CdCl_2$ was dissolved in chloroform by ultrasonicating the substrate in chloroform for 30 minutes. The obtained solution of ODT-Cd^{2+} complex was spin coated on to a silicon substrate. The spin coated film was reasonably thick and resembled a powdered sample. The structural characterization of the spin coated film was carried out using X-Ray diffractometer (Rigaku, MiniFlex II) at a wavelength of 1.54 . The 2θ scan rate was maintained at $5^{\circ}/min$.

6.2.2.7 Zeta potential Measurements

The LB film was dissolved in ethanol by ultrasonicating the substrate for 30 minutes. The dispersion medium has a refractive index of 1.3 and viscosity of 1.040 $mPa.s$ at room temperature. The zetapotential measurements was performed using Zetasizer (Malvern Instruments).

6.3 Results and Discussion

6.3.1 Fabrication of CdS nanoparticles at air-water interface

The π - A_m isotherm of the ODT molecule at air-water interface (inset Figure 6.2) exhibits gas, liquid condensed and collapse state [19]. The collapse surface pressure (π_c) was found to be around 14 mN/m. The ODT molecule was found to form stable monolayer at the A-W interface. The ODT molecules remain untilted in the condensed phase. The monolayer of ODT molecule was also found to be very sensitive on addition of monovalent, divalent and trivalent ions [19].

Figure 6.2 shows the surface pressure (π) - area per molecule (A_m) isotherm of ODT-Cd^{2+} complex for 10^{-4}, 10^{-5}, 10^{-6} and 10^{-8} M concentration of $CdCl_2$ in ultrapure water. The isotherms shows that even a very minute addition of Cd^{2+} ion into the water subphase results in deviation in the isotherm as compared to the monolayer of the ODT molecule on ion free water. As the concentration of $CdCl_2$ in the subphase increases, there is a increase in the condensation of the ODT monolayer and the isotherms shift towards lower A_m. At higher concentration of $CdCl_2$ in the subphase, the surface pressure rises very high and the monolayer does not attain collapse state.

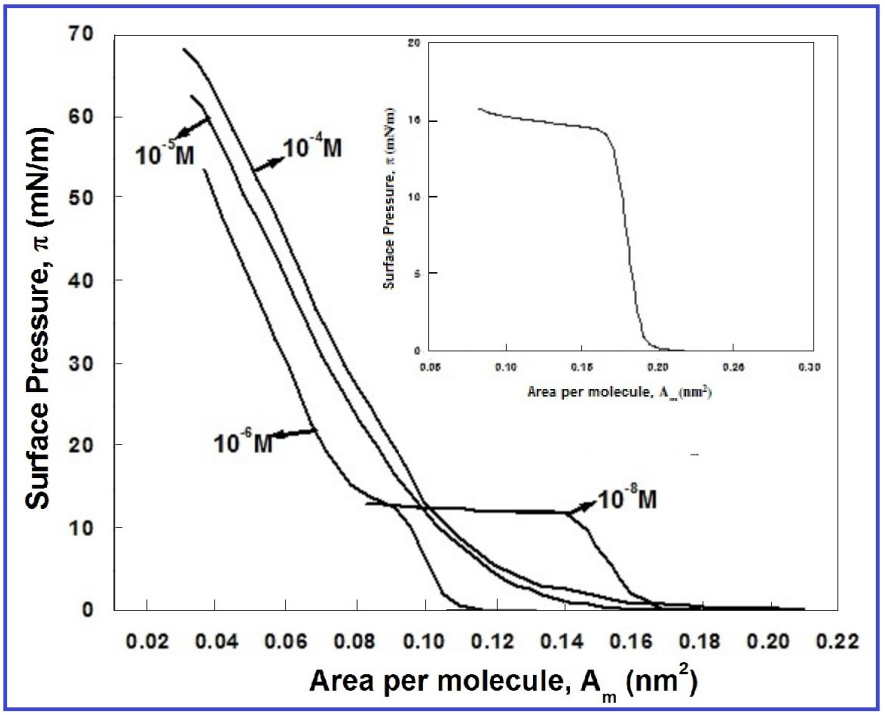

FIGURE 6.2: The surface pressure (π) - area per molecule (A_m) isotherm of octadecanethiol molecule with different concentration of $CdCl_2$ in the subphase. Inset shows the isotherm of octadecanethiol (ODT) molecule on ultrapure ion free water.

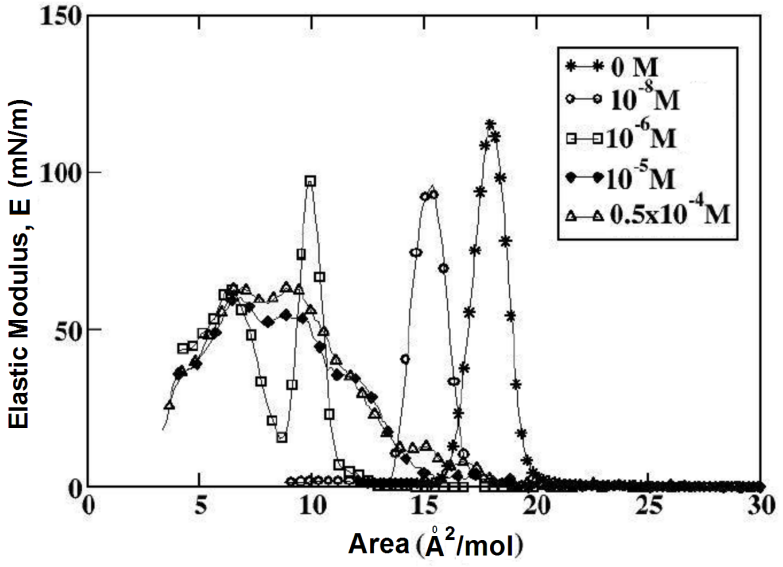

FIGURE 6.3: Plot of elastic modulus (E) vs. area per molecule (A_m) of octadecanethiol monolayer with different concentration of $CdCl_2$ in the subphase.

Figure 6.3 shows the variation of in-plane elastic modulus (E) as a function of A_m of ODT molecule with different concentration of $CdCl_2$ in the subphase. The variation of E for the ODT monolayer on the ion-free water subphase shows a peak corresponding to the untilted condensed phase. The maximum value of E in the condensed phase is around 120 mN/m. As the concentration of the $CdCl_2$ increases, the peak corresponding to the condensed phase shifts towards the lower A_m. For the concentration above 10^{-6} M of $CdCl_2$, the peak corresponding to condensed phase vanishes leading to the appearance of other broader peaks at lower A_m. The LB films were deposited from the aqueous subphase of 10^{-4}, 10^{-5} and

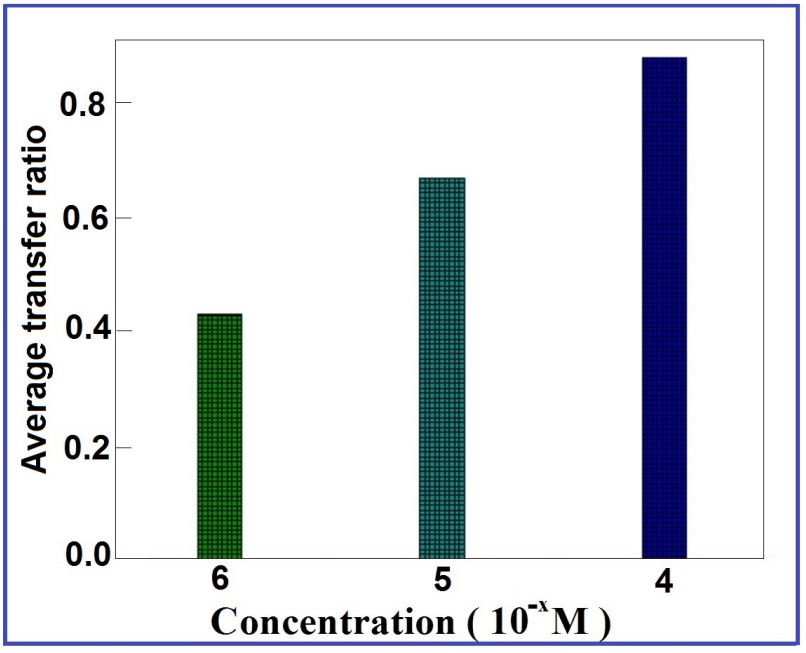

FIGURE 6.4: Average transfer ratio of LB films of ODT-Cd^{2+} complex at different concentration (10^{-x}M) of $CdCl_2$ in the aqueous subphase

10^{-6} M of $CdCl_2$ solution and at four different π_t i.e. 5, 20, 30 and 40 mN/m. The average transfer ratio increased on increasing the ionic concentration (Figure 6.4). This indicates better physical adhesion of ODT-Cd^{2+}complex to the quartz plates as the concentration of divalent Cd^{2+} ions in the aqueous subphase increases.

Table 6.1 shows the corresponding peak positions of the absorption spectra for the LB films of ODT-Cd^{2+} complex deposited at different π_t for different concentration of $CdCl_2$ in the aqueous subphase. Spectra (Figure 6.5) show absorbance at around 315 nm which is the signature of CdS nanoparticles [23]. The energy gap (E_g) is estimated from the spectra using the method discussed in chapter 5 and are summarized in Table 6.1.

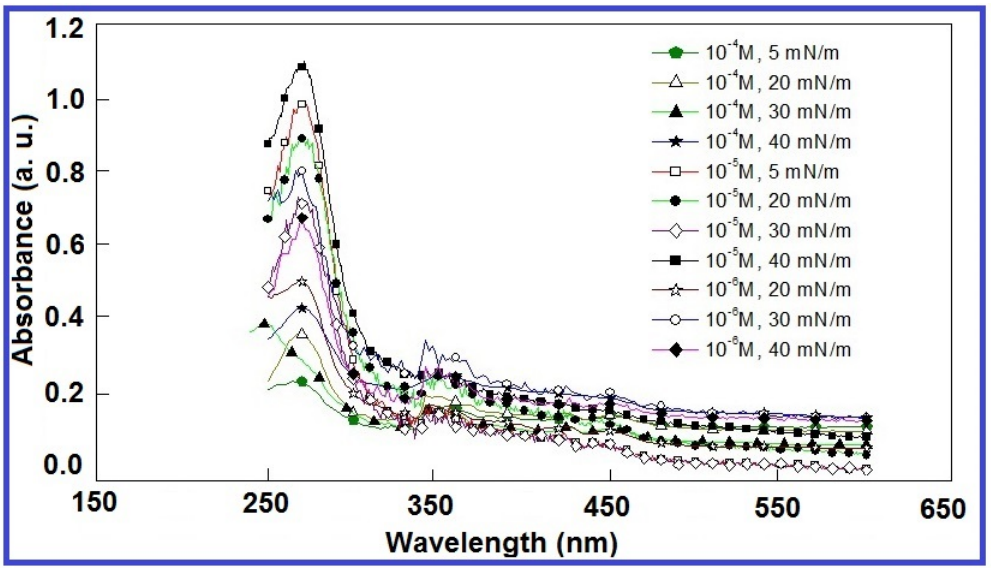

FIGURE 6.5: UV-VIS spectra of the LB film of ODT-Cd^{2+} complex deposited from the subphase having different concentration of $CdCl_2$ onto quartz plates at different π_t.

TABLE 6.1: Variation of energy gap (E_g) as the function of $CdCl_2$ concentration in the subphase and the target surface pressure (π_t) of LB deposition of ODT

$CdCl_2$ concentration (M) in subphase	**Target surface pressure (π_t) (mN/m)**	**Wavelength (λ) (nm) (Wavelength bulk = 355 nm)**	**Energy gap (E_g) (eV) E_g bulk = 3.5 eV)**
10^{-4}	5	313	3.95
10^{-4}	20	312	3.97
10^{-4}	30	311	3.99
10^{-4}	40	310	4.01
10^{-5}	5	317	3.90
10^{-5}	20	315	3.93
10^{-5}	30	313	3.95
10^{-5}	40	311	3.98
10^{-6}	20	315	3.88
10^{-6}	30	313	3.90
10^{-6}	40	311	3.95

The calculated E_g values are close to the E_g value for the cubic CdS nanoparticle i.e 3.9 eV. This suggests that the crystalline structure of the CdS nanoparticles may be cubic (zinc blend type) [24]. The average E_g of the CdS nanoparticles were found to be increasing marginally with increasing concentration of Cd^{2+} ion in the aqueous subphase. This is shown in Figure 6.6.

The LB films of ODT-Cd^{2+} complex at different π_t for 10^{-5} M concentration of $CdCl_2$ were ultrasonicated in chloroform solvent for about 30 minutes. The nanoparticles desorbed from the substrate and their suspension in chloroform was scanned using UV-VIS spectrometer. The spectra is shown in Figure 6.7. The results have been summarized in Table 6.2. The E_g values have decreased by a very small amount as compared to the E_g values of LB films of ODT-Cd^{2+} complex

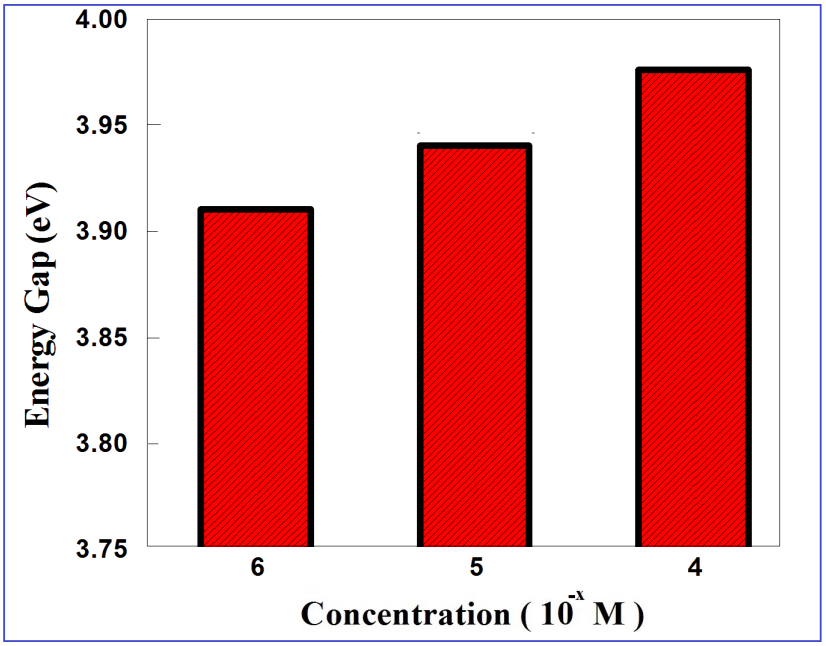

FIGURE 6.6: Plot of energy gap (E_g) of the LB films of ODT-Cd^{2+} complex deposited from different concentration (10^{-x}M) of $CdCl_2$ in aqueous subphase

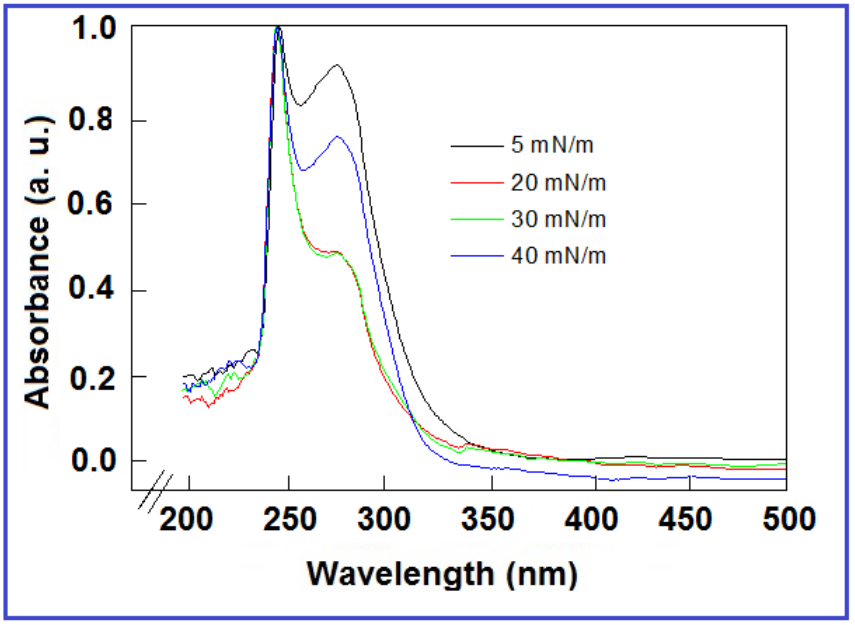

FIGURE 6.7: UV-VIS spectra of the chloroform deposited LB film of ODT transferred from the subphase having 10^{-5} M concentration of $CdCl_2$.

deposited onto quartz substrate. The broadening of the spectra may be due to agglomeration of CdS nanoparticles in the solvent.

TABLE 6.2: Variation of energy gap (E_g) as a function of target surface pressure (π_t) of LB deposition of ODT from the substrate at 10^{-5} M $CdCl_2$ concentration. The LB films were dispersed in $CHCl_3$ solvent by ultrasonication and then the UV-VIS spectra were collected.

$CdCl_2$ **concentration** (M) **in subphase**	**Target surface pressure** (π_t) (mN/m)	**Wavelength** (nm) **(Wavelength bulk =** **355** nm)	**Energy gap** (E_g) (eV) E_g **bulk = 3.5** eV)
10^{-5}	5	355	3.48
10^{-5}	20	350	3.53
10^{-5}	30	344	3.59
10^{-5}	40	328	3.77

We also tried to synthesize CdS nanoparticles by mixing and ultrasonicating ODT molecules in 10^{-5} M concentration of aqueous medium of $CdCl_2$. We scanned the sample using UV-VIS spectrophotometer and it showed no signature of CdS nanoparticles. Thus, we believe that the Cd^{2+} ion reacts chemically with the -SH group of the ODT molecules at the air-water interface and therby leading to the formation of CdS nanoparticles. The crystalline structure of the CdS nanoparticles was studied using the results of X-Ray diffraction (Figure 6.8) from the CdS nanoparticles. Prominent peaks were observed at $2\theta = 32.5°$ and $61°$. The (hkl) values at both the peaks were obtained as (100) and (111), respectively. The (hkl) values may indicate the crystalline structure of the CdS nanoparticles to be cubic (zinc blend type) [25]. Using Scherrer equation [26], we found the size of the nanoclusters to be 25 nm.

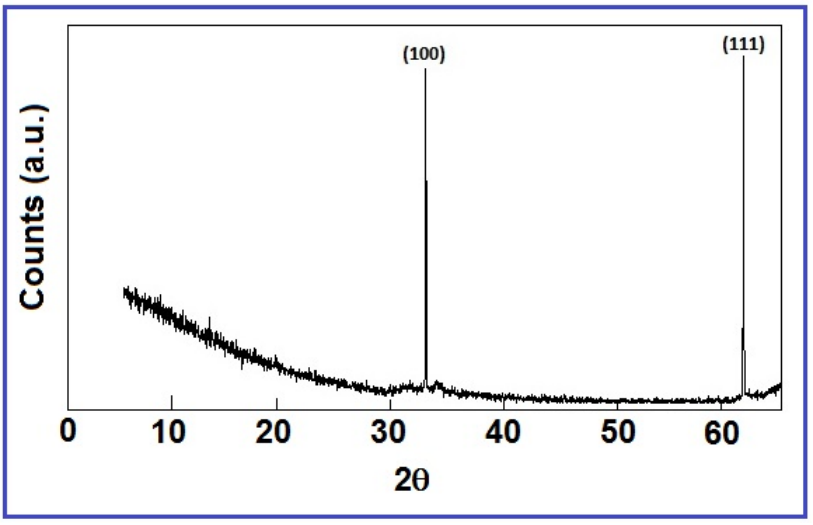

FIGURE 6.8: XRD profile of CdS nanoparticles formed at π_t of 30 mN/m. The concentration of Cd^{2+} ion in the subphase was 10^{-4} M.

The surface morphology of LB film of ODT-Cd^{2+} complex deposited at π_t of 30 mN/m onto the silicon substrate at 10^{-4} M concentration of $CdCl_2$ was studied through FESEM (Figure 6.9) and AFM (Figure 6.10). The white particles in the FESEM image indicate the CdS nanoparticles. Figure 6.9c and Figure 6.9d indicate formation of many such CdS nanoparticles. Figure 6.9a and Figure 6.9b shows that the particles are interconnected to form bigger clusters. The size of the nanoparticles was found to be 22 nm from the FESEM image. This value is nearly comparable with the size estimated through XRD. The AFM images (Figure 6.10) show aggregation of CdS nanoclusters. Figure 6.10a and Figure 6.10b are the AFM images of the LB film of ODT-Cd^{2+} complex deposited at π_t of 30 mN/m. Figure 6.10a shows interconnected clusters and Figure 6.10b shows white spherical particles which might be CdS nanoparticles. The size of the particles estimated from the AFM image was 20 nm.

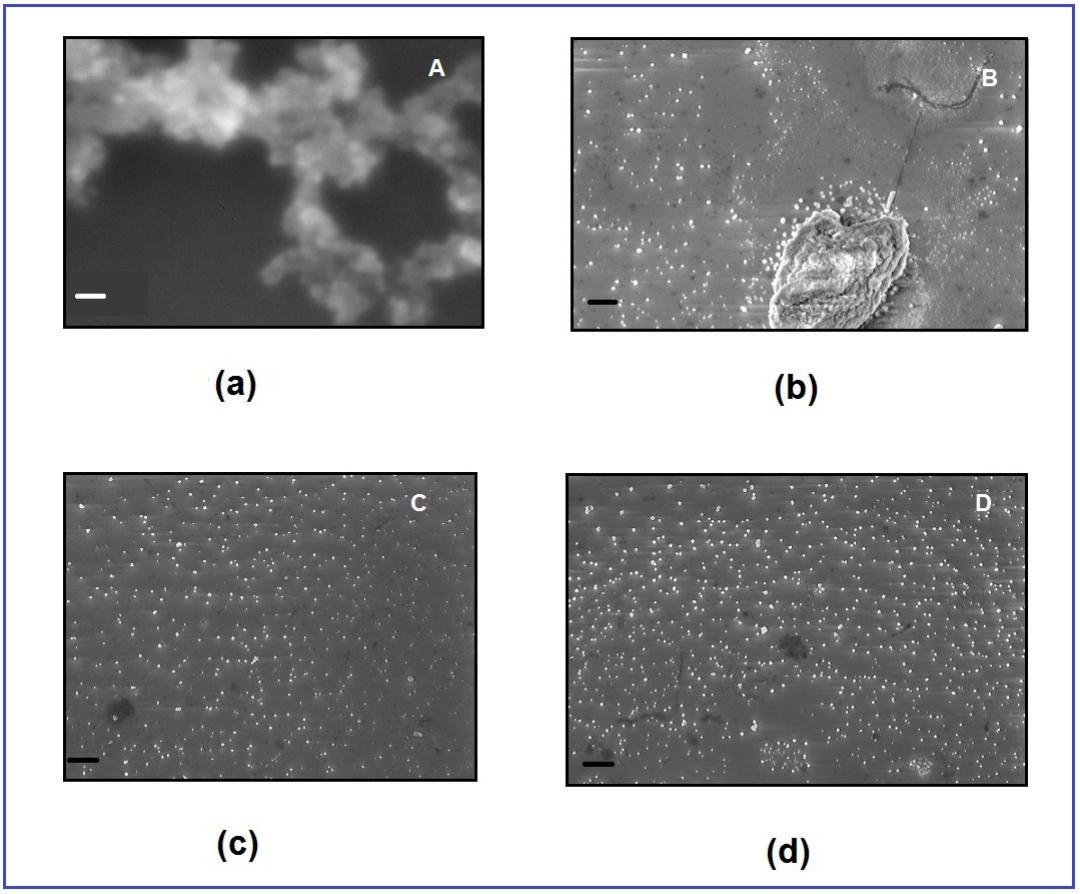

FIGURE 6.9: FESEM image of the LB film of ODT-Cd^{2+} complex deposited at π_t of 30 mN/m from the aqueous subphase of 10^{-4} M concentration of $CdCl_2$. The scale bar in (a) is 100 nm in length. The scale bar in (b), (c) and (d) is 2 μm in length.

The zeta potential results of the LB film of ODT-Cd^{2+} complex deposited at π_t of 30 mN/m from the aqueous subphase of (10^{-4} M) concentration of $CdCl_2$

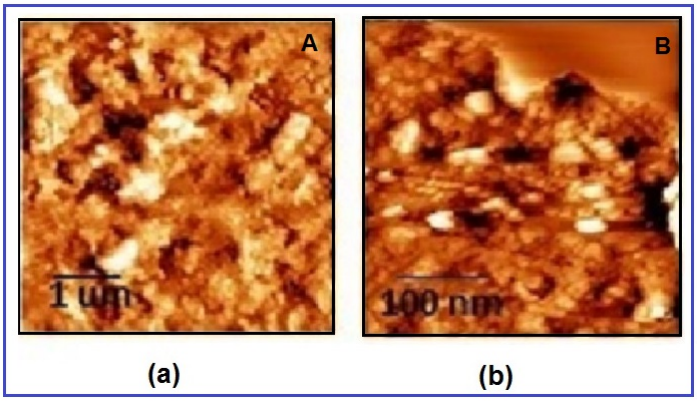

FIGURE 6.10: AFM images of the LB film of ODT-Cd^{2+} complex deposited at π_t of 30 mN/m from the aqueous subphase of 10^{-4} M concentration of $CdCl_2$. The scan area of the figure (A) 5×5 μm^2 and (B) 0.5×0.5 μm^2.

dissolved in ethanol indicated formation of stable CdS nanoparticles (Figure 6.11). We obtained negative value of zetapotential -11.1 mV with high standard deviation of 13.4. These values indicates that CdS nanoparticles are stable in ethanol solvent against coagulation [27].

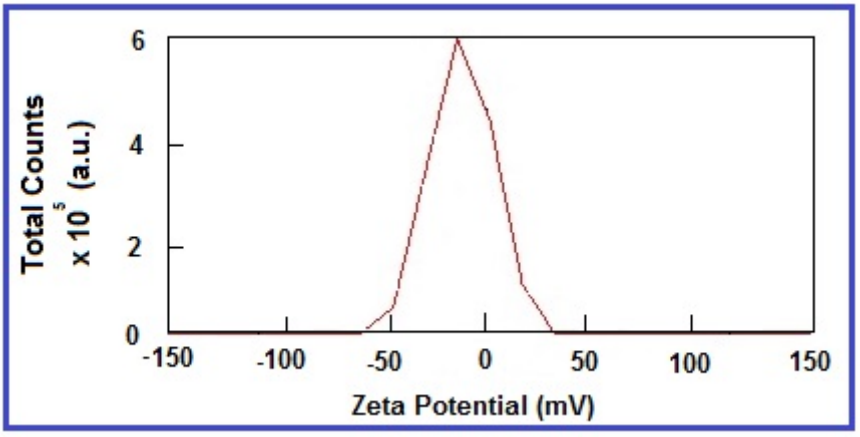

FIGURE 6.11: Zeta potential results of the ethanol dispersed LB film of ODT-Cd^{2+} complex deposited at π_t of 30 mN/m from the aqueous subphase of 10^{-4} M concentration of $CdCl_2$.

6.3.2 Incorporation of CdS nanoparticles in a liquid crystal matrix at air-water and air-solid interfaces and its role in alignment of bulk liquid crystal

In order to enhance the stability of LB film of a rod shaped LC molecule, (i.e. 8CB), we attempted to embed CdS nanoparticles in-situ in the LM of the 8CB followed by LB deposition on solid substrates. Such LB films were employed as

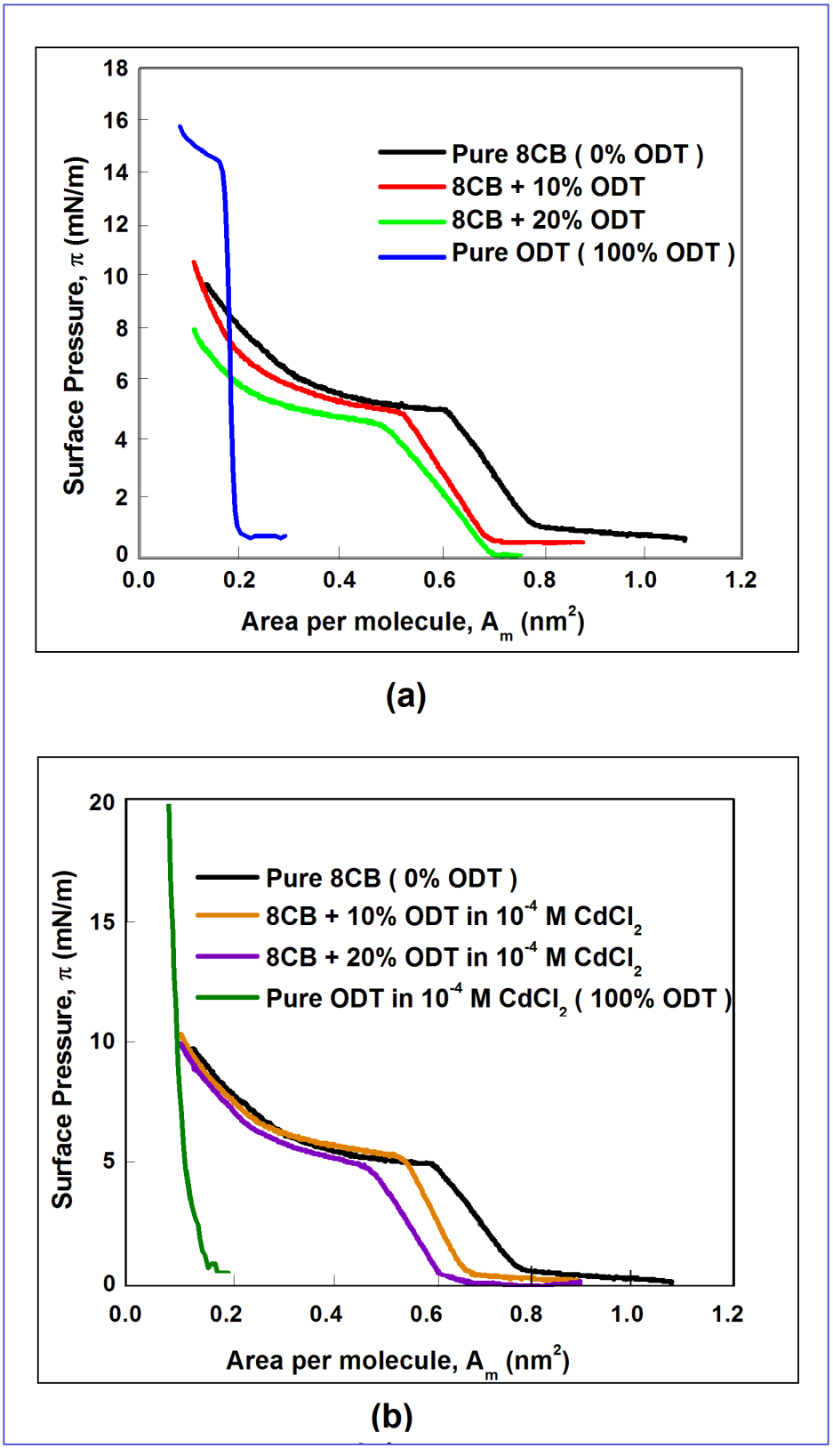

FIGURE 6.12: (a) The surface pressure (π) - area per molecule (A_m) isotherms of mixed monolayer system of 8CB with different mole percent of ODT at the ultrapure ion-free water subphase. (b) The surface pressure (π) - area per molecule (A_m) isotherms of mixed monolayer system of 8CB with different mole percent of ODT on the aqueous subphase containing 10^{-4} M concentration of $CdCl_2$.

the alignment layer during the fabrication of LC-cells and the alignment of bulk LC was studied using such LC-cells. We formed the LM of the mixed components of 8CB and ODT over the aqueous subphase possessing Cd^{2+} ions and carried out systematic surface manometry studies on such mixed system. The π - A_m isotherms of the monolayers of pure 8CB and 8CB mixed with different mole percent of ODT on ultrapure ion-free water subphase is shown in Figure 6.12a. The isotherm shift towards lower A_m with increasing concentration of ODT in 8CB and with incorporation of Cd^{2+} ion in the subphase (Figure 6.12b). This indicates condensation of the LM of 8CB due to such incorporation. The monolayer condenses as the amount of ODT molecules in 8CB matrix increases on the ion free water. The condensation of the monolayer over 10^{-4} M concentration of $CdCl_2$ in the aqueous subphase is further enhanced as the amount of ODT molecules in 8CB monolayer increases.

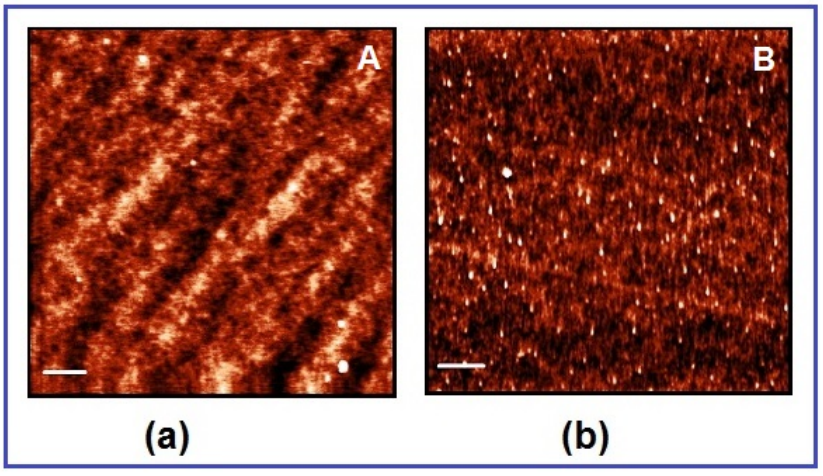

FIGURE 6.13: (a) The AFM image of LB film of 8CB with 10 mole percent of ODT deposited at π_t of 2 mN/m from the ultrapure ion-free water subphase. (b) The AFM image of LB film of 8CB with 10 mole percent of ODT deposited at the π_t of 2 mN/m from the aqueous subphase containing 10^{-4} M concentration of $CdCl_2$. The scale bar is 0.5 μm in length.

The AFM image of the LB film of 8CB with 10 mole percent of ODT deposited at π_t of 2 mN/m from the ultrapure ion-free water subphase is shown in Figure 6.13a. The image appears homogeneous over the scan area of 4×4 μm^2. This indicates that ODT and 8CB may mix well at this proportion in the LB film. Interestingly, the AFM image of LB film of 8CB with 10 mole percent of ODT deposited at π_t of 2 mN/m from the aqueous subphase containing 10^{-4} M concentration of $CdCl_2$ (Figure 6.13b) show bright dots on the uniform background. The bright dots represent clusters of CdS nanoparticles embedded uniformly in the matrix of 8CB LC. The LB films of 8CB with 10 mole percent of ODT were deposited

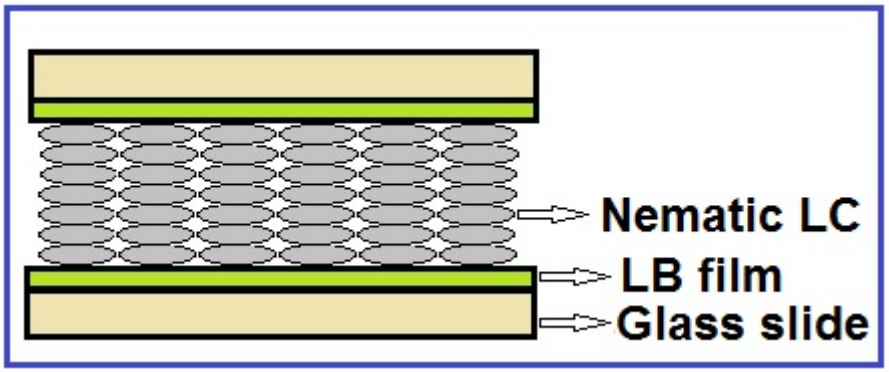

FIGURE 6.14: Schematic diagram showing LC-cell fabricated using LB film as an alignment layer.

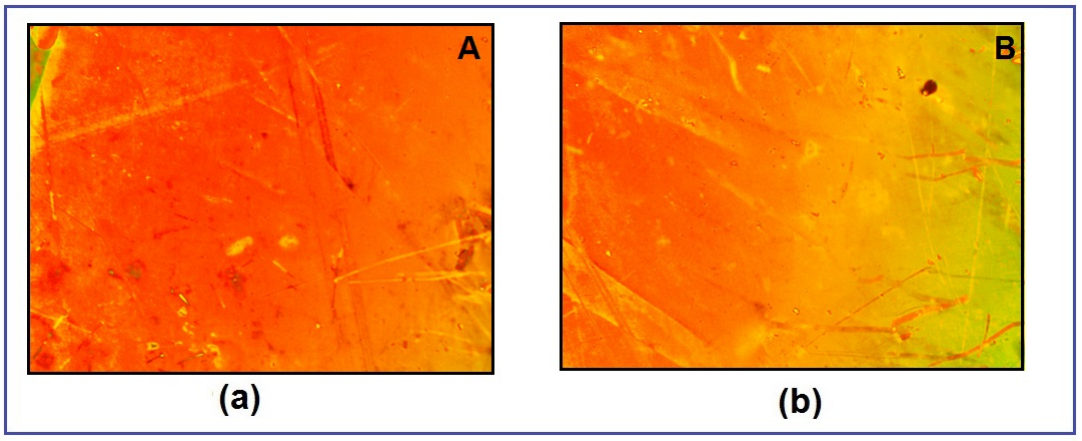

FIGURE 6.15: The polarizing microscopy textures of the LC-cell fabricated using LB films. The LB film of 8CB with 10 mole percent of ODT was deposited at π_t of 2 mN/m from the ultrapure ion-free water subphase. The intensity does not change in sequence from (a) to (b) on rotation of the LC-cell mounted on the microscope stage between crossed polarizers.

onto glass slides at the π_t of 2 mN/m from the ultrapure ion-free water subphase. The LB films of 8CB with 10 mole percent of ODT were also deposited onto glass slides at the π_t of 2 mN/m from the aqueous subphase containing 10^{-4} M concentration of $CdCl_2$. The glass slides deposited with the LB films were used for the fabrication of LC-cell (Figure 6.14).

The commonly available nematic LC, E7 was used to fill the cell. The LC-cells were placed under a polarizing microscope (Olympus BX51) and the textures were observed in the transmission mode. Figure 6.15 shows the texture of the LC-cell fabricated using LB film of 8CB with 10 mole percent of ODT as the alignment layer. On rotating the analyzer, the intensity dropped from maximum to minimum but did not get extinguished. This indicates a tendency of planar alignment of E7 LC. Figure 6.16 shows the texture of the LC-cell fabricated using LB film of 8CB with embedded CdS nanoparticles. The CdS nanoparticles are embedded in

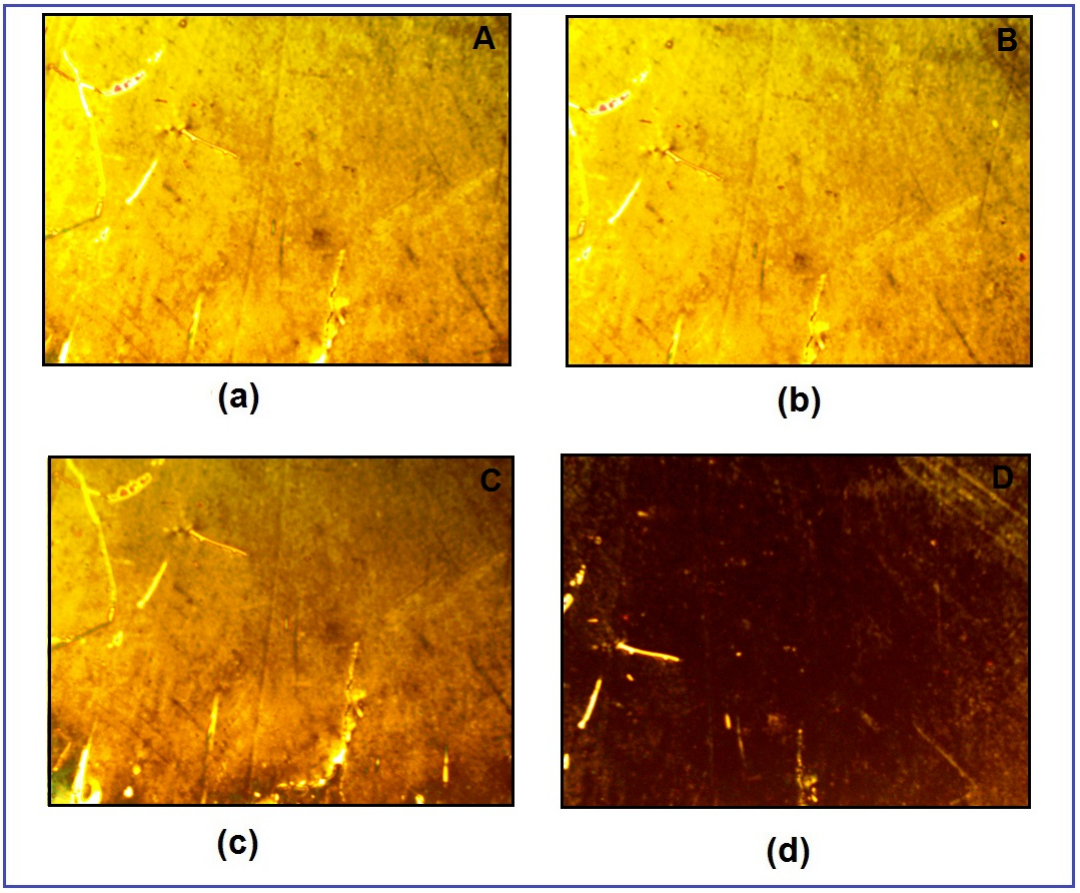

FIGURE 6.16: The polarizing microscopy textures of the LC-cell fabricated using LB films. The LB film of 8CB with 10 mole percent of ODT was deposited at π_t of 2 mN/m from the aqueous subphase containing 10^{-4} M concentration of $CdCl_2$. The change in intensity from maximum to zero can be obtained in sequence from (a) to (d) on rotation of the LC-cell mounted on the microscope stage between crossed polarizers.

the LB film by depositing the film of 8CB with 10 mole percent of ODT from the aqueous subphase containing 10^{-4} M concentration of $CdCl_2$. Here, on the rotation of analyzer, we observed drop in intensity from maximum to zero. This indicated planar alignment in E7 LC. Hence the presence of CdS nanoparticles in the 8CB matrix in the alignment layer favours the planar alignment of the bulk LC. Such technique can be successfully employed in LC display industries.

6.4 Conclusions

In the present work, we demonstrated that LM of ODT on the aqueous subphase of $CdCl_2$ can be used for the fabrication of CdS nanoparticles. Such nanoparticles can be embedded in-situ in the LM of some other material. The CdS nanoparticles were embedded in the LM of a rod shaped LC, 8CB. We transferred the LC system

onto solid substrates and characterized them using AFM. Such LB films were employed as alignment layer for the fabrication of LC-cell. The alignment of bulk LC, E7 is studied under such geometry. The presence of CdS nanoparticles favours the planar alignment of E7 in the LC-cell.

Bibliography

[1] K. R. Choudhury, M. Samoc, A. Patra and P. N. Prasad, J. Phys. Chem. B, 108, 1556, 2004.

[2] P. Michler, Single quantum dots: Fundamentals, applications and new concepts, Springer, 2004.

[3] M. Bruchez, M. Moronne, P. Gin, S. Weiss and A. P. Alivisatos, Sci., 281, 013, 1998.

[4] W. C. W. Chan and S. M. Nie, Sci., 281, 016, 1998.

[5] S. Chaudhary, M. Ozkan and W. C. W. Chan, Appl. Phys. Lett., 84, 2925, 2004.

[6] V. Colin, M. C. Schlamp and A. P. Alivisatos, Nat. (London), 370, 374, 1994.

[7] C. J. Murphy and J. L. Coffer, Appl. Spectrosc., 56, 16A, 2002.

[8] C.B. Murray, D.J. Norris and M.G. Bawendi, J. Am. Chem. Soc., 115, 8706, 1993.

[9] Y. Wang and N. Herron, Phy. Rev. B, 42, 7253, 1990.

[10] R. Banerjee, R. Jayakrishnan and P. Ayyub, J. Phys.: Cond. Matt., 12, 10647, 2000.

[11] C. C. Chen, A. Herhold, C. Johnson and A. Alivisatos, Sci., 276, 398, 1997.

[12] El-Sayed and A. Mostafa, Acc. Chem. Res., 37, 326, 2004.

[13] Frenzel, Johannes, Jan-Ole Joswig and G. Seifert, J. Phys. Chem. C, 111, 10761, 2007.

[14] L. Qi, H. Colfen and M. Antoniett, Nano Lett., 1, 61, 2001.

[15] A. Ahmad, P. Mukherjee, D. Mandal, S. Senapati, M. I. Khan, R. Kumar and M. Sastry, J. Ame. Chem. Soc., 124, 12108, 2002.

[16] J. Zhu, M. Zhou, J. Xu and X. Liao, Mat. Lett., 47, 25, 2001.

[17] A. Agostiano, M. Catalano, M. Curri, M. Della Monica, L. Manna and L. Vasanelli, Micron, 31, 253, 2000.

[18] A. Ulman, Langmuir-blodgett films, The Handbook of Surface Imaging and Visualization, 1995.

[19] R. K. Gupta, K. Suresh, R. Guo and S. Kumar, Anal. chimi. acta, 568, 109, 2006.

[20] Ruths, Marina, Suzi Steinberg and Jacob N. Israelachvili, Langmuir, 12, 6637, 1996.

[21] S. Bardon, et al., Phys. Rev. E, 59, 6808, 1999.

[22] J. Y. Fang, Z. H. Lu, G. W. Ming, Z. M. Ai, Y. Wei and P. Stroeve., Phys. Rev. A, 46, 4963, 1992.

[23] S. L. Murov, G. L. Hug and I. Carmichael, Handbook of photochemistry, CRC Press, US, 1993.

[24] R. Banerjee, R. Jayakrishnan and P. Ayyub, J. Phys. Cond. Matt., 12, 10647, 2000.

[25] B. E. Warren, X-ray Diffraction, Dover Publications, 1969.

[26] A. Patterson, Phys. rev., 56, 978, 1939.

[27] B. Salopek, D. Krasi and S. Filipovi, Measurement and Application of Zeta-Potential, Rudarsko-geolo sko-naftni fakultet, 1992.

Chapter 7

Langmuir monolayer (LM) and Langmuir-Blodgett (LB) films of H-Type liquid crystal molecule

7.1 Introduction

The liquid crystal (LC) molecules with different shapes may exhibit different surface phases at the air-water (A-W) interface. Due to different shape anisotropy, chirality and chromophore groups of such LC molecules, the molecular aggregation in the Langmuir Blodgett (LB) films may yield interesting patterns. The formation of such patterns essentially governed by inter-molecular, molecule-substrate interactions and the external force fields e.g. electromagnetic, thermal and magnetic fields.

Spatiotemporal patterns like spiral waves and concentric circular stripe waves are found in many physical, chemical and biological systems [1–3]. In LCs, formation of striped patterns is due to asymmetry in molecular shape, which results in change in molecular orientation. Molecular chirality gives rise to striped or spiral patterns in freely suspended liquid-crystalline films [4, 5]. Patterns may also arise at an interface between two phases due to asymmetry between the phases, as observed at the free surface of LCs [6]. These patterns are also observed in Langmuir monolayers (LMs) on the aqueous subphase [7–12]. Gupta et al. [13] have observed spatiotemporal patterns in a Langmuir monolayer (LM) of a chiral LC, cholestric acid. The reason for such patterns were due to collective precession of the mesogenic molecules, driven by the evaporation of water through the monolayer.

There are several studies on LB films of chiral LCs [14–19] reported in the literature. Charra et al. [14] have observed chiral patterns in molecular assemblies of discotic liquid crystal (DLC), hexakis-2,3,6,7,10,11-alkyloxytriphenylene. Yuan et al. [18] have studied chiral molecular assemblies of amphiphilic 2-(heptadecyl) naphtha [2, 3] imidazole.

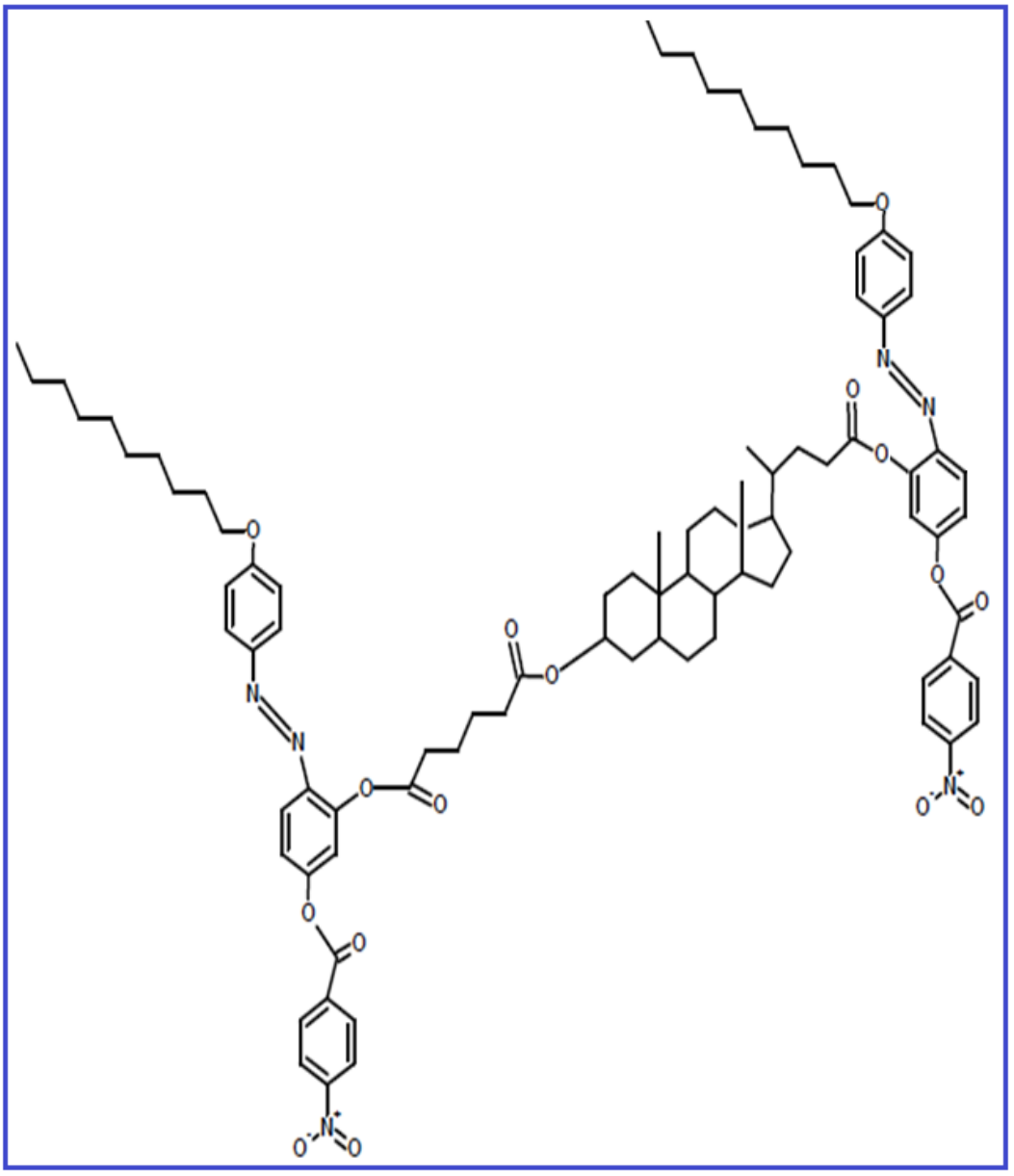

FIGURE 7.1: Chemical structure of H shaped LC (HLC) molecule.

Chiral LCs containing the azobenzene group are promising materials for devices involving photomechanics, optical switching, and image storing because of their high resolution and sensitivity [20–22]. It will be interesting to study the LM of such mesogenic LCs at A-W and air- solid (A-S) interfaces [23–25].

Suresh et al. [23] has shown that H-shaped mesogenic azobenzene molecule $bis[5-(4-n-dodecyloxybenzoyloxy)-2-(4-methylphenylazo)phenyl]$ adipate are photosensitive and, by shining ultraviolet (UV) light, it can be switched from trans to cis isomer state.

In this chapter, we studied LM of H-shaped mesogenic LC molecule (HLC) at the A-W interface under different illumination - bright and ultra-violet (UV) light and under dark condition. The chemical structure of the molecule is shown in Figure 8.11. The LB film of HLC molecule was transferred onto the hydrophilic silicon substrate at target surface pressure (π_t) of 1 mN/m and 20 mN/m using LB technique. The LB deposition was done under different illumination - bright and UV light and under dark condition. The surface morphology of HLC was studied using atomic force microscopy (AFM) and field emission scanning electron microscopy (FESEM).

7.2 Experimental Methods

The HLC molecule was procured from Prof. Sandeep Kumar of Raman Research Institute, Bengaluru. On cooling, smectic phase appears from temperature range, 76∘C to 50∘C. We studied surface manometry of HLC molecules at the A-W interface under different illumination - bright and UV light and under dark condition. The bright and UV light was achieved by using a compact fluorescent lamp (CFL) sources. The LM of HLC at the A-W interface was formed by spreading the HPLC grade chloroform solution of HLC onto the ultrapure ion-free water. The concentration of the HLC molecule in HPLC grade chloroform was 0.5 mg/ml. The monolayer was compressed by moving the barriers laterally at the rate of 20 mm/min. The phases of the LM of HLC under bright light were observed using a Brewster angle microscopy (BAM). A single layer of LB film of HLC was deposited under different illumination - bright and UV light and under dark condition on to Si substrate at π_t of 1 and 20 mN/m. The dipper speed was maintained at 2 mm/min during LB deposition. The film was scanned using AFM in semi contact mode. The spring constants and the resonance frequencies of the Si tips were in the ranges of 10-20 N/m and 180-270 KHz, respectively. The LB film of HLC was scanned using a FESEM at extra high tension of 0.5 kV, maintaining working distance of 4.1 mm at magnification of 1 KX. All the experiments were carried out at room temperature of ∼22°C.

7.3 Results and Discussion

The suface pressure (π) - area per molecule (A_m) isotherms of HLC molecule at A-W interface under different illumination - bright, UV and dark are shown in Figure 7.2. The isotherms show zero π at very large A_m. This indicates HLC molecule at high A_m to be in gas phase. The lift-off area per molecule (A_i) for the LM of HLC under dark condition is found to be 0.8 nm^2. Under the illumination of bright and UV lights, the A_i was changed marginally. The A_i of the LM under bright and UV light were found to be 1.0 and 0.7 nm^2 respectively. The regions of the isotherms, B to C, F to G and I to J under different illumination - bright and UV light and under dark condition respectively show slow and gradual rise in π. The regions, B to C, F to G and I to J in the isotherms indicate HLC molecule

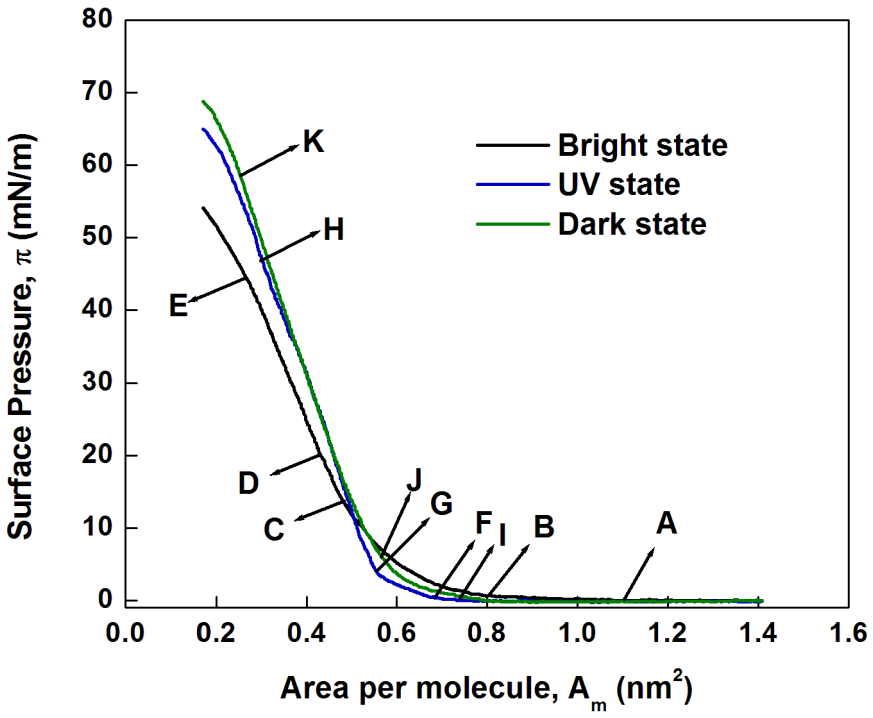

FIGURE 7.2: Surface pressure (π) - area per molecule (A_m) isotherm of HLC molecule at air-water (A-W) interface under different illumination - bright and UV light and under dark condition. Different regions of the isotherms are labelled from A to K.

to be in low density liquid (L_{1H}) phase. The isotherms show kinks indicated by C, G and J. Such kinks may indicate a phase transition. On further reduction in A_m, the π rises sharply in all three isotherms followed by a slow collpase. The regions, C to E, G to H and J to K in the isotherms indicate HLC molecules to be in high density liquid phase (L_{2H}) phase. The values of lift-off area per molecule

(A_i), limiting area per molecule (A_o) and collapse surface pressure (π_c) have been summarized in Table 7.1.

The HLC molecule mainly comprises of three parts - backbone, photoactive area and the hydrophilic part (Figure 7.3). Under different illuminating conditions on the HLC molecules, we observe no considerable change in the molecular area at A-W interface. Due to irradiation of light there is change in the conformation of photoactive part. Under different illuminations, there is no change in the conformation of the backbone and hydrophilic part. As a consequence of that, we observe no significant change in the surface manometry results of HLC molecule.

TABLE 7.1: Surface manometry results for HLC molecule

Illumination	**Lift-off area per molecule** A_i (nm^2)	**Limiting area per molecule** A_o (nm^2)	**Collapse** π π_c (mN/m)
Bright	1.0	0.5	45
UV	0.7	0.5	49
Dark	0.8	0.6	60

The planar area of the HLC molecule was estimated to be 4 nm^2 and its area in edge on configuration was estimated to be 0.35 nm^2. The A_o of HLC molecule for the isotherms is lesser than the planar area and larger than the edge on area of HLC molecule. This does not support molecule to be in planar (face on) configuration. Hence, we propose HLC molecule to have edge-on conformation with tilted molecules.

The variation of in plane elastic modulus (E) for the HLC monolayer (Figure 7.4) under different illumination - bright, UV and dark on the ion-free water subphase shows a peak corresponding to the L_{1H} (Peaks 1, 3 and 5 in Figure 7.4) and L_{2H} (Peaks 2, 4 and 6 in Figure 7.4) phase. The maximum value of E for HLC in the L_{1H} phase is around 42.7, 85.1 and 58.7 mN/m under different illumination - bright and UV light and under dark condition, respectively. The maximum value of E for HLC in the L_{2H} phase is around 63.6, 102.5 and 85.3 mN/m under different illumination - bright and UV light and under dark condition respectively. Such small values of E for HLC in L_{1H} and L_{2H} phase suggest that the monolayer is fluidic in nature in both the phases. From Figure 7.4, we observed that the specific area range of the L_{2H} phase is minimum under UV light and maximum under bright light. We observed that as the specific area range of the L_{1H} and L_{2H} phase increases, the value of E decreases.

The LM of HLC at A-W interface under bright light is subjected to isocycles (Figure 7.5) by compressing and expanding the monolayer repeatedly.

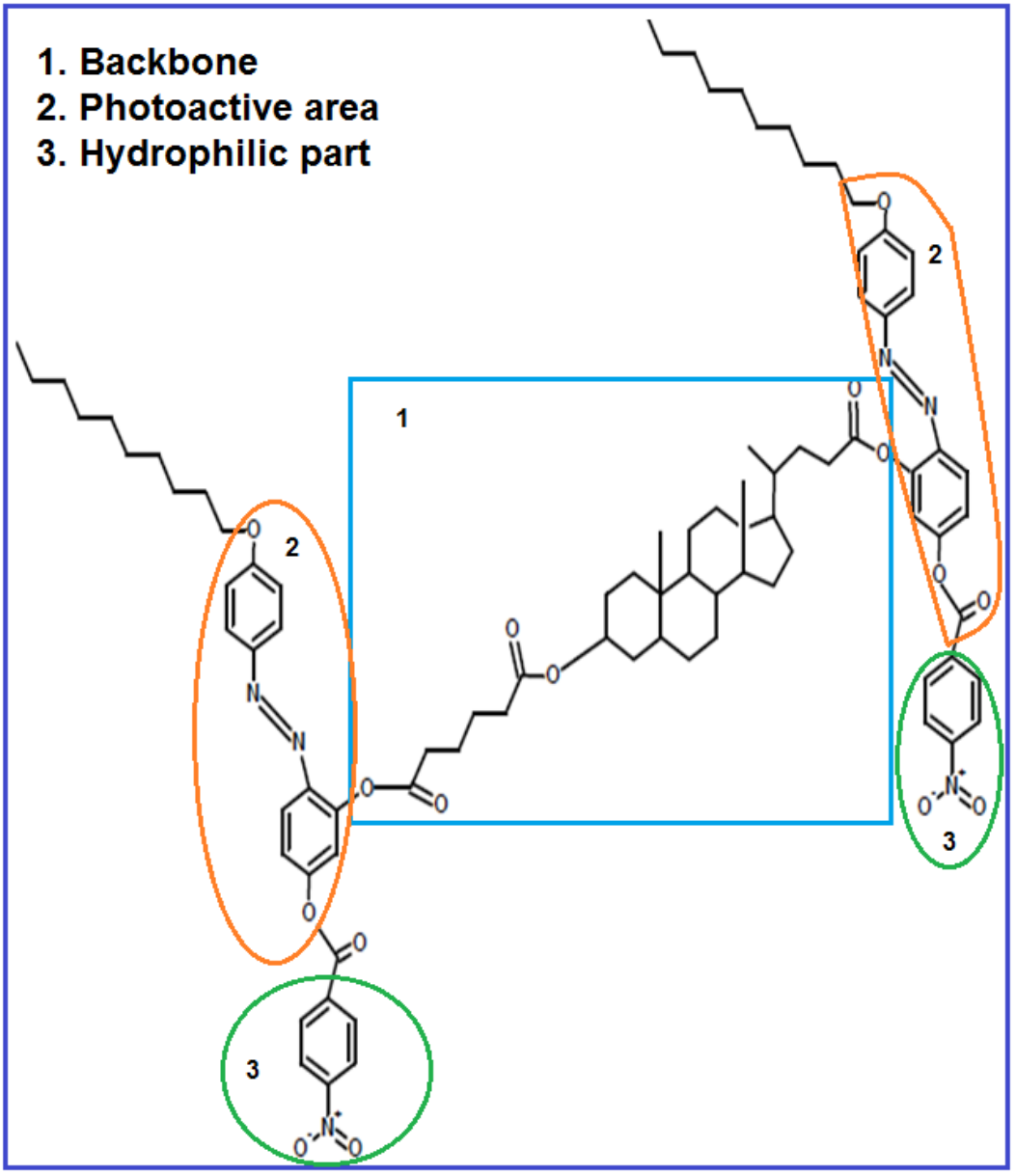

FIGURE 7.3: Chemical structure of H shaped LC (HLC) molecule indicating the 1) backbone, 2) photoactive area and the 3) hydrophilic part.

The results show considerable hysteresis and indicate that the isotherm is not reversible in nature. The second and the third cycle in Figure 7.5 was shifted by 0.3 and 0.6 nm^2 respectively w.r.t first isocycle on x-axis for visual clarity. The hysterisis in the isocycles also indicate the change in molecular conformation of HLC molecules at A-W interface due to repeated compression and expansion. The amount of hysterisis decreases as we increase the number of cycles from 1 to 3. This indicates that the molecules may attain some stable conformation due to repeated compression and expansion. We visualized the LM of HLC molecule under bright light using a BAM. At large A_m (Figure 7.6a), we found complete

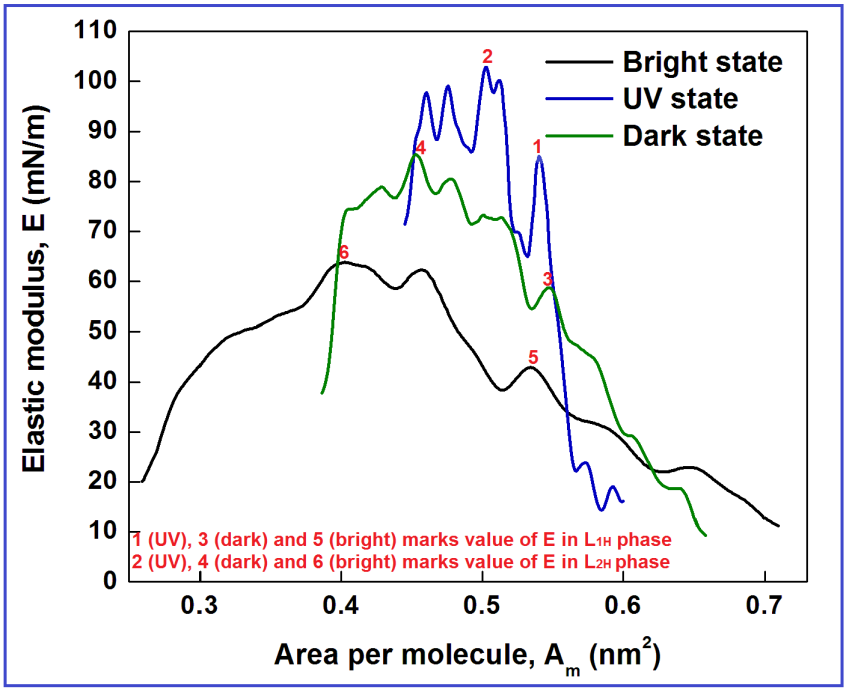

FIGURE 7.4: In-plane elastic modulus (E) - A_m of the HLC molecule under different illumination - bright and UV light and under dark condition.

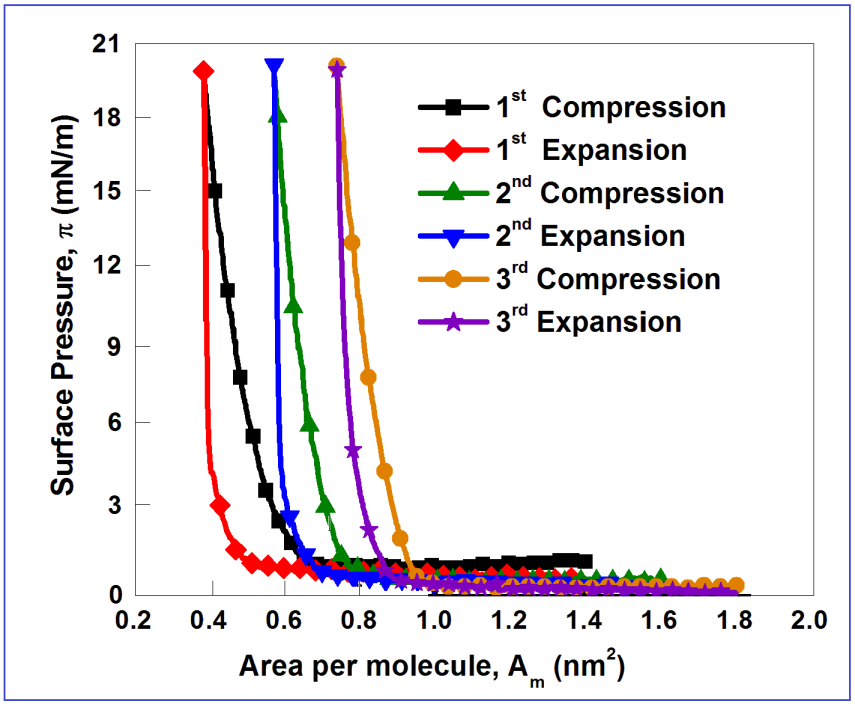

FIGURE 7.5: Isocycles obtained during repeated compression and expansion of the HLC monolayer at A-W interface under bright light. With respect to the first isocycle, the second and third cycles have been shifted by 0.3 and 0.6 nm^2 respectively on x-axis for visual clarity.

dark region. The dark region indicated HLC molecule to be in gas phase. On compressing the LM, the BAM image (Figure 7.6b) showed co-existence of bright and dark region. The bright region indicated onset of a liquid phase. On further reduction in A_m at (Figure 7.6c), the gas phase appears vanishing and we found almost complete liquid phase. The image shows few traces of gas phase, which may be due to non-uniformity in the LM of HLC at the length scale of 6.4 x 4.8 mm^2.

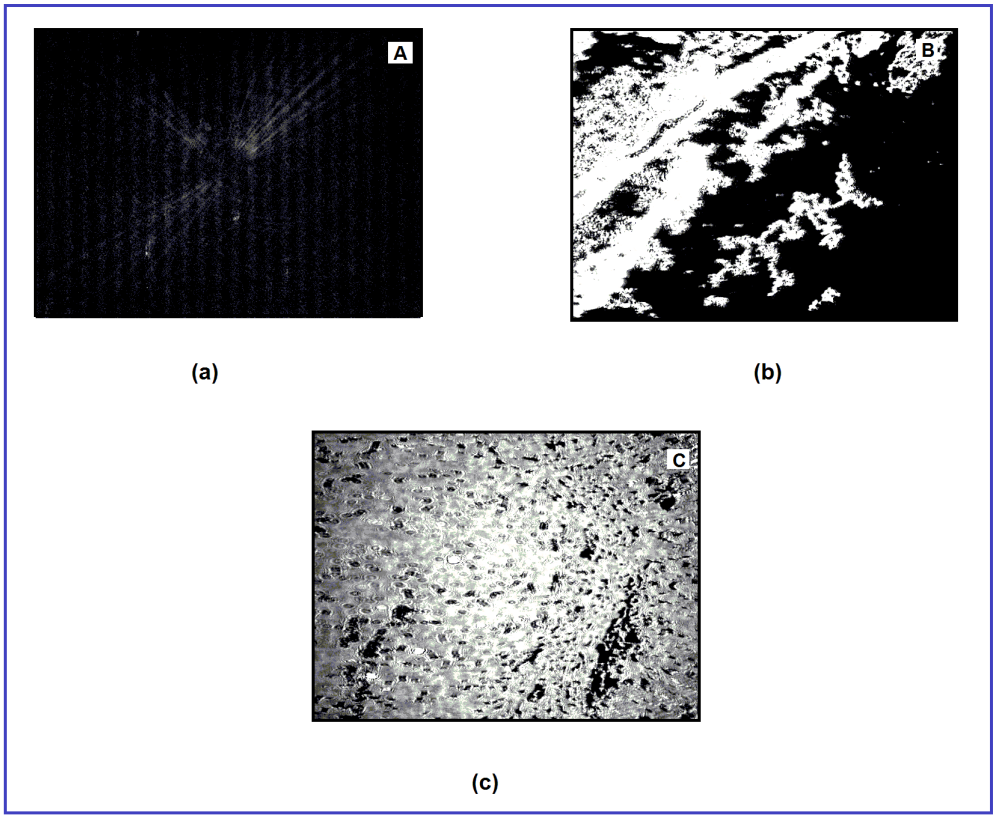

FIGURE 7.6: BAM images of LM of HLC molecule under bright light at A-W interface. The size of the image is 6.4 x 4.8 mm^2.

The FESEM images of LB film of HLC (Figure 7.7 and Figure 7.8) deposited under different illumination - bright and UV light and under dark condition at π_t of 1 and 20 mN/m shows interesting textures. The FESEM image shows a strong dependence of pattern formation onto the substrate due to the exposure of radiation. The pattern consists of dendritic growth revealing flower like patterns. It can be noted that the LB film of HLC deposited at π_t of 1 mN/m show larger flower-like pattern in case of presence of bright light (Figure 7.7A) and UV light (Figure 7.7B). However, the size of the pattern becomes smaller, if the ambient light is switched off during the deposition process. The image of the LB film deposited under dark condition also reveals wire strand like pattern (Figure 7.7C). With increase in π_t of LB deposition, the density of the

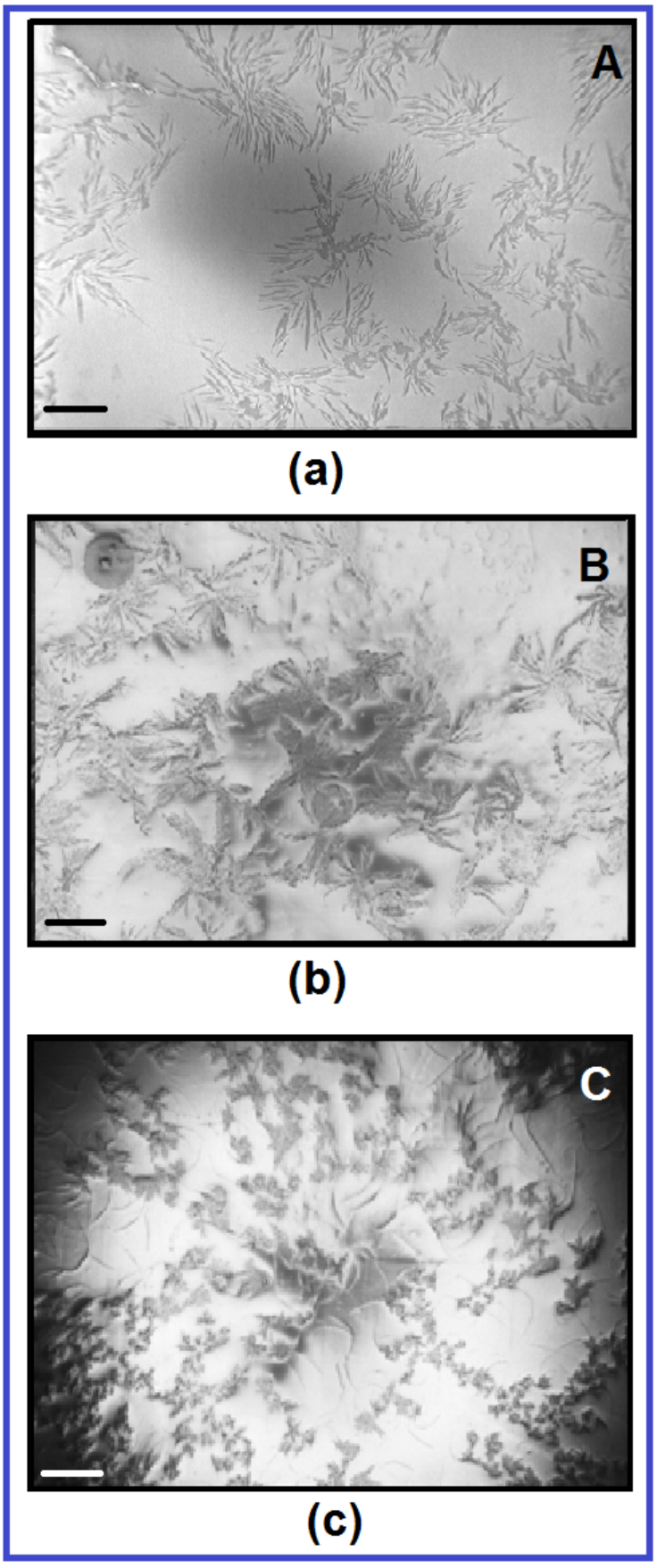

FIGURE 7.7: FESEM image of HLC molecule under different illumination - (a) Bright light (b) UV light (c) Dark condition at π_t of 1 mN/m. The scale bar is 100 μm in length.

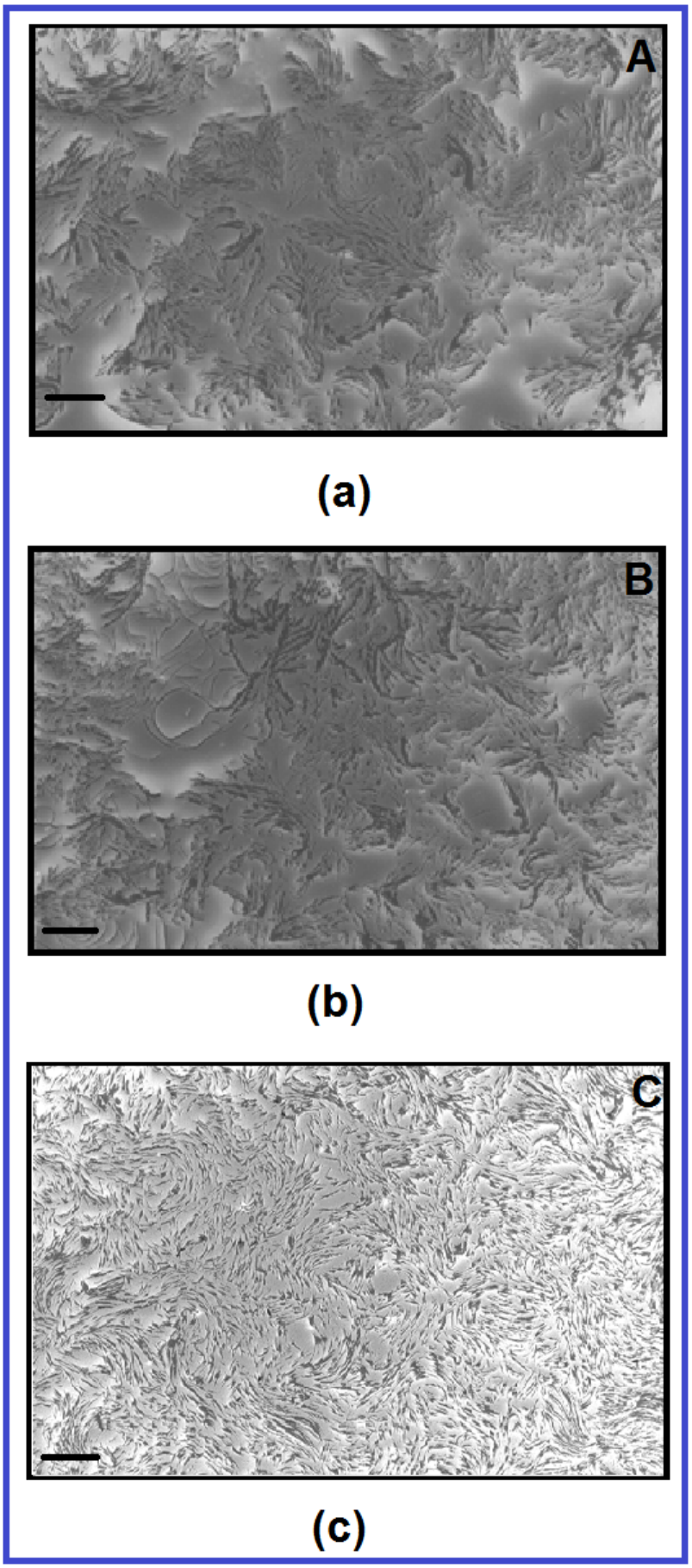

FIGURE 7.8: FESEM image of HLC molecule under different illumination - (a) Bright light (b) UV light (c) Dark condition at π_t of 20 mN/m. The scale bar is 20 μm in length for images A and C. The scale bar is 30 μm in length for the image B.

pattern increases. However, the flower pattern vanishes and swarm-like pattern forms (Figure 7.8).

In order to understand the sub-microstructure of the patterns obtained in FESEM images of the LB films, high resolution AFM with low scan area is performed. The AFM images (Figure 7.9 and Figure 7.10) reveal step-like layered structures. The sharp boundary of the layers also indicate its crystalline nature. The minimum height of the layers is calculated from the AFM images at different locations and in different images, and statistical average of the minimum height of the layers is calculated. The summary of the average minimum step height of the crystal like layer of the LB film deposited under different illumination is presented in Table 7.2. The minimum layer height is found to be largest for the LB films deposited under dark condition. Since the cis-isomer is less stable than trans-isomer, it may be possible that the isomeric state of the azobenzene part of the HLC is trans under dark condition. Hence, on LB deposition under dark condition, the overall step height of the crystalline layers increases. The average minimum height of the crystalline layer of LB film deposited in UV light is found to be the least.

TABLE 7.2: Minimum average step height of HLC layers observed in AFM.

Illumination	**Minimum average step height** (nm) **at** π_t **of 1** mN/m	**Minimum average step height** (nm) **at** π_t **of 20** mN/m
UV	3 ± 0.5	5 ± 0.5
Bright	4 ± 0.5	8 ± 0.5
Dark	6 ± 0.5	60 ± 0.5

This is due to the fact that on UV light during LB deposition, the azobenzene part of the HLC switches to cis-isomeric state and therefore the overall thickness of the layer reduces. Due to partial trans-cis transformation of the azobenzene part of the HLC molecule during the LB deposition in the presence of bright light, the average minimum height is found to be intermediate value between those obtained for LB films deposited in UV light and under dark condition. The patterns observed in LB films do not change on changing the illumination over the deposited LB films on the Si substrates. The patterns do not change due to strong cohesive interaction between the molecules and strong physical interaction between the molecules and the underlying surface of the substrate.

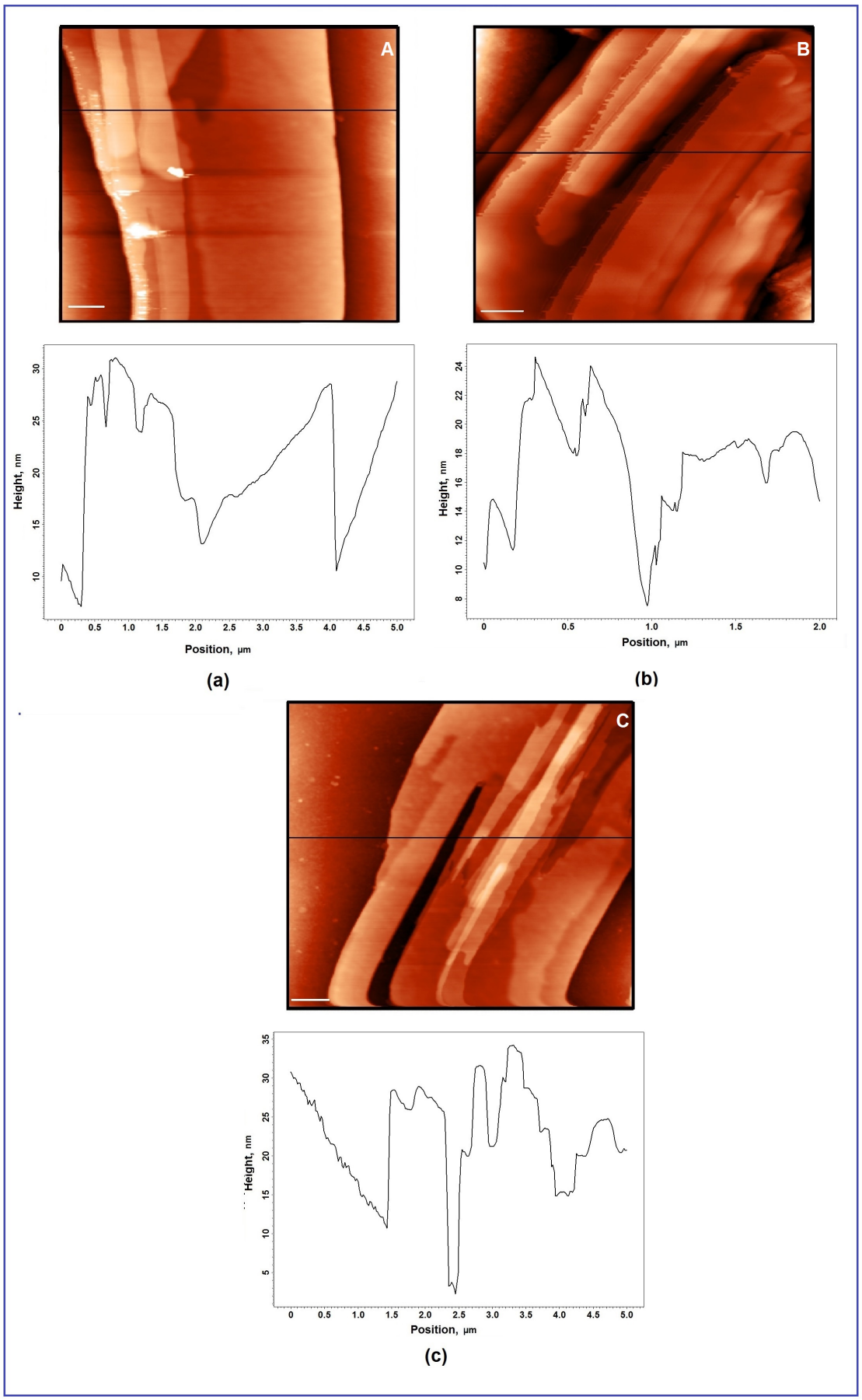

FIGURE 7.9: AFM images of single LB film of HLC molecule under different illumination - (a) UV light (b) Bright light (c) Dark condition at π_t of 1 mN/m. The scale bar is 0.5 μm in length for images A and C. The scale bar is 0.25 μm in length for image B.

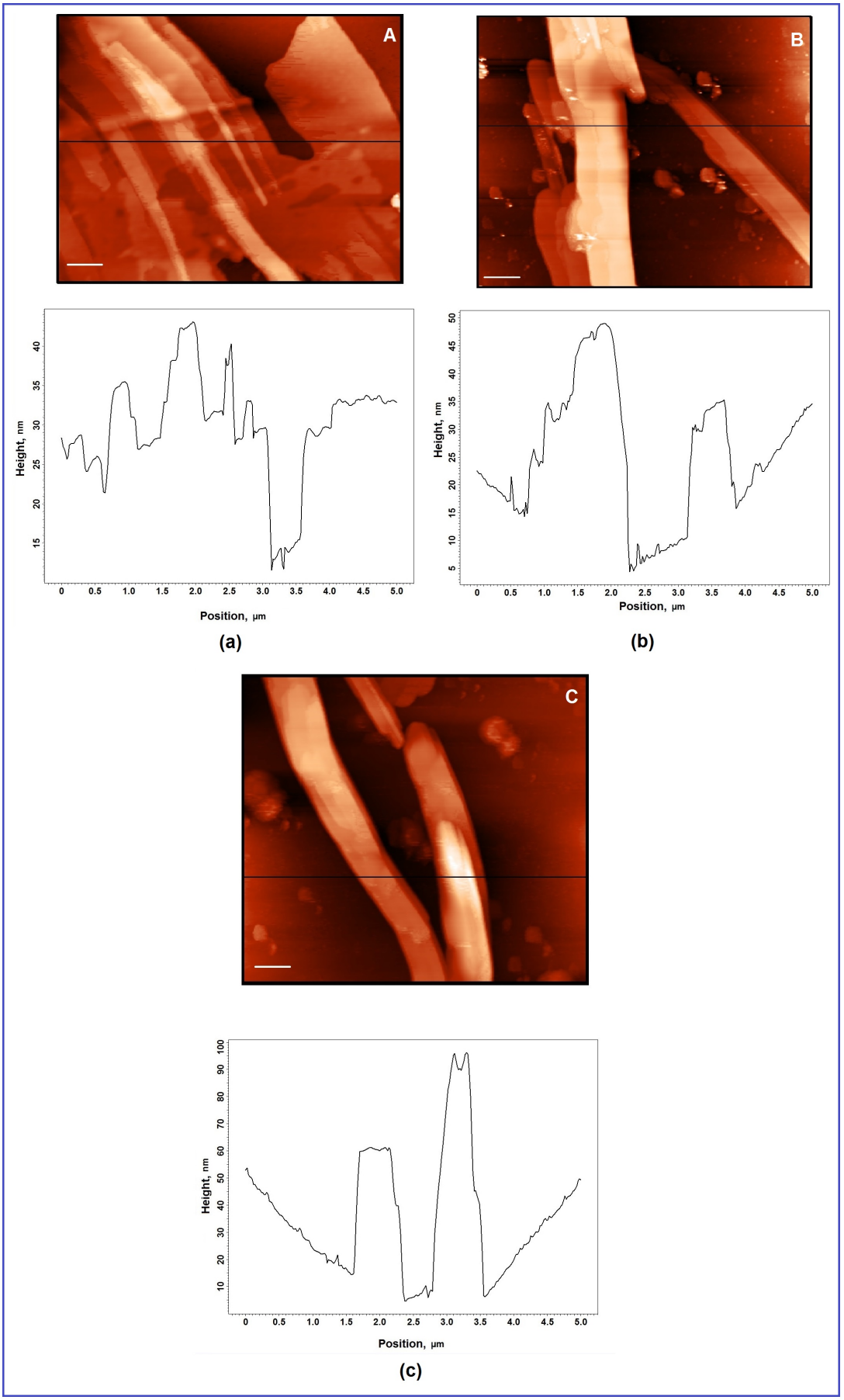

FIGURE 7.10: AFM images of single LB film of HLC molecule under different illumination - (a) UV light (b) Bright light (c) Dark condition at π_t of 20 mN/m. The scale bar is 0.5 μm in length.

7.4 Conclusions

We studied LM and LB of HLC molecule under bright, UV and dark illumination at A-W and A-S interfaces. In all three cases, the HLC molecule exhibits gas, L_{1H} and L_{2H} phase. We propose HLC molecule to be in edge-on conformation with tilted molecules in the liquid like phase. FESEM images of LB film of HLC under different illumination - bright and UV light and under dark condition at 1 mN/m indicate flower like patterns. The flower like dendritic patterns are smaller for the LB film of HLC under dark condition when compared with the deposited films under UV and bright light at 1 mN/m. The density of such patterns increase as the π_t is increased to 20 mN/m. Such features may arise due to molecular chirality. The AFM results for the LB film of HLC at 1 mN/m under different illumination - bright and UV light and under dark condition show crystal layered structures of HLC molecule. We found that the layer thickness depend strongly on the illumination during the LB.

Bibliography

[1] A. N. Zaikin and A. M. Zhabotinsky, Nat. London, 225, 535,1970.

[2] K. I. Agladge and V. I. Krinsky, Nat. London, 296, 424, 1982.

[3] I. Krinsky, Nat. London, 353, 740, 1999.

[4] V. K. Vanag and I. R. Epstein, Sci., 294, 835, 2001.

[5] S. A. Langer and J. P. Sethna, Phys. Rev. A, 34, 5035, 1986.

[6] S. B. Dierker, R. Pindak, and R. B. Meyer, Phys. Rev. Lett., 56, 1819, 1986.

[7] R. B. Meyer and P. S. Pershan, Solid State Commun., 13, 989, 1973.

[8] X. Qiu, J. Ruiz-Garcia, K. J. Stine, C. M. Knobler and J. V. Selinger, Phys. Rev. Lett., 67, 703, 1991.

[9] S. Rivière, S. Hénon, and J. Meunier, Phys. Rev. E, 49, 1375, 1994.

[10] Y. Tabe and H. Yokoyama, J. Phys. Soc. Jpn., 63, 2472, 1994.

[11] J.-L. Gallani, S. Mery, Y. Galerne, and D. Guillon, J. Phys. Chem. B, 108, 11627, 2004.

[12] J. V. Selinger and R. L. B. Selinger, Phys. Rev. E, 51, R860, 1995.

[13] R. K. Gupta, K. A. Suresh, S.Kumar, L. M. Lopatina, R. L. B. Selinger and J. V. Selinger, Phys. Rev. E, 78, 041703, 2008.

[14] Charra, Fabrice, and Jacques Cousty, Phys. Rev. Lett., 80, 1682, 1998.

[15] Ruiz-Garcia, Jaime, et al., J. Phys. Chem. 97, 6955, 1993.

[16] M. K. Durbin, et al., J. Chem. Phys., 106, 8216, 1997.

[17] Seul, Michael and David Andelman, Sci., 267, 476, 1995.

[18] Yuan, Jing and Minghua Liu., J. Ame. Chem. Soc., 125, 5051, 2003.

[19] Fasel, Roman, Manfred Parschau and Karl Heinz Ernst., Ang. Chemi. Int. Ed., 42, 5178, 2003.

[20] C. J. Barrett, J. I. Mamiya, K. G. Yager and T. Ikeda, Soft Matt., 3, 1249, 2007.

[21] Y. Yu, M. Nakano and T. Ikeda, Nat., 425, 145, 2003.

[22] T. Ikeda and O. Tsutsumi, Sci., 268, 1873, 1995.

[23] B. Kumar, A. K. Prajapati, M. C. Varia and K. A. Suresh, Langmuir, 25, 839, 2009.

[24] Tabe, Yuka and Hiroshi Yokoyama, J. Phys. Soc. Jp., 63, 2472, 1994.

[25] Ichimura, Kunihiro, et al., Langmuir, 4, 1214, 1988.

Chapter 8

Conclusions and future scope of our studies

8.1 Conclusions

A thin film is a layer of material whose thickness ranges from a fraction of nanometer to several micrometers. The surface to volume ratio of a material increases enormously when spread on to a substrate to form thin film which results in enhancement of performance and efficiency of the thin film based devices. Thin films find application in microelectronics, optical devices, microelectromechanical systems (MEMS) devices, photovoltaics and as an anti corrosion agent. A single layer of molecules onto the substrate can be considered as ultrathin film. The possibility of molecules to orient in ultrathin films can be used for several applications ranging from display devices to molecular electronics. Ultrathin films can be fabricated using different techniques e.g. chemical vapour deposition (CVD), plating, physical vapour deposition (PVD), dip coating, spin coating, self assembly (SA) and Langmuir Blodgett (LB) technique. This thesis mainly focuses on Langmuir monolayer (LM) and LB films of thermotropic and lyotropic liquid crystals at air-water (A-W) and air-solid (A-S) interfaces. LM is a stable film of single layer of amphiphilic molecules at the A-W interface. The LM gains stability due to balance between hydrophilicity and hydrophobicity of the amphiphilic molecule. LM can be considered as a two-dimensional system on smooth water surface, and it is known to exhibit several interesting surface phases. Such phases can be characterized using several techniques e.g. surface manometry, Brewster angle microscopy (BAM), epifluorescence microscopy (FM), grazing angle x-ray diffraction and second harmonic generation techniques. We have employed surface

manometry, BAM and FM for our studies. Using LB technique, the monolayer in a particular phase at the A-W interface can be transferred layer-by-layer onto a solid substrate by vertically moving the substrate in and out of the aqueous subphase in a highly controlled manner. LB films at the A-S interfaces can be characterized using numerous techniques. We have employed scanning probe microscopy (SPM), scanning electron microscopy (SEM), ultraviolet-visible (UV-VIS) spectroscopy and fourier transform infrared (FTIR) spectroscopy for our studies.

Liquid crystals (LCs) are states of condensed matter whose symmetries lie between those of 3-dimensionally ordered crystals and completely disordered isotropic liquid. There are two types of LCs: thermotropic and lyotropic LCs. The thermotropic LCs exhibit mesophases as a function of temperature whereas lyotropic LCs exhibit mesophases as a function of concentration, ion-contents, pH, temperature and humidity. The thermotropic mesophases are dependent on various factors including the molecular interaction and molecular shape anisotropy. Several thermotropic LCs are amphiphilic in nature and can form stable LM. In this thesis, we aim to study the LM and LB of LCs with different functional groups and different shape anisotropy. There are few studies on the LM and LB of the discotic liquid crystals (DLCs) at the A-W and A-S interfaces. Such systems are known to exhibit monolayer phases where the disk-plane of the molecules are either planar to the water surface (face-on conformation) or perpendicular to the water surface (edge-on conformation). There is a large scope to observe new phases in the LM, and molecular nucleation and aggregation at the A-S interface due to alteration of molecular interaction.

Chapter 1 is the introduction to LM, LB films and the techniques used for their characterization. We have also discussed about the LCs and other materials. The recent scenario of research and development of thin film of LCs is reviewed and the research gap is identified. In **Chapter 2** of this thesis, we present the results of LM of tricycloquinazoline (TCQ) based amphiphilic DLCs (AmTCQ) at the A-W interface. The chemical structure is shown in Figure 8.1. We report that due to weaker pi - pi interaction between the TCQ core of the discotic molecules, a new phase in the LM was observed. We found a stable LM of AmTCQ molecules. The monolayer exhibits gas phase, low density liquid (L_1) phase with face-on molecular configuration, and a novel high density liquid (L_{12}) phase exhibiting both the face-on and edge-on conformations of the molecules.

In the proposed model for face-on conformation, the core of the molecules lie planar to the water surface where the flexible ethylenoxy side-chains are interdigitated

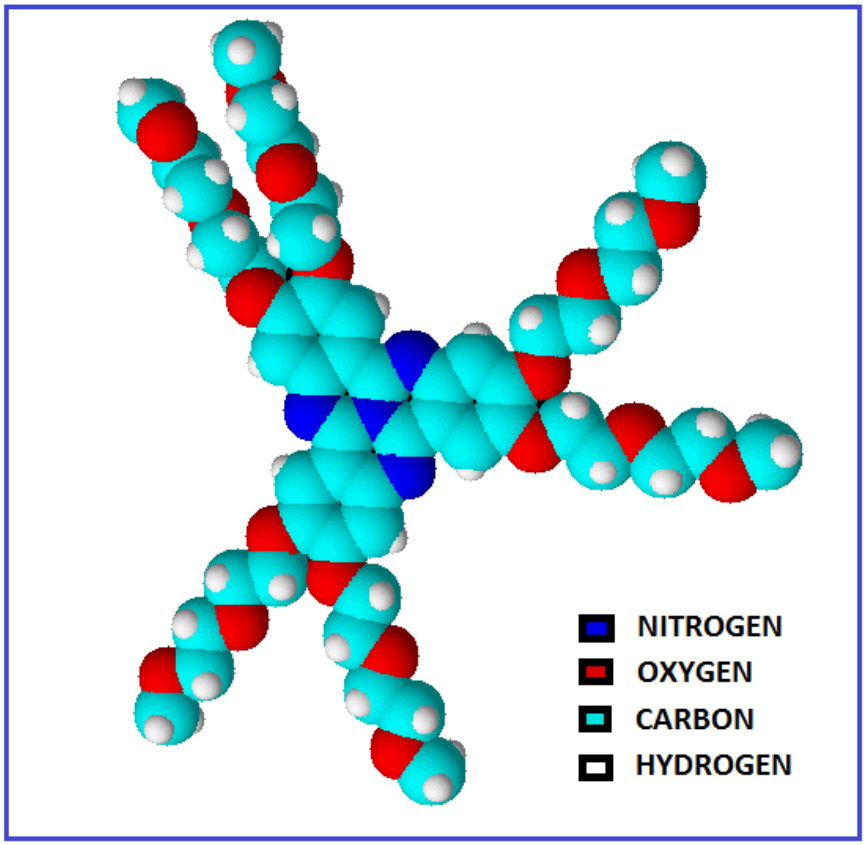

FIGURE 8.1: Discotic liquid crystal (DLC) molecule possessing tricycloquinazoline (TCQ) core and six ethelenoxy side chains (AmTCQ).

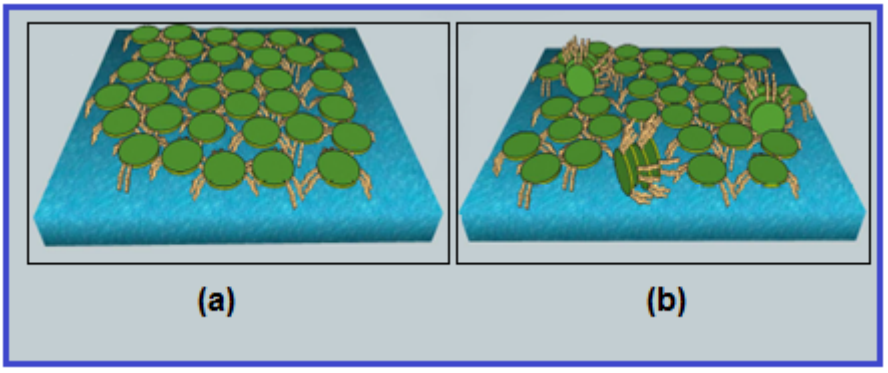

FIGURE 8.2: The possible molecular conformation of AmTCQ molecules at the A-W interface in a) L_1 and b) L_{12} phases.

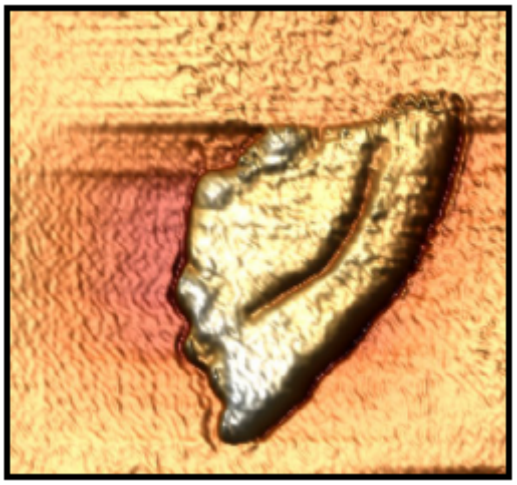

FIGURE 8.3: Triangular domain of AmTCQ molecule.

with the neighboring molecules (Figure 8.2a). The appearance of both face-on and edge-on conformations in the L_{12} phase might be due to the weak intermolecular interaction (Figure 8.2b). We transferred the LB films of the AmTCQ molecules onto the silicon (Si) substrate at different target surface pressure (π_t) and the films were scanned using atomic force microscopy (AFM). The LB films deposited in the gas phase (zero value of π_t) show flat domains with face-on conformation of the molecules. The LB films deposited at a low π_t of 1 mN/m show nucleation sites for the growth of triangular domains. As the π_t of LB deposition increases, AFM images of the film show triangular domains (Figure 8.3). The shape and size of such domains appear to be stable with respect to π_t provided if π is less than the equilibrium spreading pressure (ESP) of the AmTCQ molecules (i.e. greater than 20 mN/m). As π_t increases, the number of triangular domains increases. We have estimated percentage of area coverage of the triangular domains in the LB films deposited at different π_t. This is shown in Figure 8.4.

The triangular domain exhibit crack-line defect (Figure 8.3). The triangular domains deform as the π_t increases above ESP of the AmTCQ molecules indicating instability. Such instability arises as the monolayer approaches collapse above the ESP. The triangular domains may be formed due to the relaxation of strained LB films of the AmTCQ molecules. The strain in the LB films develops due to the lattice mismatch of the films and Si (100) substrate. Our study demonstrates that π_t to be a controlling parameter for altering the number of triangular domains in the LB films.

Further, it will be interesting to understand the role of molecular interactions in the nanostructure formation at interfaces. Hence, we extended our study on

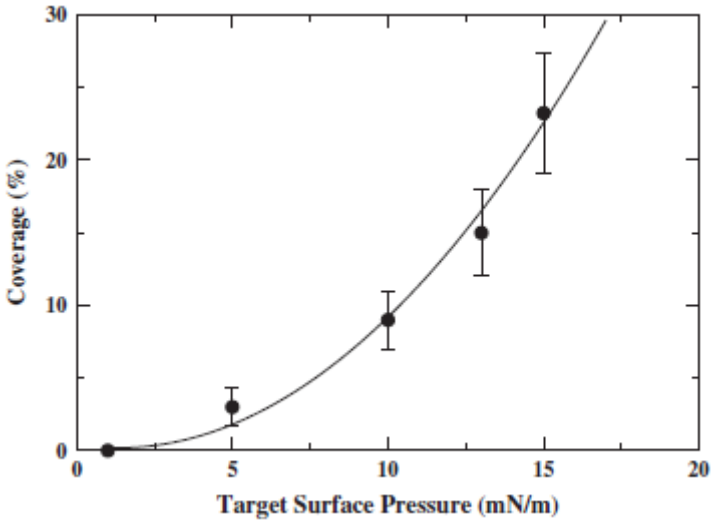

FIGURE 8.4: Percentage area coverage (c) of triangular domains in the LB films of AmTCQ deposited at different target surface pressure (π_t). The dark circles are the experimental data points. The solid line is a fit polynomial curve: $c = 0.4 - 0.32\pi_t + 0.12\pi_t^2$.

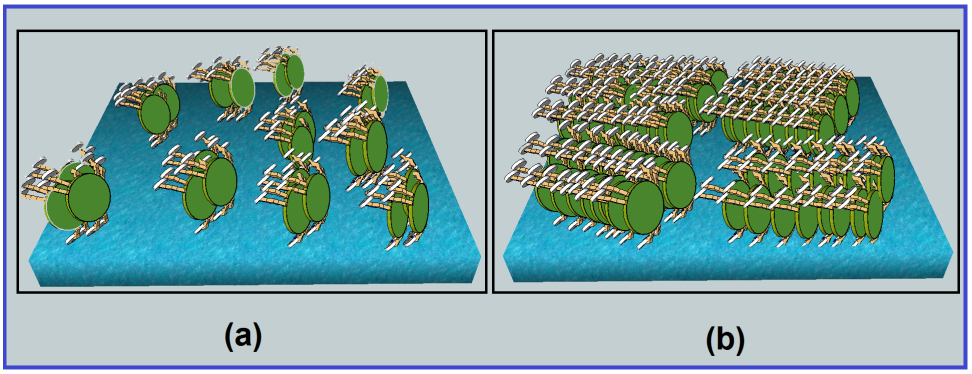

FIGURE 8.5: The possible molecular conformation of TCQCB molecules at the A-W interface in a) L_1 and b) L_2 phases. In L_1 phase, the molecules may prefer edge on conformation with a tilt. In L_2 phase, the molecules exhibit edge-on conformation in a highly dense surface layer where the side chains of the molecules are shown interdigitated with the side chains of the neighbouring molecules

surface behavior by altering the side chains of the AmTCQ molecules. Novel liquid crystalline (TCQCB) molecule has been synthesized by covalently linking rod shaped cyanobiphenyl to the central disk shaped TCQ core. The presence of rod shaped cyanobiphenyls at the periphery provides additional polarity to the discotic molecules. The surface behavior of such molecules is presented in **Chapter 3**. We found a stable LM of TCQCB molecules.The monolayer exhibits gas phase, low density liquid (L_1), and high density liquid (L_2) phases. The molecular orientation in L_1 and L_2 phases were found to be edge-on (Figure 8.5). The AFM images of the LB films deposited at $\pi_t \leq 10\ mN/m$ reveal the domains with vertical and tilted orientation of molecules. With increasing π_t, the elongated

domains were observed. The elongated domains as observed in L_1 phase undergoes a structural transformation to form a dense grainy texture in L_2 phase.

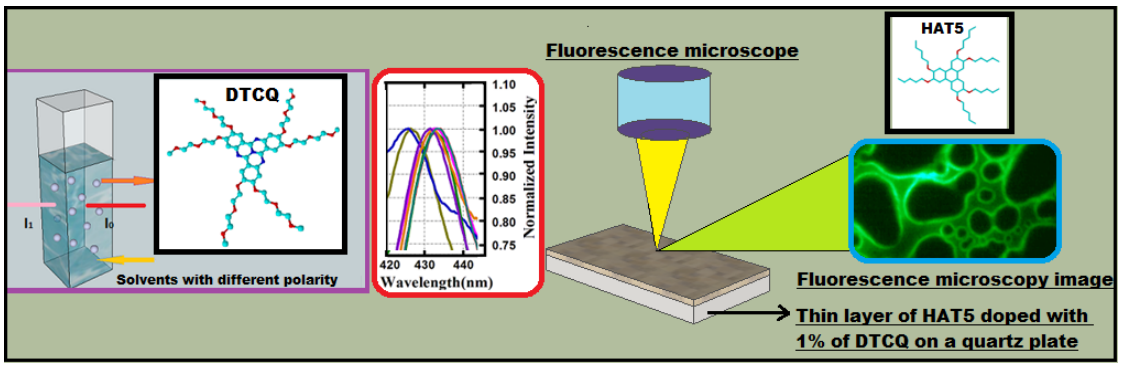

FIGURE 8.6: Graphical abstract of Chapter 4

AmTCQ is fluorescent in nature and can be used for fluorescence imaging of bulk LCs and thin films. In **Chapter 4**, the effect of various solvents of different polarity on photophysical properties of AmTCQ was studied. We observed red shift in the emission spectra as polarity of the solvent was increased. The Stoke's shift, Lippert's, Bakshiev's, and Kawski–Chamma–Viallet's polarity function were estimated from the experimental data. We found the ground and excited state dipole moment value of the molecule to be 2.56 D and 3.59 D respectively. Computationally, the ground state dipole moment value was calculated to be 3.20 D using Gaussian'03 package. We demonstrated that AmTCQ molecules can be employed for imaging another non-fluorescent DLC in the bulk state (Figure 8.6). The AmTCQ molecules are spread on the water surface to form a stable LM. The epi-fluorescence imaging of the LM of AmTCQ molecules reveals good contrast in the gas and liquid phases.

Studies on surface behavior of hybrid system of organic DLCs and metal oxide nanoparticles may find application in the field of photovolatics. In **Chapter 5**, the LM of pure hexaalkoxy triphenylene (HAT5) and HAT5+TiO_2 nanocomposites with different wt.% of TiO_2 nanoparticles are studied. We found condensation effect on the monolayer of HAT5+TiO_2 nanocomposites due to the presence of TiO_2 nanoparticles. The LB films of HAT5 and HAT5+TiO_2 nanocomposites with 5 and 20 wt.% of TiO_2 nanoparticles are deposited at π_t of 2 and 20 mN/m. The UV-Vis spectroscopy results indicate the reduction in energy gap with the increase in concentration of TiO_2. The reduction is found to be significant for the LB films deposited at higher surface pressures. As the wt.% of TiO_2 nanoparticles increases, the density and the size of clusters of TiO_2 nanoparticles increases (Figure 8.7).

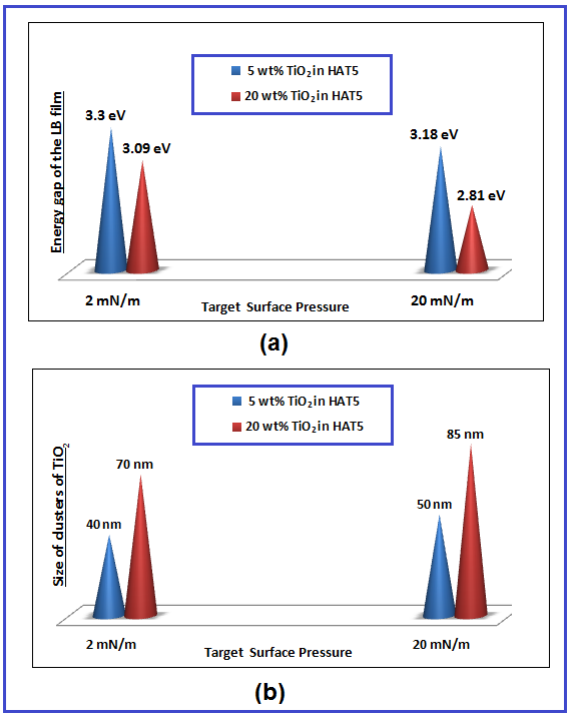

FIGURE 8.7: Variation of a) energy gap b) size of clusters of TiO_2 nanoparticles of the LB films deposited at π_t of 2 mN/m and 20 mN/m and 5 and 20 wt.% of TiO_2 in HAT5.

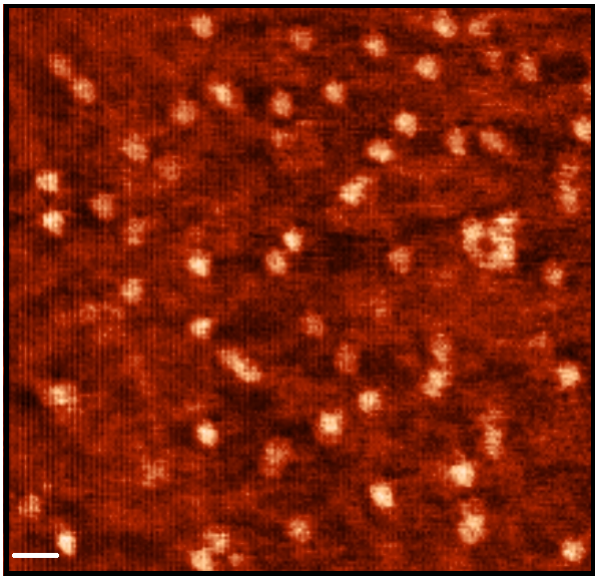

FIGURE 8.8: The AFM images of LB film of HAT5+ 20 wt.% of TiO_2 nanoparticles. The films were deposited in the L_2 phase at π_t of 20 mN/m. The scale bar is 0.2 μm in length.

The surface morphology of the LB films of pure HAT5 and HAT5+TiO_2 nanocomposites was obtained using AFM. We found increase in density of clusters of TiO_2 nanoparticles with the increase in wt.% of the nanoparticles in HAT5 matrix (Figure 8.8). We observe reduction in the energy gap of the HAT5 system on appropriately doping the system with TiO_2 nanoparticles. Our study indicates a dependence of energy gap of the LB films of HAT5 + TiO_2 nanocomposites on wt.% of TiO_2 nanoparticles in the HAT5 matrix.

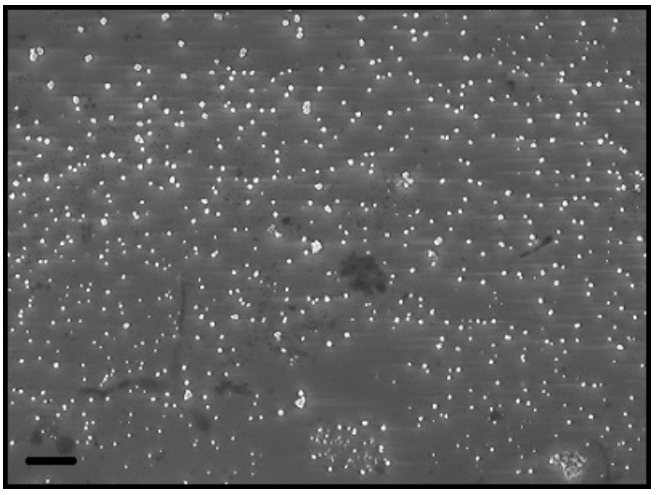

FIGURE 8.9: FESEM image of the LB film of ODT-Cd^{2+} complex deposited at π_t of 30 mN/m from the aqueous subphase of 10^{-4} M concentration of $CdCl_2$. The scale bar is 2 μm in length.

In **Chapter 6**, we demonstrated that LM can be employed for the fabrication of cadmium sulphide (CdS) nanoparticles. A LM of octadecanethiol (ODT) molecules is formed on the ionic subphase. The aqueous subphase is made ionic by adding a salt, cadmium chloride ($CdCl_2$) in ultrapure ion free water. The hydrophilic SH group of the ODT molecule interacts with the metal ion dissolved in the aqueous subphase resulting in formation of CdS nanoparticles. The surface morphology of LB film of ODT-Cd^{2+} complex deposited at π_t of 30 mN/m onto the Si substrate at 10^{-4} M concentration of $CdCl_2$ was studied through FESEM (Figure 8.9). The white particles in the FESEM image indicate the CdS nanoparticles. The average size of the particles obtained through AFM, FESEM and X-ray diffraction (XRD) was found to be $\sim$23 nm. The CdS nanoparticles were embedded in the LM of a rod shaped LC, 4-octyl-cyanobiphenyl (8CB) molecules and transferred onto the substrate. Such LB films were used as alignment layer during the fabrication of LC cell. We observed that with the LB films of 8CB+CdS nanoparticles as alignment layer, the bulk LC in the cell can align planar. The presence of CdS nanoparticles in the LB film of 8CB LC matrix enhances the planar orientation in the bulk LC (Figure 8.10).

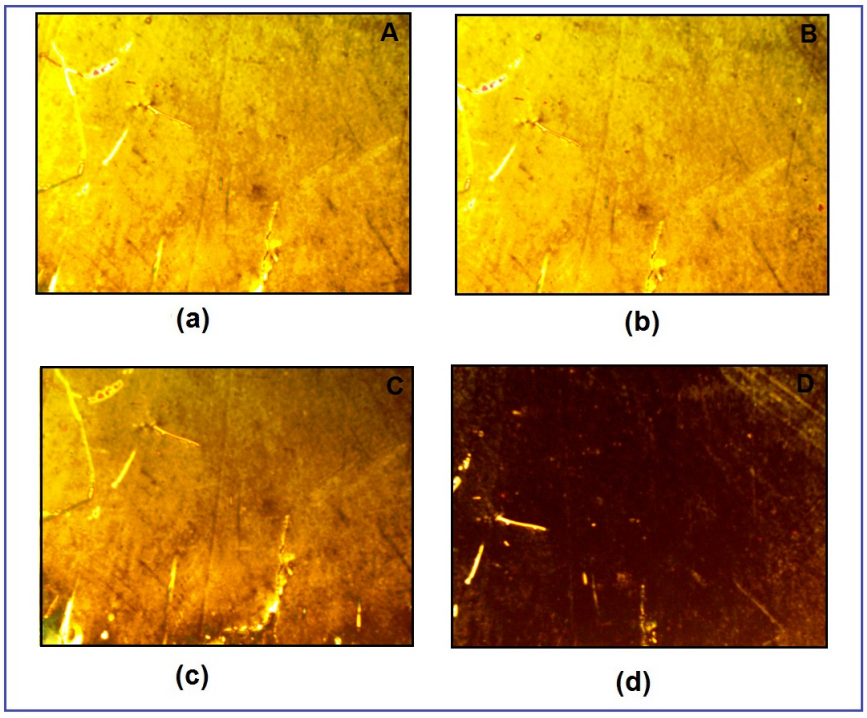

FIGURE 8.10: The polarizing microscopy textures of the LC-cell fabricated using LB films. The LB film of 8CB with 10 mole percent of ODT was deposited at the π_t of 2 mN/m from the aqueous subphase containing 10^{-4} M concentration of $CdCl_2$. The change in intensity from maximum to zero can be obtained in sequence from (a) to (d) on rotation of the LC-cell mounted on the microscope stage between crossed polarizers.

LCs in which conventional mesogenic units are pre-organized in a classical shape can produce unusual phase structures and can exhibit unique physical properties. It will be interesting to study the surface behaviour of such unconventional LC. In **Chapter 7**, we have studied the LM and LB films of unconventional H-Shaped LC molecules (HLC). The chemical structure of the molecule is shown in Figure 8.11. The molecule posseses azo group which can switch from cis-trans-cis on the application of appropriate radiation. The LB films of such molecule showed different patterns under UV light and dark condition. The high resolution AFM images of LB films of HLC indicate crystal like layered structure. Such patterns may arise due to intermolecular and molecule substrate interactions.

8.2 Future Scope

In our studies, we found that the π_t of LB deposition as a factor to control the nanostructures in the LB films of AmTCQ molecule. It will be interesting to study the role of factors like temperature, substrates and shape of the molecules in the nanostructure formation at the A-S interface. The molecular states of

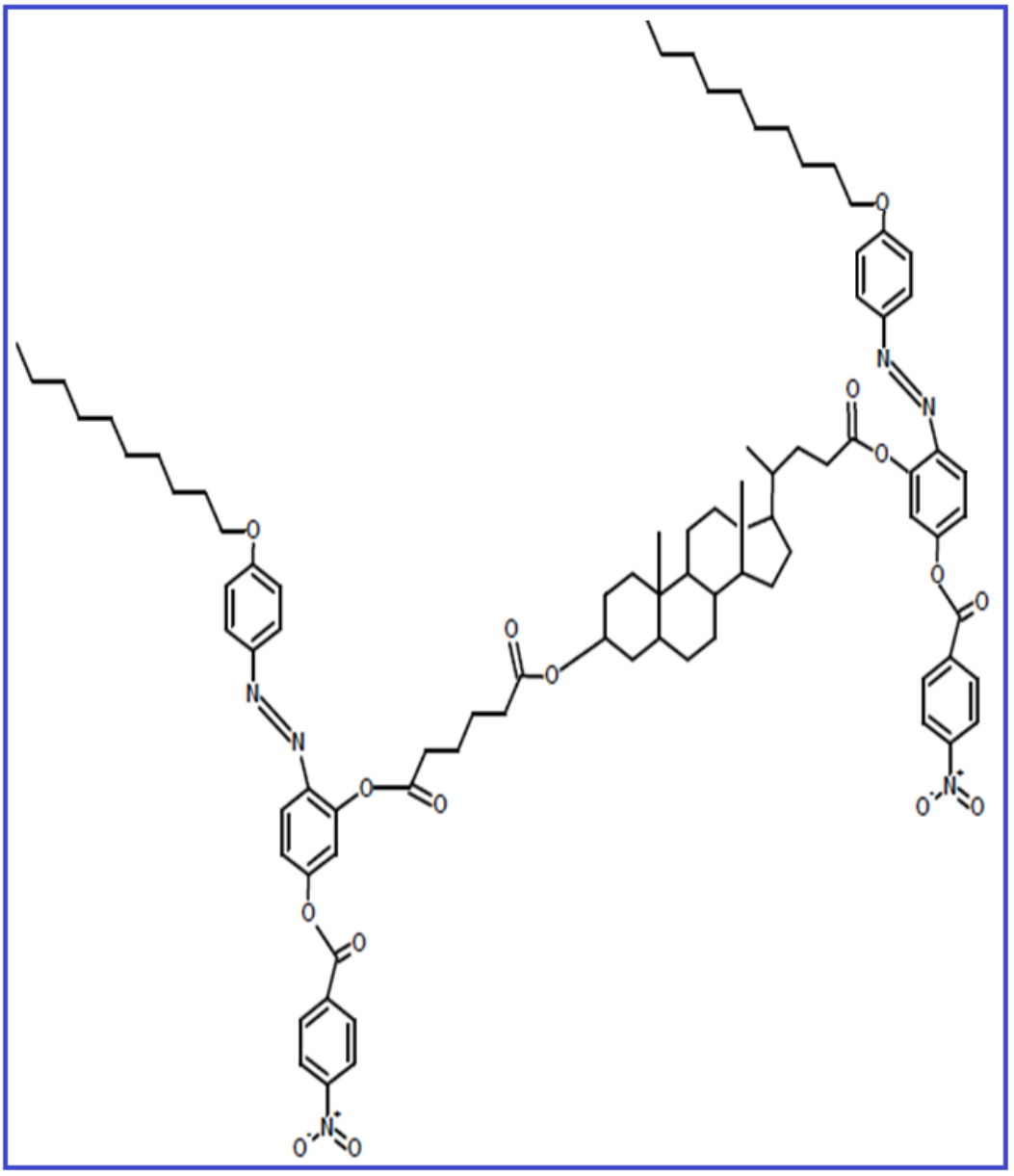

FIGURE 8.11: Chemical structure of H shaped LC (HLC) molecule.

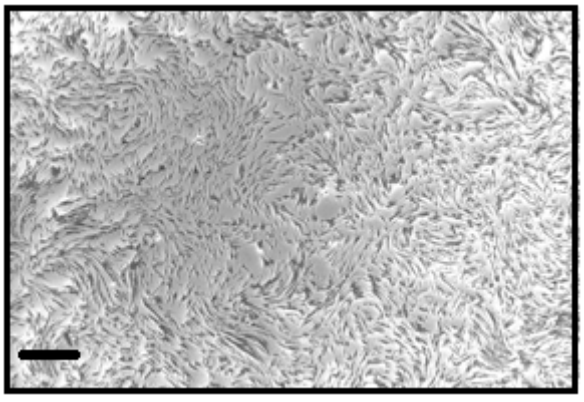

FIGURE 8.12: FESEM image of HLC molecule indicating flower like patterns under dark condition at π_t of 20 mN/m. The scale bar is 20 μm in length.

the thermotropic LCs can be significantly affected due to change in temperature. Therefore, it will be interesting to perform a systematic study on pattern formation in LB films of thermotropic LCs under the influence of temperature. Such patterns can be employed for the alignment of bulk LCs for display device application. The fluorescence nature of the TCQ based DLC molecules can be used as a molecular probe for imaging disc-shaped molecular systems. We studied the surface behavior of a unique nanocomposite comprises of HAT5 molecule and TiO_2 nanoparticles. Here we demonstrated that the energy gap of the LB films of the nanocomposite can be altered systematically on changing the wt.% of the TiO_2 nanoparticles in the HAT5 matrix. The LB film of such nanocomposites can be employed for the fabrication of organic solar cell and the performance of the device can be studied under the influence of various physical parameters. We demonstrated that CdS nanoparticles can be embedded in-situ into LM of amphiphilic molecules. Such nanoparticles not only enhance the adhesion of the LB films but also can alter the physical properties of the film. We embedded CdS nanoparticles in the LB film of 8CB and employed the LB film as alignment layer during the fabrication of LC cells. The presence of CdS nanoparticles in the alignment layer facilitates the planar orientation of the bulk liquid crystal in the LC cell. This may be a cost effective way to align the LCs in the planar geometry which is a vital factor for the fabrication of liquid crystal display devices. HLC molecule possesses azobenzene group which can switch from cis-trans-cis on the application of electromagnetic wave radiation. The LB film of HLC molecule show interesting patterns. The molecular conformations in such patterns will be studied at the subnanometer resolution and the effect of electromagnetic wave radiation will be studied. The thin film of such material can be used for devices involving photomechanics, molecular switching, nano-lithography and memory storage.

Appendix A

LIST OF PUBLICATIONS

Publications in international journals

1. **Studies on Langmuir monolayer of tricycloquinazoline based disk-shaped liquid crystal molecules**
Raj Kumar Gupta, Manjuladevi V., C. Karthik, Sandeep Kumar, and K.A. Suresh
Colloids and Surfaces A: Physicochemical and Engineering Aspects, 410, 91-97 (2012).

2. **Pattern formation in Langmuir - blodgett films of TCQ based discotic liquid crystal molecule**
C. Karthik, Manjuladevi V., Raj Kumar Gupta, and Sandeep Kumar
Journal of molecular structure, 1070, 52-57 (2014).

3. **Studies on thin films of hexa-alkoxy triphenylene (HAT 5) and composite of HAT5 – TiO2 nanoparticles**
C. Karthik, Keerti Choudhary, Aditya Joshi, Adbhut Gupta, Manjuladevi V., Raj Kumar Gupta, and Sandeep Kumar
Advanced Science Letters, 20, 1138-1142 (2014).

Publications in conferences

1. **Studies on ultrathin films of tricycloquinazoline (TCQ) based discotic liquid crystal molecules**
C. Karthik, Manjuladevi V., Raj Kumar Gupta and Sandeep Kumar
Journal of Physics, 417, 012068 (2013).

2. **Formation of H-type liquid crystal dimer at air-water interface**
C. Karthik, Keerti Choudhary, Adbhut Gupta, Aditya Joshi, Manjuladevi V., Raj Kumar Gupta, Mahesh C. Varia and Sandeep Kumar
AIP proceedings, 1591, 1036 (2014).

3. **Atomic force microscopy of Langmuir Blodgett films of disk shaped molecules**
C. Karthik, Raj Kumar Gupta, Manjuladevi V., Sandeep Kumar
Journal of Physics and Mathematical Sciences ISSN: 2277-2111 (Online).

4. **Effect of cadmium ions on ultrathin films of octadecanethiol molecules**
Sartaj S. Manhas, C. Karthik, Raj K. Gupta and Manjuladevi V.
Journal of Physics and Mathematical Sciences ISSN: 2277-2111 (Online).

Papers to be communicated

1. **Photophysical properties of tricycloquinazoline based discotic liquid crystal and its application in fluorescence imaging**
C. Karthik, Manjuladevi V., R. K. Gupta and S. Kumar

2. **Langmuir monolayer assisted fabrication of cadmium sulfide (CdS) nanoparticles and its role in alignment of bulk LC**
C. Karthik, Manjuladevi V. and R. K. Gupta

3. **Light dependent pattern formation in Langmuir Blodgett films of H-shaped liquid crystal**
C. Karthik, Manjuladevi V., R. K. Gupta, M. C. Varia and S. Kumar

Appendix B

LIST OF PRESENTATIONS

1. **Oral presentation** in **National conference on Nano- and Functional Materials**, Birla Institute of Technology and Sciences, Pilani from 7-8 November, 2014, *"Application of disk shaped Tricycloquinazoline molecule in fluorescence imaging".*

2. **Poster presentation** in **DAE- Solid State Physics Symposium**, Patiala, 17-21 December 2013, *"Formation of thin films of H-Type Liquid Crystal Dimer".*

3. **Poster presentation** in **International E-Workshop on Computational Condensed Matter Physics and Materials Science**, Gwalior, 27-29 November 2013, *"Physicochemical studies on a novel discotic liquid crystal".*

4. **Oral presentation** in **International conference on Nanoscience and Nano technology**, Lucknow from 18-20 November, 2013, *"Investigating optical properties of suspension of Tricycloquinazoline disk-shaped liquid crystals in various solvents".*

5. **Poster Presentation** in **International conference on Nanoscience and Nano technology**, Lucknow from 18-20 November, 2013, *"Studies on thin films of Hexa-alkoxy triphenylene (HAT5) and composite of HAT5-TiO2 nanoparticles".*

6. **Oral presentation** in **International Conference on Surface Science and Engineering**, Indore from 4-5 March, 2013, *"Cadmium Sulfide nano particles at*

air-water interface".

7. **Poster presentation** in **National conference in condensed matter physics**, Birla Institute of Technology and Sciences, Pilani, 24-25 February 2012, *"Atomic force microscopy of Langmuir Blodgett films of disc shaped molecules".*

8. **Poster presentation** in **3rd International Conference on Current Developments in Atomic, Molecular, Optical and Nanophysics**, Delhi University, 14-16 December, 2011, *"Nanostructured domains in ultrathin films of discotic liquid crystals molecules".*

9. **Oral presentation** in **15th International Conference on Thin Films**, Kyoto, Japan from 8-11 November, 2011, *"Studies on ultrathin films of tricycloquinazoline (TCQ) based discotic liquid crystal molecules".*

Appendix C

BIOGRAPHY OF THE CANDIDATE

Mr. C. Karthik is a full time research scholar in Department of Physics, BITS, Pilani since January 2011. He holds M.Sc. (HONS) Physics from Birla Institute of Technology and Science, Pilani in the year 2010. He is the founder of Gurukul, Department of music, BITS, Pilani and a junior diploma holder from Prayag Sangeet Samiti, Allahabad in vocal music.

His research interests are focused on surface manometry of liquid crystals with different functional groups and different shape anisotropy using Langmuir Blodgett Technique. He also works on fabrication and characterization of ultra-thin films of different materials, and controlling the nanostructures in the thin films. He is currently pursuing Ph.D. from BITS, Pilani in soft condensed matter physics (experimental) as "Studies on thin films of liquid crystalline molecules". He published three papers in international journals and presented his work in nine national or international conferences in India and abroad.

Appendix D

BIOGRAPHY OF THE SUPERVISOR

Prof. Raj Kumar Gupta is an experimental soft condensed matter physicist. He obtained his Ph.D. from Raman Research Institute, Bengaluru in soft condensed matter physics (experimental) in the year of 2005. He works on thin films of mesogenic molecules, nanomaterials and the composites. Currently, his research interests are focused on understanding the change in properties of materials in the ultrathin film regime and its application for device fabrication. He and his team comprising Prof. Manjuladevi V. and Mr. Devanarayanan in BITS Pilani have developed a low cost portable surface plasmon resonance instrument with the financial support from DST, India. The instrument is ready for any sensing application. His current research interests are:-

1. Optics: Surface Plasmon Resonance Instrumentation and related software development
2. Scanning probe microscopy of thin films of nanoparticles
3. Controlling parameters for defect formation in thin films
4. Scanning tunneling microscopy/spectroscopy
5. Application of ultrathin films for device development

He has published several research articles in reputed international journals. He has authored few book chapters in the field of his research interest. At present, he is associate professor in the department of physics at BITS, Pilani.